ACS OMEGA

Open Access

http://pubs.acs.org/journal/acsodf

Review

A Review of Synthesis Methods, Modifications, and Mechanisms of ZnO/TiO_2-Based Photocatalysts for Photodegradation of Contaminants

Reza Ghamarpoor,* Akram Fallah, and Masoud Jamshidi

Cite This: *ACS Omega* 2024, 9, 25457−25492

Read Online

ACCESS | Metrics & More | Article Recommendations

ABSTRACT: The environment being surrounded by accumulated durable waste organic compounds has become a critical crisis for human societies. Generally, organic effluents of industrial plants released into the water source and air are removed by some physical and chemical processes. Utilizing photocatalysts as cost-effective, accessible, thermally/mechanically stable, nontoxic, reusable, and powerful UV-absorber compounds creates a new gateway toward the removal of dissolved, suspended, and gaseous pollutants even in trace amounts. TiO_2 and ZnO are two prevalent photocatalysts in the field of removing contaminants from wastewater and air. Structural modification of the photocatalysts with metals, nonmetals, metal ions, and other semiconductors reduces the band gap energy and agglomeration and increases the affinity toward organic compounds in the composite structures to expand their usability on an industrial scale. This increases the extent of light absorbance and improves the photocatalytic efficiency. Selecting a suitable synthesis method is necessary to prepare a target photocatalyst with distinct properties such as high specific surface area, numerous surface functional groups, and an appropriate crystalline phase. In this Review, significant parameters for the synthesis and modification of TiO_2- and ZnO-based photocatalysts are discussed in detail. Several proposed mechanistic routes according to photocatalytic composite structures are provided. Some electrochemical analyses using charge carrier trapping agents and delayed recombination help to plot mechanistic routes according to the direction of photoexcited species (electron−hole pairs) and design more effective photocatalytic processes in terms of cost-effective photocatalysts, saving time and increasing productivity.

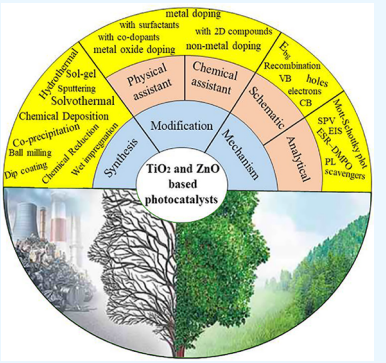

1. INTRODUCTION

Emerging organic pollutants (EOPs) are derived from pharmaceuticals, herbicides, pesticides, industrial products, or byproducts. These compounds show significant stability against biological degradation and thus remain long after being released into the environment in the form of effluents of water resources and air pollutants.[1,2]

The removal of pollutants from wastewater depends on the physical states of these compounds, with solid and oil waste removed by coagulation-flocculation,[3] sedimentation,[4] electrocoagulation,[5] and chemical oxidation[6] methods. Shi et al.[7] worked on the removal of organic pollutants in wastewater by using a red mud/graphitic carbon nitride ($g\text{-}C_3N_4$) composite (RM-CN) as a sorbent. Several properties like large surface area, high porosity, and numerous functional groups as active sites are necessary for sorbent active sites.[8,9] $g\text{-}C_3N_4$ as a semiconductor and RM as a mixture of some metal oxides like Fe_2O_3 and TiO_2 act as photocatalysts that, due to their adsorbent properties, are synergistically used for wastewater treatment for antibiotics and dyes. Degradation processes using photocatalysts as heterogeneous, accessible, and cost-effective compounds under light luminescence have been extensively utilized for the removal of organic pollutants in the air and bodies of water.[10]

General applications of ZnO and TiO_2 are as photocatalysts for the photodegradation of organic and inorganic pollutants, electrodes for water splitting,[11] H_2 production,[12] CO_2 reduction,[13] solar cells,[14] support of drug delivery,[15] sensors,[16,17] and energy storage.[17,18] These compounds act as n-type semiconductor photocatalysts for the degradation of a wide range of organic pollutants from air to wastewater domains. TiO_2 crystallizes in three structures: (1) anatase, (2) rutile, and (3) brookite, with Ti^{4+} in the center and six oxides in an octahedral arrangement. Band gap and excitation binding energies of ZnO and TiO_2 are large and equal to 3.3 eV and 60 meV (ZnO) and 3.1 eV and 53 meV (TiO_2), respectively.[19] The extent of striking light that can excite and pick up electrons from the valence band (VB) and transfer them to the conduction band (CB) is placed in the UV range.[20−23]

Received: November 3, 2023
Revised: May 22, 2024
Accepted: May 24, 2024
Published: June 6, 2024

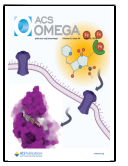

Scheme 1. Overview of Investigated Parameters in TiO_2- and ZnO-Based Photocatalysts

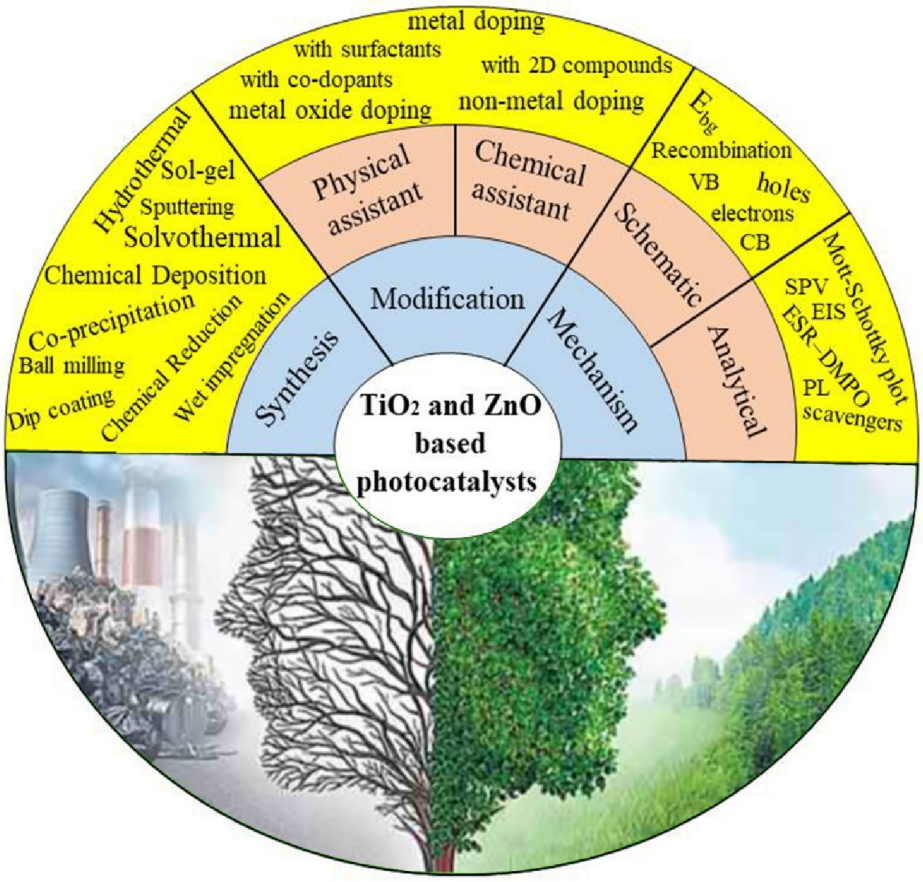

Some other semiconductors with photocatalytic effects are known, such as CeO, CdS, and ZnS, which have preferable properties compared to other conductive and insulating compounds due to their appropriate band gap energy to sufficiently decrease the recombination time of photoactive species.[24,25] Some of the significant characteristics of ZnO and TiO_2 as semiconductor oxides are their suitable electronic constructions, long lifetimes in the excited state, and magnificent light absorption from the UV to visible regions with slight modifications in their chemical structures.[26,27]

On the basis of limited access to the UV area, it is necessary to modify these precious semiconductors to shift their functional area from the UV to visible region. Enhancement with several structural modification methods include the following: loading with some transition metals,[28−30] doping with metal ions[31] or nonmetal ions,[32] coupling with other semiconductors with narrower band gap energies,[33] loading with some noble metals on the surface of photocatalysts,[34] including nitrogen, iodine, sulfur and carbon in the TiO_2 and ZnO lattice with their p orbitals coordinating with the O $2p_z$ orbital of the photocatalysts,[35,36] doping with some transition metals such as V, Cr, Fe, Mg, Ag, Co, Zn, and Mo,[37,38] some synthetic techniques like coatings, and surface sensitization with the introduction of some definite impurities[39] to increase the extension of irradiated light trapping by narrowing the band gap or increasing the specific surface area,[40] which are alternative approaches to narrow the band gap energy of pristine ZnO and TiO_2 and shift to them the visible light region.[23]

Different methods have been used to synthesize TiO_2, ZnO, and their modified forms with outstanding properties such as high porosity, low density, and high specific surface area. Hydrothermal,[41] solvothermal,[42] sol−gel,[43,44] chemical deposition,[45] and sol−hydrothermal[46] methods are some synthetic methods that provide superb electronic and optical properties and high shell penetrability. Hu et al.[47] synthesized hollow spheres of black titanium containing mesoporous structures by sequence reactions including the solvothermal method in template-free conditions, an encircling process in reflux conditions with an amine compound, and then hydrogenation at high temperature. The obtained black titanium had mesoporous walls with high crystallinity and frameworks with Ti^{3+} and disarray on the surface.

Kozlova et al.[48] modified pristine titanium photocatalysts with Pt metal to overcome fast electron−hole recombination in the photocatalysts. Pt plays an electron trap role in the photocatalytic degradation progress, delays the recombination time of charge carriers, and improves the photocatalytic activity. This phenomenon occurs through the formation of Schottky barriers at the interface of the metal and semiconductor. Maheswari et al.[49] fabricated CuO and ZnO that were dispersed sufficiently throughout titania (TiO_2) to form Schottky barriers. The antioxidation and photocatalytic activities of the prepared composites were analyzed against MB photodegradation. Dong et al.[50] synthesized a TiO_2/GM composite to degrade pharmaceutical compounds from medicinal wastewater. The significant advantage of the composite was its simple separation from the mixture and superb recyclability in comparison to pristine titanium.

Degradation of organic pollutants involves tandem photooxidation reactions that occur on the surface of photocatalysts

https://doi.org/10.1021/acsomega.3c08717
ACS Omega 2024, 9, 25457−25492

and initiate from the simultaneous transfer of photoexcited electrons from the VB to the CB and the remaining holes in the VB of semiconductors with light excitation.[51] Photoexcited electrons face two routes: (1) falling down to the VB and recombining with holes and/or (2) reacting with surface-adsorbed O_2 and participating in photo-oxidation reaction to degrade the pollutant. Electrons and holes as charge carriers themselves reach the surface of the photocatalyst and start reduction and oxidation reactions, respectively. Electrons reduce dissolved O_2 adsorbed on the surface of the photocatalyst to the superoxide radical anion ($O_2^{\bullet-}$), and holes oxidize adsorbed H_2O to the hydroxyl radical ($OH^{\bullet}$). These new reactive oxygen species (ROS) as indirect photoreaction products degrade organic pollutants in the solution to nontoxic compounds (i.e., H_2O and CO_2). Qiang et al.[52] synthesized a $RuTe_2$/black TiO_2 composite and proposed a mechanistic route where photoexcited electrons move from the VB to CB of black TiO_2 and then fall down to the CB of $RuTe_2$, which is more negative than that of black titanium.

Surveys of the literature show that there is increasing interest in exlpoiting semiconductor oxides as photocatalysts for the removal of pollutants. Significant features of photocatalytic compounds are their potential to exploit environmental light (sunlight) and transform photoelectric energy into chemical bonds. Power source accessibility, economic cost effectiveness, renewability, reusability, and heterogeneity are critical properties of these compounds that cause their inescapable applications in the field of solar cells, batteries, supporting and carrier compounds, and drug delivery. Studies show that there are many ways to improve the properties of TiO_2 and ZnO nanoparticles and widen their absorbance area from the UV region to the visible region. In this Review, we examine different synthesis methods, structural and surface modifications, and photoreaction mechanisms of these nanoparticles and their composites.

2. RESEARCH METHODOLOGY

The aim of this study is focused on the application of TiO_2- and ZnO-based photocatalysts for organic pollutant degradation in air and water. A relevant approach must be taken to arrange fraught information in a variety of articles.[53] As a result, this approach leads to particular literature that are precisely consistent with the research question of evaluating photocatalytic effects on environmental pollutants. For the purpose that was presented by Tranfield et al.,[54] it is necessary to take four imperative steps, namely, planning, searching, screening, and reporting. This direction is surveyed in the following section to help reviewers more effectively access it[55] and is demonstrated in Scheme 1.

2.1. Planning. The Review was established on researching four queries including synthetic methods, modification strategies, and mechanistic routes of semiconductors as photocatalyst compounds. This panel covers critical conditions, the importance of organic pollutant treatments in wastewater and air, and identifying properties of TiO_2 and ZnO as photocatalysts with reusability for the photodegradation of any pollutant in trace amounts, as well as acquaintance with several analytical methods of structural and mechanistic routes.

RQ1.
What compounds are considered as environmental pollutants?

RQ2.
What kinds of synthetic methods are used to prepare solid photocatalytic compounds?

RQ3.
How can modification cause an improvement of photocatalytic efficiency?

RQ4.
What are the mechanisms of photocatalytic reactions?

2.2. Searching. Literature survey was performed among the articles published between 1991 and 2024 (until June 2024). The scopus database including Elsevier, Springer, Wiley, and American Chemical Society was chosen as the search engine. A range of keywords about the photocatalytic field were used to find the best appropriate literature, which involved the four query areas mentioned before. Some keywords included "organic pollutants", "wastewater pollutants", "air pollutants", "dyes as wastewater pollutants", "synthetic methods of photocatalytic compounds", "synthetic methods of heterogeneous compounds", "TiO_2 as photocatalyst", "ZnO as photocatalyst", "semiconductors as photocatalyst", "modification of TiO_2", "modification of ZnO", "mechanistic routs of photocatalysts", and "mechanistic routs of photocatalytic reactions".

2.3. Data Selection and Reporting. In order to avoid exceeding the number of similar articles in the target area, at first some criteria were considered to classify appropriate articles. For example, all selected articles were from the Scopus database and published in English. Similar articles in terms of synthetic routes, modification strategy, and/or mechanistic routes were set aside, and only 314 articles were used. The articles with related titles and subjects were screened. Second, in order to rewrite the main contents of the articles, the focus was on the photodegradation of organic pollutants by photocatalytic reactions, modification strategies, and suggested mechanistic routes. The photocatalytic articles with semiconductors other than TiO_2 and ZnO based were ignored. In total, articles from Elsevier, American Chemical Society, Springer, and Wiley, among other, were selected; among these, only 314 articles passed successfully through filtering factors and were therefore studied in detail and summarized in the Review.

3. COMMON ORGANIC POLLUTANTS IN THE ENVIRONMENT

3.1. Air Pollutants. Air pollutants and water contaminants are a severe problem that has afflicted creatures in the recent century. They are classified into two main groups as particulate and gaseous pollutants. The first group can be refined by suitable sieves that remove the pollution physically. The latter group of air pollutants must be removed through purification by some chemical conventional methods such as adsorption, ionization, plasma technologies, and photocatalytic decomposition.[56,57] The second group of air pollutants primarily consists of NOx,[58] SOx,[59] CO_2,[60] and volatile organic compounds (VOCs).[61] The origins of gaseous pollutants are some processes that occur in the landfill naturally and or industrial activities of human beings.[62] NOx, SOx, and CO_2 gases originate from fuel combustion and are considered as industrialization outcomes. Because they derive from the greenhouse effect, acid rain and other corrosive compounds must be controlled to protect the green environment and health of humans.[63] VOCs include alcohols; aromatics

https://doi.org/10.1021/acsomega.3c08717
ACS Omega 2024, 9, 25457−25492

Table 1. Some Synthetic Routes of Photocatalyst Preparation

no.	photocatalyst	precursors	synthesis method	efficient parameters	analyses	ref
1	graphene oxide-based ZnO	graphene-based nanomaterials produced by Hummers's method, $Zn(NO_3)_2$, basic reagent	hydrothermal	temperature, time	(1) using solar energy as an inexhaustible source (2) graphene oxide (GO)-based zinc oxide (ZnO) nanocomposites to overcome the drawbacks of ZnO photocatalysts: light absorption, charge separation, charge transportation, and photo-oxidation of dyes	130
2	S-doped TiO_2/WS_2/calcium alginate beads	$Na_2WO_4{\cdot}2H_2O$, $TiCl_4$, $CaCl_2$ (76.5%) and $Na_2S{\cdot}xH_2O$ (30% Na_2S), sodium alginate	hydrothermal	temperature, time, pH, concentration	(1) removal of oxytetracycline (OTC) from aqueous solution (2) S-TiO_2/WS_2 semiconductor as a hybrid photocatalyst (3) calcium-substituted sodium alginate as adsorbent support	131
3	TiO_2 nanoparticles	titanium tetraisopropoxide (TTIP)	wet ball milling sol–gel	solvent, time, temperature, TTIP/MeOH molar ratio of 1:15, TTIP/DI water ratio of 1:4	(1) TiO_2 characteristics: the smallest particle size, the narrowest size distribution, and the highest photocatalytic degradation of MB (2) characterization analyses: XRD, DRS, TEM	115
4	TiO_2–HA	titanium(IV) butoxide ($Ti(OBu)_4$), acetic acid as stabilizer, agen, hydroxyapatite (HA) nanoparticles (60 nm average size)	sol–gel synthesis and a supercritical CO_2 drying process	solvent, time, temperature, amount of hydroxyapatite (HA) in the dioxide of titanium (TiO_2) matrix	(1) drying of the TiO_2–HA composite gels with supercritical CO_2 (2) characterization analyses: XRD, Raman, FTIR, SEM (3) the interaction of HA with TiO_2 was confirmed by the Raman band at 796 cm^{-1} in the TiO_2–HA composites	132
5	ZnO-poly(lactide)/poly (butylene adipate-*co*-terephthalate) (PBAT) composite	poly(lactide) (PLA) and PBAT as resins, zinc acetate dihydrate, zinc chloride, zinc nitrate hexahydrate	chemical precipitation	temperature, pH	(1) preparation of three different zinc oxide nanoparticles–PLA/PBAT composite films (2) characterization analyses: FE-SEM, Chroma meter, FTIR	133
6	CdS/TiO_2	titanium(IV) isopropoxide (TTIP), cadmium chloride	chemical bath deposition and microwave-assisted hydrothermal	solvent, temperature, time	(1) characterization analyses: X-ray, XRD, BET, SEM, chroma meter, FTIR (2) the CdS/TiO_2 nanocomposites were composed of anatase TiO_2 and hexagonal CdS phases with strong absorption in the visible region	134
7	SiO_2@TiO_2	titanium(IV) isopropoxide, tetraethylorto-silicate	solvent-controlled deposition	solvent, temperature, time	(1) obtaining photocatalysts with enhanced photoactivity (2) unique properties associated with core@shell architecture (3) solvent-based synthetic strategy for the reproducible and controlled coating of anatase nanocrystals over submicrometer SiO_2 spheres	135
8	TiO_2-coated ZnO nanorods	$Zn(NO_3)_2$, hexamethylenetetramine (HMTA), titanium tetraisopropoxide (TTIP)	chemical vapor deposition	solvent, reductant, concentration, deposition temperature, deposition and coating time	(1) fabrication of ZnO/TiO_2 core–shell nanostructures, (2) coating time affecting the morphological, structural, optical, and photoluminescence properties of the ZnO/TiO_2 core–shell structures	136
9	black TiO_2 hollow spheres	tetrabutyl titanate (TBOT), hexamethylenetetramine, ethylenediamine	solvothermal, high-temperature hydrogenation	(1) a template-free solvothermal approach (2) combination with a small amine molecule reflux-encircling process (3) the encircled protectors, especially ethylenediamine (4) pH = 11–12	(1) hydrogenated black TiO_2: tune the bandgap (2) utilize solar energy	47
10	Cu–ZnO/S-gC_3N_4 nanocomposites	$(NH_2)_2CS$, $(Cu(NO_3)_2{\cdot}3H_2O$, $Zn(NO_3)_2{\cdot}6H_2O$	chemical reduction	(1) synthesis of ZnO: pH = 11, the white precipitates (2) synthesis of Cu–ZnO NPs: adding 25% ammonia solution, white precipitates (3) synthesis of sulfur-doped g-C_3N_4 (S-g-C_3N_4): heating thiourea at 3 °C/min to 550 °C for 5 h in a muffle furnace, yellowish porous product	(1) characterization analyses: TEM, XRD, EDX, FTIR, SEM (2) evaluation of photocatalytic MB degradation	137
11	ZnO nanoparticles	Zinc nitrate ($Zn(NO_3)_2$), leaf samples of *Salvia officinalis*	bioreduction	concentration, time, pH	(1) aqueous leaf extract of *Salvia officinalis* L. as an efficient stabilizing/capping agent (2) characterization analyses: TEM, XRD, EDX, UV–vis, SEM, TGA/DTG, BET (3) under optimum experimental conditions: 92.47% degradation of MO by ZnONPs	138

https://doi.org/10.1021/acsomega.3c08717
ACS Omega 2024, 9, 25457−25492

Table 1. continued

no.	photocatalyst	precursors	synthesis method	efficient parameters	analyses	ref
12	ZnO nanoparticles	Zn metal	ball milling	calcination temperature, time	(1) synthesis of ZnO nanoparticles, different calcination temperatures ranging from 400 to 900 °C (2) calcination temperature affected size and morphology (3) characterization analyses: XRD, FTIR, FESEM, Raman (4) inhibition of bacteria with UV light as a photocatalyst	139
13	TiO_2 mixture	titanium oxide(IV)	ball milling	rotational speed, milling time	(1) high-pressure TiO_2 (II) as an intermediate for the polymorphic transformation from anatase to rutile (2) characterization analyses: XRD, TEM, SEM, BET, XPS, FTIR (3) use of tailored mixtures of titania phases (4) increase in oxygen vacancies, reducibility, and oxygen mobility of the supports with milling time	140
14	Fe_2O_4/ZnO nanowires	zinc acetate dehydrate ($Zn(CH_3COO)_2$, $2H_2O$), iron(III)chloride anhydrous ($FeCl_3$, H_2O), Monoethanolamine	dip coating	temperature, stabilizer, time	(1) photocatalytic activities against orange II dye (O−II) degradation (2) characterization analyses: XRD, AFM, SEM, UV−vis (3) Fe_2O_4/ZnO-nanowires were grown successfully on glass substrate (4) without any additional seed layer or pressure and temperature control	141
15	ZnO nanoparticles coated onto the SiC foam	macroporous SiC foam filter used as solid filter support with a porosity of 74%, two hydrated zinc acetate ($Zn(Ac)_2{\cdot}2H_2O$)	dip coating	negative pressure suction, concentration, temperature	(1) ZnO NPs coated onto the surface of the pore channel of SiC foam (2) fabrication of a novel antibacterial air filter material (3) no evident N_2 permeability difference was detected in gas permeation tests before and after the coating of ZnO nanoparticles	142
16	ZnO/rGO nanocomposites	zinc chloride ($ZnCl_2$) as precursor, $KMnO_4$, H_2O_2, PEG-400, hydrazine hydrate	wet impregnation	temperature, stabilizer, time, oxidants	(1) template/surfactant-free hydrothermal method (2) annealing the ZnO at 400 °C modified the rod-like structures into irregularly shaped structures (3) the optical band gap of the as-synthesized ZnO nanoparticles was slightly shifted from 3.09 to 3.02 eV in ZnO/rGO	124
17	Cu and Pt clusters deposited on TiO_2 powders	commercial P25 TiO_2 powders	sputtering	Pt clusters on the TiO_2 surface are beneficial to the photoactivity of the material, regardless of their amount	(1) copper and platinum were deposited onto commercial P25 TiO_2 powders by pulsed direct current magnetron sputtering method (2) the metal targets were sputtered at 250 W, 350 kHz, 50% duty cycle (corresponding to a pulse-off period of 1.4 μs, when the cathode voltage is reversed) (3) methanol photosteam reforming	125
18	Fe_2O_3-modified TiO_2	commercial TiO_2 powders with anatase phase, ferrocene ($Fe(Cp)_2$)	sputtering (atomic layer deposition)	X cycles of ALD Fe_2O_3 (X = 200, 400, 600, and 800) were coated on TiO_2 powder at 300 °C, the samples are marked as TiO_2@ X-Fe_2O_3	(1) visible light photocatalytic activity (2) the ultrathin Fe_2O_3 coating having a small bandgap of 2.20 eV can increase the visible light absorption of TiO_2 supports (3) characterization analyses: XRD, SEM, HRTEM, XPS	143
19	ZnO−SnO_2 thin films	tin target, Sn, and zinc target, Zn	cosputtering	(1) ZnO−SnO_2 films deposited at different working pressures (2) influence the growth of preferential planes of each one of the present phases	(1) a magnetron cosputtering method was used to deposit ZnO−SnO_2 thin films over glass substrates using Zn and Sn targets (2) deposition of ZnO−SnO_2 thin films (3) characterization analyses: X-ray (XRD), SEM, EDS, RI (4) ZnO−SnO_2 films were evaluated as photocatalysts to produce hydrogen under UV light irradiation	22

https://doi.org/10.1021/acsomega.3c08717
ACS Omega 2024, 9, 25457−25492

like benzene, toluene, ethylbenzene, and xylene (BTEX); aldehydes like acetaldehyde and formaldehyde; and halocarbons. The emission and distribution of VOCs in the air result from consuming fossil fuel in industries and the transportation system (procedure of petrochemical combustion, purification of petroleum, and so on).[61,64,65]

3.2. Water-Soluble Pollutants. There are a variety of pollutants in wastewater bodies like rivers, lakes, and oceans that originate from discharge sources, plants, hospitals, municipal sewage, and chemical laboratories; pathogenic organisms, organic and inorganic chemical scaffolds, microplastics, radioactive particles, and oil leaks are generally the main sources of water pollutants.[66−69] Dyes are an important class of organic compounds considered as dangerous pollutants if their amount exceeds the allowed concentration in the wastewater of industrial plants. These compounds are mostly separated into two groups named azo and thiazine dyes, like methyl orange (MO) and methyl blue (MB), respectively. The most serious issue about organic dyes is their high color density, persistence against biodegradation, and oxygen consumption during the oxidation process that results in a decrease of the dissolved oxygen level in bodies of water.[70,71] Amines are the main products of azo dye biodegradation and are very toxic for living organisms. Discharge of dye effluents into water resources by the textile industry is the main source of pulltion by dyes (up to 80%) because around 15−50% of dyes can not bind to the fabric and misspend. It is noteworthy that around 7.0×10^5 tons of azo dyes are produced annually throughout the world.[72]

In addition to the slow biodegradation method, there are some conventional physical techniques like adsorption, coagulation-flocculation, electro-coagulation, ion exchange, membrane filtration, and chemical oxidation that are used for the removal of dyes. Apart from having good properties like being environmentally friendly and cost-effective, these methods also have some drawbacks like the disposal of the solid residue of the absorbent after treatment and recyclability.[73,74] Protection of the environment including water and air has attracted a lot of attention to avoid exceeding the danger threshold for human survival.

Other organic pollutants are phenolic compounds, which include phenol and its derivatives. This group is contained in in chemical structures of agricultural compounds, pharmaceutical materials, paper and pulp compounds that are thrown away during industrial chemical processes, and their effluents that are discharged into water sources.[75] 2,4-Dichloro phenols as a model of phenolic derivatives are also used widely in the preparation of pesticides, disinfectants, herbicides, dyes, and pharmaceutical compounds.[76] Other crucial sources of organic pollutants are polycyclic aromatic hydrocarbons (PAHs) that are produced inescapably during the incomplete combustion of any carbonaceous compounds. It has been determined that the level of PAHs in the air is equivalent to the population of that area because PAHs mainly result from human activities during the consumption of organic materials like oil, petroleum gas, wood, and urban waste. This group of pollutants mostly belongs to soil pollutants as opposed to water and air, although soil and sediment pollutants originate from atmospheric deposition and movement from air to the water and soil.[77−80] On the other hand, some properties like low volatility and high hydrophobicity cause PAHs to last a long time without change or remediation in the landfill.[81] Among 16 PAHs that the United States Environmental Protection Agency (U.S. EPA) set as priority pollutants, two of them, i.e., phenanthrene and pyrene, are more common than others and are distributed in environmental bodies.[82] Heavy metals in wastewater are considered as independent pollutant sources resulting from agricultural fertilizers, mining process, and effluents from industrial plants, but they also complex with other contaminations like medicines, causing their endurance against removal. Some oxidation numbers of transition metals like Cr(VI) in chromates (CrO_4^-) have dangerous effects on live organisms and are considered as toxic pollutants that threaten the ecosystem.[83] The discharge of harmaceutical effluents into rivers is a critical problem due to the direct effect on biological systems. Antibiotics, vaccines, and other medicines with different organic scaffolds like tetracyclines, phenolics, and heterocyclic compounds accumulate in bodies of water.[84]

Our focus will be on water-soluble pollutants because of their greater distribution and restriction of water resources. Air pollutant treatments have also been investigated in detail. The main route of pollutant photodegradation occurs on the surface of the photocatalysts. In fact, water media facilitate the access of pollutants to the surface of the photocatalyst and are considered as the origin of secondary active species. In the following, at first, we discuss the diversity of synthetic methods for TiO_2 and ZnO preparation.

4. PHOTOCATALYSTS

4.1. Synthesis Approaches. Some synthetic routes of photocatalyst preparation as composites and/or hybrids are gathered and are represented in Table 1. Hydro/solvothermal, sol−gel, chemical deposition, chemical reduction, dip coating, wet impregnation, and sputtering are among the main synthetic routs of photocatalyst synthesis. In this section, the impact of temperature is studied, which along with other determining factors of synthetic methods improves distinct properties of photocatalysts. Improvements in photocatalyst efficiency are also produced by changes in the crystallinity of the pure form. TiO_2 in different lattice arrangements has different photocatalytic activities under distinct light irradiation. For example, the anatase form has better photocatalytic activity than the rutile form, although the presence of rutile TiO_2 as an impurity within the anatase state improves the overall photocatalytic performance. It is worth noting that the duration and temperature of calcination have an effect on the level of crystallinity and oxygen vacancies and the number of defects in the photocatalytic bulk. Crystallinity determines the amount of specific surface area that can adsorb pollutants, and oxygen vacancies and deficiencies act as photoexcited electron trapping agents and overall affect the photocatalytic efficiency.

4.1.1. Hydrothermal. Solution-based synthesis has attracted more attention due to the potential of preparing nanoparticles in a variety of morphologies such as nanowires, nanotubes, nanosheets, and tunable sizes. This approach ensure a simple, straightforward, and controllable route for the synthesis of nanosized crystals, porous compounds, and high-level purity under mild conditions.[85,86] Siwińska-Stefańska et al.[87] reported the synthesis of a multifunctional TiO_2−ZnO system with effective photocatalytic properties by the hydrothermal method. The reaction time and the molar ratio of TiO_2 and ZnO as two main factors of hydrothermal synthesis and their effect on the physicochemical and structural properties of the binary system were studied. The authors found that several characteristics such as morphology, crystallinity, and porosity, along with chemical surface functionality, were improved and caused better photocatalytic and antibacterial efficiencies. Saleh et al.[88] studied the

https://doi.org/10.1021/acsomega.3c08717
ACS Omega 2024, 9, 25457−25492

synthesis of ZnO nanospheres as photocatalysts for the bleaching of methyl orange (MO) as an azo dye. The prepared nanosized particles of zinc oxide spheres had diameters in the range of 200−250 nm. The results of utilizing the ZnO nanospheres in the MO solution (10 mg/L) at pH = 6.0 demonstrated that approximately the whole of MB was degraded and bleached. Gupta et al.[85] reported the synthesis of one-dimensional TiO_2 nanorods (NRs) by the hydrothermal method. This scientific group overcame some conventional restrictions of hydrothermal methods to reduce the reaction time and provide uniform TiO_2 NRs, which provided significant photocatalytic efficiency arising from good retardation of recombination during photocatalytic degradation.

4.1.2. Sol−Gel. The sol−gel technique is utilized extensively for the synthesis of a variety of heterogeneous photocatalysts. The advantages of the sol−gel method generally include ambient conditions, low cost, and uncomplicated and reproducible processes. Also, the final particles have good crystallinity, uniform morphology, and a narrow particle size distribution.[89] Chen et al.[21] worked on the preparation of ZnO by sol−gel methods and used Zn $(OAc)_2$ as a precursor of ZnO. This photocatalyst was used for the degradation of azo dyes like MO, Congo red (CR), and Direct Black 38 (DB38) in the UV region. Phin et al.[90] synthesized a zinc oxide/carbon nanotube composite to photocatalytically degrade MB dye as a pollutant in water media. In this work, zinc oxide/carbon nanotube composites were produced by the sol−gel method. In order to conquer some prevalent problems in the synthesis of solid materials, this group used a modified sol−gel technique and ignored the use of organic additives and postannealing treatment. Palanisamy et al.[91] used the sol−gel method for the synthesis of a photocatalytic binary system of Fe_2O_3/TiO_2 on a mesoporous scale. This team used Pluranic P123 (as structure-directing agent) in a soft-template sol−gel method. Extended light absorption by TiO_2, shifting from the UV to visible region due to Fe_2O_3 loaded on the surface of TiO_2, and photosensitization under solar irradiation were reported, which improved the photodegradation of 4-chlorophenol.

4.1.3. Solvothermal. The efficient photocatalytic activity of heterogeneous nanoparticles against the degradation of any organic pollutants in the media depends on their morphology, particle size, and specific surface area. All these factors can be controlled by solvothermal methods in the presence of morphology-controlling agents.[92,93] Surveys of the literature show that there are many fluorine-containing compounds that are utilized as morphology-controlling agents, such as ammonium fluoride, ammonium bifluoride, BF_4^-, fluoroboric acid, lithium fluoride, and sodium fluoride.[94] Venkatraman et al.[95] announced the synthesis of a purely anatase structure of TiO_2 by the solvothermal method in a mixed solution of ethanol/water. Titanium nanoparticles prepared under controlled hydrolysis and low temperature had an approximately spherical shape with a narrow size distribution. Titanium tetraisopropoxide (TTIP) and anhydrous ethanol were used as the titanium precursor and solvent, respectively. Zulfiqar et al.[96] reported the synthesis of a purely anatase crystalline structure of TiO_2 nanosheets (TNSs) and spherical shape TiO_2 nanoparticles (TNPs) with a narrow distribution size of by the solvothermal method under alkaline conditions. They used *N*,*N*-dimethylformamide (DMF) as a morphology-controlling agent instead of any compounds containing fluorine because of their hazardous and corrosive nature. Control of time and temperature and the transfer of absorption edge from UV (TNPs had a band gap energy of 3.22 eV) to the visible region (TNSs had a band gap energy of 2.62−2.85 eV) were reported as the precious modification results by the solvothermal method. Mao et al.[71] disclosed the synthesis of ZnO in micro- and nanostructures by the solvothermal method modified with some surfactants, including sodium dodecyl sulfate (SDS), polyvinylpyrrolidone (PVP), and polyethylene glycol (PEG, MW = 10000). SEM image analysis of ZnO synthesized with and without SDS surfactant shows a uniform spherical shape in nanosize and hexagonal disks (HDs), respectively. Nano- and microspheres of ZnO were tested against the photodegradation of RhB under UV light irradiation.

4.1.4. Chemical Deposition. The chemical deposition method is used for the synthesis of nanocatalysts in alkaline media in order to deposit crystalline structures of dissolved metal ions in the solution. There are three chemical deposition methods: (1) simple chemical deposition, (2) chemical vapor deposition, and (3) electrochemical deposition. Wu et al.[97] synthesized amorphous TiO_2 as a shell layer that was coated on the surface of Ag_2CO_3 by the simple precipitation method (SCD) in a $NaHCO_3$ solution. The results showed that the amorphous structure as well as core−shell arrangement of the nanocomposite led to a decrease in the recombination time and prevented Ag_2CO_3 corrosion. Improved photocatalyst efficiency toward the visible light region was obtained. The electrochemical deposition (ECD) method is used to transfer metal ions from their electrolyte to the surface of the cathode by passing sufficient electricity through electrodes and electrolytes.[98] Many researchers in the field of photocatalyst synthesis have taken advantage of this method to prepare solid crystalline materials with high purity and efficiency against photocatalytic degradation of organic pollutants. Çırak et al.[99] reported the synthesis of ZnO-deposited TiO_2 nanotubes using tandem electrochemical (anodic oxidation) and chemical bath deposition methods. The experimental analysis showed that the TiO_2/ZnO photocatalyst prepared by this method has significant outstanding photocatalytic performance in comparison with pure TiO_2 or ZnO for the photodegradation of RhB. It is worth mentioning that increasing in the number of ZnO deposition cycles on the surface of TiO_2 in the chemical bath process led to the formation of larger crystals, improved ZnO crystallinity, and more efficient photocatalytic activity. The chemical vapor deposition method (CVD) is a cost-effective technique for preparing composites in the form of film with a homogeneous morphology and complete coverage. Generally, this technique was coupled with other techniques to modify and overcome its limitation and improve the quality of the film. Plasma-enhanced chemical vapor deposition and aerosol-assisted chemical vapor deposition are some modified techniques.[100,101] Taylor et al.[102] synthesized titanium dioxide coatings by chemical vapor deposition with assistance from the aerosol technique. This group used titanium isopropoxide (TIPP) as a precursor of TiO_2 coatings modified with acetyl acetone (acac) and coupled an aerosol technique with chemical vapor deposition. The aerosol technique was used to modify chemical vapor deposition method such as moderating temperature and pressure. The resultant nanoparticles had approximately 10−25 nm size with controlled morphology and photocatalytic activity against the degradation of Resazurin in an equal ratio of TIPP to acac.

4.1.5. Chemical Reduction. A survey of the literature shows that black TiO_2 nanomaterials were synthesized by two distinct routes of chemical reduction techniques. First, they were synthesized reduction by some materials containing active

https://doi.org/10.1021/acsomega.3c08717
ACS Omega 2024, 9, 25457−25492

hydrogen like H_2 in the pure gas state or mixed with an inert gas like Ar, N_2, etc., as well as with $NaBH_4$, CaH_2 and some other metal hydrides. Second, they were synthesized by chemical reduction with reductive metals, such as aluminum, zinc, magnesium, etc. The latter contains some organic reductants like hydrazine, ascorbic acid, imidazole, etc.[103,104] Malik et al.[105] synthesized ZnO nanoparticles by the bioreduction method mediated by *Ocimum basilicum* extract as a reduction agent and decorated the nanoparticles on sheets of reduced graphene oxide. The reaction was carried out under room temperature, and zinc acetate dihydrate was used as the ZnO precursor for the chemical reduction reaction in alkaline media. Nanospheres of ZnO had an average size of 25 nm, were arranged in wurtzite hexagonal structure, and were used for the photodegradation of RhB.

4.1.6. Coprecipitation. Concurrent precipitation of two or more particles from the same solution is considered as the coprecipitation method, which has been used extensively for the synthesis of binary, ternary, and mixed crystals and composites. Coprecipitation occurs by several techniques, like hydrothermal, solvothermal, coagulation, flocculation, etc.[106] Ali et al.[107] worked on the synthesis of ZnO/SnO_2 honeycomb nanoparticles and modified them with TiO_2 through the self-assembly coprecipitation method. This technique was carried out by sequence processes including dispersing semiconductor salt in water, increasing the pH up to 9.0, collecting precipitated compounds, and calcination. This group reported that increasing the calcination temperature causes a decrease in the photocatalytic activity because heat decreases the crystalline nature, forms some inactive phases of Ti, Sn, and Zn like $ZnTiO_3$ and Zn_2SnO_4, and decreases oxygen opening bulk responsible for charge recombination. Lassoued et al.[108] reported the preparation of of TiO_2 nanoparticles doped with cobalt by the coprecipitation technique under alkaline media of NH_3, followed by thermal annealing treatment under 500 °C. 6% cobalt-doped TiO_2 nanoparticles demonstrated 79.98% degradation of MO under visible radiation. Higher degradation of dyes was attributed to the lower size of Co-doped TiO_2 nanocrystals and better amelioration of captured light in UV and visible domains. Mahendran et al.[109] studied the synthesis of TiO_2 nanoparticles doped with Fe by the coprecipitation method and evaluated their photocatalytic efficiencies against Acid Scarlet 3R degradation in wastewater. This group employed the ultrasound technique along with the coprecipitation method to improve the photocatalytic efficiency of Fe-doped TiO_2 nanostructures under UV light compared with solar irradiation.

4.1.7. Ball Milling. Among a variety of photocatalyst synthesis methods, the ball milling technique in an agate jar is a cost-effective, highly productive, and accessible process. In this method, mechanical force causes chemical changes in the structures. Several benefits have been reported through using this simple technique and its modified methods, such as the fabrication of nanoparticles, the application of solvent-free conditions, the possibility of reducing particle size, an increase in specific surface area, the introduction of more functional groups, homogeneity and narrow size distribution of nanoparticles, the creation of surface functional groups, and defects in lattice structures that generally are triggers of improving photocatalytic and photodegradation efficiencies.[110] Wu et al.[111] synthesized TiO_2 nanoparticles modified with Gd_2O_3 and TiO_2 nanoparticles doped with Gd^{3+} by the ball milling method. The XPS and EDS analyses proved that doping gadolinium into the lattice caused a decrease in the number of oxygen-containing nanocomposites, resulting in defects and distortion. The removal of the lattice as a hole trap is a perfect driving force for increasing photocatalytic efficiency. Yu et al.[112] prepared ZnO/biochar nanocomposites by the ball milling method and evaluated their photocatalytic efficiencies for the degradation of MB as a wastewater pollutant. This group attributed increases in the amount of meso- and macropores in the prepared nanocomposites to the use of the ball milling method. Increasing the pore content and size together with using biochar resulted in expansion of the specific surface area of the nanocomposites and led to better MB adsorption and degradation compared to pure ZnO (more than 95.19%).

4.1.7.1. Ball Milling-Assisted Sol−Gel. The ball milling method in dry or wet conditions is used to prepare small-scale particles. The wet ball milling has more benefits than dry because of it provides powdered particles with smaller sizes and more narrow size distributions.[113] Shafei et al.[114] synthesized Cu-doped TiO_2 nanocomposites by the ball milling-assisted sol−gel method. This group evaluated the efficiency of the ball milling method in the photocatalytic performance of synthesized nanocomposites before calcination. The results demonstrated that doping with Cu and using ball milling method are two key factors in line with amplifying photocatalytic efficiency, which resulted in potent separation of electron−hole pairs and a decrease in band gap from 3.4 eV in pure TiO_2 to 2.8 eV in Cu-doped TiO_2 nanocomposites. Phromma et al.[115] synthesized TiO_2 nanoparticles with the wet ball milling-assisted sol−gel method (WBMS) and studied the effects of calcination temperature on the photocatalytic efficiency related to the kind of phase formation. The wet ball milling process was performed in isopropyl alcohol (2 mm diameter balls, 500 rpm, 2 h) after dry ball milling of yellow-white xerogels (10 mm diameter balls at 300 rpm, 20 min).

4.1.8. Dip Coating. The dip coating method consists of coating particles on a plate in the solution state that was prepared by the sol method and calcination to prepare thin films.[116] Two efficient factors to fabricate thin films are (1) the rate of plate immersion into the solution and removal from the solution media (by millimeters per minute) and (2) the number of immersion cycles. The significant properties that must be noticed in the preparation of thin film are homogeneity and lack of any pores according to standard cleaning operation, for example, some pretreatments like etching in HCl, cleaning with deionized water and ethanol, and assisted ultrasonication during all the processes. The procedure finishes with the plate drying at 100 °C in the oven for a restricted time, which results in excellent adherence of dissolved particles on the plate surface.[117,118] Thongsuriwong et al.[119] reported the synthesis of ZnO thin films prepared by the sol−gel dip coating method. The initial concentration of zinc ions affected the prepared photocatalyst activity, optical properties, and morphology of ZnO thin films. A higher concentration of Zn^{2+} in the solution resulted in increased granule size and film thickness and therefore a lower optical band gap energy because of particle agglomeration in the solultion. It has been reported that in the optimum situation, a 0.1 M Zn^{2+} solution, results in the fabrication of the best ZnO thin film as a photocatalyst for MB degradation. Compared with other experimental conditions, the photocatalyst had the largest specific surface area according to BET analysis, which originated from its uneven surface. Tekin et al.[120] synthesized a ZnO/TiO_2 thin film photocatalyst using the dip coating method. The solution of this method was prepared

https://doi.org/10.1021/acsomega.3c08717
ACS Omega 2024, 9, 25457−25492

Table 2. Modification Strategies in the Synthesis of Photocatalysts

no.	modified photocatalyst	type of dopants	fabrication method	photoactive region	organic pollutant	performances	ref
TiO_2-based							
1	$Cu^{\delta+}/CeO_2-TiO_2$	transition metal/n-type semiconductor	interface-engineering strategy: metal−organic framework (MOF) of MIL-125-NH_2, $Cu(NO_3)_2$, $Ce(NO_3)_3$, and titanium as precursors	simulated sunlight	CO_2 reduction to ethylene	(1) ethylene production rate: 4.51 $\mu mol^{-1} \cdot g_{cat}^{-1} \cdot h^{-1}$ and 73.9% selectivity (2) with H_2O as hydrogen source and hole scavenger	230
2	PRGO-TiO_2 photocatalyst	p-n heterojunction; PRGO: p-type; titanium: n-type	ultraviolet (UV)-assisted photoreduction method	UV and visible	volatile organic pollutants (VOCs)	the main reactive species responsible for the photocatalytic activities were h_{VB}^+ species and $O_2^{\bullet-}$ radicals	220
3	RCP/TiO_2 composite	recycled concrete powder (RCP)	mechanical chemical method; nanotitanium precursor: Degussa, AEROXIDE-P25	visible	RhB	(1) enhanced photocatalytic efficiency because of surface hydroxylation (2) excellent reusability (3) high stability	231
4	W−Mo/Mo−V/V−W-codoped titanium	transition metals	plasma electrolytic oxidation (PEO) process: Cp-Ti, $Na_2WO_4 \cdot 2H_2O$, $Na_2MoO_4 \cdot 2H_2O$, NH_4VO_3	sunlight	MB	(1) The bandgaps of the pure and codoped samples T, WM, MV and VW are 3.21, 2.96, 2.51, and 2.58 eV, respectively (2) PEO electrolyte systems used to prepare the coatings and pH and conductivity of electrolytes	232
5	$RuTe_2$/black titanium	Ru: transition metal; Te: semiconductor	black TiO_2: sol−gel and calcination method; loaded $RuTe_2$ cocatalyst on B-TiO_2: microwave method; tetrabutyl titanate ($C_{16}H_{36}O_4Ti$), ruthenium chloride hydrate ($RuC_{l3} \cdot xH_2O$), and sodium tellurite (Na_2TeO_3) as precursors	simulated sunlight	diclofenac (DCF)	(1) 0.5% $RuTe_2$/B-TiO_2 with high structural stability, good electrical conductivity and surface concavities creating more active sites (2) the favorable energy band position between B-TiO_2 and RuTe2	52
6	Ag/MoO_3/TiO_2	transition metals	sol−gel method: $C_{12}H_{28}O_4Ti$; $AgNO_3$ and $(NH_4)_6Mo_7O_{24} \cdot 4H_2O$ as precursors	UV	MO	(1) construct anatase phase of titanium photocatalysts based (2) immobilized borosilicate glass (BG) reactors (3) E_{bg} = 2.89 eV	233
7	$CaTiO_3$/Cu/TiO_2	$CaTiO_3$: perovskite composite oxide; Cu: transition metal	two-step hydrothermal method: $Ca(NO_3)_2.4H_2O$; $[Ti(C_4H_9O)_4]$ and $Cu(CH_3COO)_2.H_2O$ as precursors	simulated sunlight irradiation	hydrogen generation	(1) vector Z-scheme $CaTiO_3$/Cu/TiO_2 photocatalyst (2) assisted by cocatalyst Cu nanoparticles as non-noble-metal electron mediator	234
8	Ru−Ti_3CN MXene-TiO_2	Ti_3CN nitride-based MXene; Ru: transition metals	Ti_3CN MXene: Lewis acidic etching method; growth of TiO_2 and Ru nanoparticles: in situ hydrothermal; RuC_{l3}, Ti_3AlCN, and CuC_{l2} as precursors	visible	CO_2 photoreduction	(1) synergy between in situ growth of TiO_2 on Ti_3CN MXene and Ru nanoparticles (2) nitride-based MXenes have stronger metallic property and higher electrical conductivity	235
9	Pd/H−TiO_2	transition metal	photodeposition method: $C_{12}H_{28}O_4Ti$ and PdC_{l2} as precursors	visible	selective photocatalytic oxidation of methane to methanol	(1) hollow porous Pd/H-TiO_2 nanocages (2) $OH^{\bullet}$ and $O_2^{\bullet-}$ as the main active species involved in the photocatalytic process	236
10	Zr/Y codoped titanium	transition metals	sol−gel method: $C_{16}H_{36}O_4Ti$, $Zr(NO_3)_4 \cdot 5H_2O$, and $Y(NO_3)_3.6H_2O$ as precursors	UV	hydroquinone	(1) titanium: 100% anatase structure with a specific surface area of 42.36 m^2/g and a pore size of about 4.25 nm (2) Y−ZrO_2−TiO_2: higher photocatalytic activity when Ti/Zr/Y = 100:6:0.5, calcination temperature is 500 °C, and time is 2 h	237
11	Fe-doped titanium	transition metal	coprecipitation method: tetrabutyl titanate (TBT) and Fe $(NO_3)_3 \cdot 9H_2O$ as precursors	visible	MO	(1) $E_{bg}(TiO_2)$ = 3.07 eV (2) E_{bg}(Fe-doped TiO_2) = 2.71 eV (3) single anatase structure between 200 and 400 °C	238
12	$LaFeO_3$/TiO_2	$LaFeO_3$: a perovskite type	sol−gel and wet impregnation method: iron(III) nitrate nonahydrate, lanthanum nitrate hexahydrate, and Pluronic L-64 as surfactant	visible	antibiotic: ciprofloxacin	(1) nonionic surfactant Pluronic L-64 for synthesizing nanocrystalline mesoporous TiO_2 (2) highly effective porous $LaFeO_3$/TiO_2 photocatalysts by impregnation of $LaFeO_3$ on TiO_2 (3) $LaFeO_3$ with E_{bg} = 2.0−2.7 eV and a superior visible-light-induced photocatalyst	239

https://doi.org/10.1021/acsomega.3c08717
ACS Omega 2024, 9, 25457−25492

Table 2. continued

no.	modified photocatalyst	type of dopants	fabrication method	photoactive region	organic pollutant	performances	ref
ZnO-based							
13	multilayer graphene/ZnO nanocomposite (MLG/ZnO)		green synthesis of ZnO in the presence of *Ageratum houstonianum* leaf extract as reduction agent, ZnO in wurtzite structure, corn husk waste biomass as MLG precursor	visible light (natural solar light)	brilliant black (BB)	(1) the optical band gaps obtained through Tauc plots were found to be 3.09, 2.08, and 2.66 eV for ZnO, MLG, and MLG/ZnO_1, respectively (2) monitoring degradation peak of BB at 570 nm (3) the decrease in the percentage degradation of BB in the presence of scavengers was as follows: EDTA (holes scavengers) > p-BQ (superoxide radicals scavengers) > *t*-BuOH (hydroxyl radicals scavengers) (4) holes play a major role in the photodegradation of BB: $h^+ > O_2^{\bullet -} > HO^\bullet$	240
14	β-CD-CuO/ZnO nanocomposite	transition metal	sol−gel method: binary nanocomposite CuO/ZnO, ternary nanocomposite β-CD-CuO/ZnO, Zn $(CH_3COO)_2{\cdot}2H_2O$, $CuSO_4{\cdot}5H_2O$, and β-CD as precursors	visible	MG and MB	(1) the coupling of metal oxides increases the efficiency due to their broad light absorption, fast dynamic process, and natural p-n characteristics (2) β-CD-CuO/ZnO has a good adsorption tendency because of its hydrophilic exterior and hydrophobic interior cavity, which can encapsulate pollutant molecules in the cavity	241
15	Cu-doped ZnO nanocomposite	transition metal	biosynthesis in the presence of leaf extracts of *Synadenium grantii* as reductant agent: Zn $(NO_3)_3{\cdot}6H_2O$, $Cu(NO_3)_3{\cdot}6H_2O$, wurtzite crystal structure of ZnO	UV	MB, Indigo Carmine (IC), and RhB	(1) the emission peaks in photoluminescence spectra at 424, 446, and 573 nm are associated with the electron movement from the deep donor level, zinc interstitial to the zinc vacancy, and oxygen vacancy, respectively (2) reasons for enhanced photocatalytic efficacy: lowest lattice strain, reduced recombination rate of photoinduced charge carriers	242
16	$ZnFe_2O_4$@ZnO nanocomposite	transition metal	solution combustion method: $Zn(NO_3)_2{\cdot}6H_2O$, $Fe(NO_3)_3{\cdot}9H_2O$	visible	RhB	(1) reactive oxygen species ($O_2^{\bullet -}$, $OH^\bullet$) play a major role in the photodegradation of RhB (2) band gap energies (E_{bg}, eV) of $ZnFe_2O_4$-0%@ZnO, $ZnFe_2O_4$-10%@ZnO, $ZnFe_2O_4$-30%@ZnO, and $ZnFe_2O_4$-50%@ZnO are 3.14, 2.89, 2.09, and 1.89, respectively.	243
17	$ZnFe_2O_4$−ZnO hybrid nanostructures (ZFZ)	zinc ferrite ($ZnFe_2O_4$): transition metal ferrites	simple coprecipitation method: $Zn(NO_3)_2{\cdot}6H_2O$ and Fe $(NO_3)_3{\cdot}9H_2O$ as precursors	sunlight	MB, MG, MO, and RhB	(1) band gap variation from 1.91 to 2.07 eV (2) the PL intensity of the sample ZFZ3 was much lower compared to those of other samples, indicating better suppression of the recombination (3) the p-type $ZnFe_2O_4$ and n-type ZnO coupled together to form type II p-n heterojunction since the CB and VB of $ZnFe_2O_4$ are more negative compared to those of ZnO	244
18	MoS_2/ZnO (MZ) composites	transition metal	hydrothermal method: $Zn(NO_3)_2{\cdot}6H_2O$ and MoS_2	visible	ciprofloxacin antibiotic and hydrogen production	(1) reasons for enhanced photocatalytic efficacy: excellent visible light absorption capacity, effective charge transfer, minimized recombination of charge carriers (2) the fluorescence technique was employed to detect the formation of hydroxyl radicals using MZ-30 catalyst	245
19	Zn/ZnO heterostructures	semiconductor	sustainable route method: the recycling of metals from alkaline batteries waste	UV	Direct Red 80 dye (DR80)	(1) photocatalysts were synthesized from anodic paste of alkaline batteries waste (2) removal occurs by direct oxidation in photogenerated vacancies and indirectly by •OH radicals (3) the presence of oxygen vacancies can be associated with different calcination temperatures, causing the occurrence of defects in the material structure (4) the active species h^+_{BV}, and $^\bullet OH$ are responsible for the DR80 photodegradation	246

https://doi.org/10.1021/acsomega.3c08717
ACS Omega 2024, 9, 25457−25492

Table 2. continued

no.	modified photocatalyst	type of dopants	fabrication method	photoactive region	organic pollutant	performances	ref
ZnO-based							
20	Ag-doped ZnO/MgO nanocomposite (NCPs)	alkaline earth metal and transition metal	biosynthesis in the presence of *Caccinia macranthera* seed extract as reducing agent: $Mg(NO_3)_2{\cdot}4H_2O$, $Zn(NO_3)_2{\cdot}6H_2O$, and $AgNO_3$ as precursors	UV	MB	(1) evaluation of photocatalytic activity and cytotoxicity (2) NCPs can function as sensors of heavy metal ions, specially Pb^{2+} ions (3) the active species $O_2^{\bullet-}$ and $OH^{\bullet}$ are responsible for the MB photodegradation	247
21	FeV_2O_4–ZnO nanocomposites (NCs)	FeV_2O_4: spinel single system	ZnO NPs: chemical coprecipitation; FeV_2O_4 decorated ZnO NCs: sonochemical/coprecipitation method; $ZnSO_4{\cdot}7H_2O$, FeC_{l3}, and $VOSO_4$ as precursors	white light	MB	(1) the reaction rate was enhanced 3.6× in NCs cmpared to pure FeV_2O_4 and ZnO (0.003 min^{-1}) (2) The $OH^{\bullet}$ radical played a key role in MB degradation (3) excellent antibacterial activity against *E. coli* and *B. subtilis*	248
22	ZnO-CoTe binary photocatalyst	metal tellurides	hydrothermal method: $Zn(NO_3)_2{\cdot}6H_2O$, tellurium powder, and $CoC_{l2}{\cdot}2H_2O$ as precursors	sunlight	methyl red and MB	(1) the S-scheme charge transfer mechanism of the ZnO-CoTe binary photocatalyst: effectively improves charge carriers migration and separation and has a high photocatalytic degradation capability than pure ZnO and CoTe catalysts (2) the bandgaps of ZnO, CoTe, and ZnO-CoTe were observed at 3.37, 2.24, and 2.80 eV, respectively	249
23	Nd_2O_3eZnO nanostructure	Nd: lanthanide element	solution combustion method: $Zn(NO_3)_2{\cdot}6H_2O$ and elemental neodymium (Nd) as precursors	visible	RhB and MB	(1) the direct energy band gap values of the Nd–ZnO nanocomposites: 3.35 eV (pure ZnO) to 3.26 eV (Nd_2O_3eZnO) (2) Nd 3p ions take the substitutional site of Zn 2p ions and form cationic vacancies because of the unlike ionic levels (3) scavenger experiments suggested that the peroxide free-radical plays a key role: $O_2^{\bullet-} > HO^{\bullet} > h^+ > e^-$	250
24	$ZnO/SrZnO_2$	ZnO: n-type semiconductor; $SrZnO_2$: p-type semiconductor	sol–gel method: zinc acetate ($ZnC_4H_6O_4$) and $Sr(NO_3)_2$	natural solar light	azo dye (Congo red) and bacterial strain (*Escherichia coli*)	(1) scavenger experiments suggested that the peroxide free-radical play a key role, while the holes play a minor role in the mineralization of Congo red dye: $O_2^{\bullet-} > HO^{\bullet} > e^- > h^+$ (2) the optical band gaps of ZnO, $SrZnO_2$, and $ZnO/SrZnO_2$ nanostructures were estimated to be 3.19, 3.13, and 3.04 eV, respectively (3) in the $ZnO/SrZnO_2$ nanohybrid, the free electrons moved from ZnO to $SrZnO_2$ until the Fermi level of both materials was aligned, resulting in a narrowing of the bandgap	43
25	Sn-doped ZnO/CdS	Sn: heavy metal p-block; CdS: n-type semiconductor	simple chemical precipitation methods: $(CH_3COO)_2{\cdot}Zn{\cdot}2H_2O$, Cd $(NO_3)_2$, and Na_2S as precursors	solar light	reduction of Reactive Blue 160 (RB 160)	(1) there was a decrease in photocatalytic activity when the Sn content was increased (optimum percent of Sn doped ZnO/CdS nanocomposite: 0.6%) (2) ZnO/CdS/Sn nanocomposites degrade the RB 160 solution thoroughly in 120 min even when used for the third time (3) the composites have excellent stability in acidic conditions	251

https://doi.org/10.1021/acsomega.3c08717
ACS Omega 2024, 9, 25457−25492

via a sol−gel process and coated on the quartz glass plate. In this experiment, after calcination, about 14.76 mg of photocatalyst was coated on the plate for use in orange G photodegradation. Al Farsi et al.[121] prepared a ZnO photocatalyst doped with Al (AZO) as a thin film by the dip coating method. The thin films had perfect transparency under visible and near IR regions, with a value of more than 80%, and demonstrated good photocatalytic activity under visible light irradiation. It is noteworthy to mention that ZnO intrinsically has some point defects in the lattice that demonstrated an active trap center in the UV and visible regions; this property is also seen in the AZO, which makes the Urbach energy greater than that of pure ZnO because of Al doping.

4.1.9. Wet Impregnation. This method is utilized for synthesis of nanocomposites because of its ease of use, cost-effectiveness, low-temperature usability, reducibility, and adhesion to suitable substrates, with an even coating on the plate.[122] It is important that the structure, size, and morphology of the prepared crystals in the wet impregnation method are controllable. Some factors that are critical to achieve these aims are pH, solvent, and hydrolysis speed.[123] Pryia et al.[123] reported the synthesis of $BiFeWO_6$/ZnO nanocomposites and evaluated their photocatalytic activity against RhB under visible light irradiation. At first, $BiFeWO_6$ and ZnO as precursors were prepared by the coprecipitation method, then various amounts of $BiFeWO_6$ (1.0, 5.0 and 10.0%) were added to ZnO to synthesize $BiFeWO_6$/ZnO nanocomposites through the wet impregnation method. In this process, ethanol was used as the solvent, and the media was sonicated, stirred, and finally evaporated at 80 °C. The optimum nanocomposite was 5% BiFeWO6 loaded on ZnO, which degraded RhB at a rate 2× faster than pristine ZnO under visible light irradiation. Kumaresan et al.[124] reported the synthesis of ZnO/rGO nanocomposites by the wet impregnation method. The synthesis of ZnO was performed using a hydrothermal method in the presence of a template under solvent-free conditions to prepare rod-like ZnO nanoparticles. In the wet impregnation method, the reaction medium was deionized water. The efficiencies of the prepared nanocomposites were evaluated by the photodegradation of RhB and 4-chloro phenol (4-CP) dyes under UV irradiation.

4.1.10. Sputtering Method (MS). MS is performed to deposit a layer of photocatalysts on a solid or liquid support by pulsed-direct current (DC) and radio frequency (RF) modes. This method is extensively applied in industrial processes because of scalability, adaptability, and replicability to produce high-quality thin films.[125] Yu et al.[122] reported the synthesis of $Ag−Ag_2O−TiO_2$ photocatalysts as thin films on polyester fabrics using this method. The photocatalytic efficiency for the degradation of RhB was evaluated for both polyester modified $Ag−Ag_2O−TiO_2$ and simple TiO_2 coatings. Photodegradation results showed that the modified coating was able to degrade RhB under UV light irradiation with more differentiation compared to simply a TiO_2 coating polyester. Mekasuwandumrong et al.[126] worked on the synthesis of some Cu/TiO_2 photocatalysts by reactive magnetron sputtering with the DC mode. In this manner, TiO_2 was used as a support, and Cu clusters were deposited on the support with various amounts. The rate of Cu loading on the TiO_2 supports was determined by the time of the reactive magnetron sputtering process in constant Cu flux.

4.1.11. Effect of Calcination Temperature on the Photocatalytic Efficiency. Changing the calcination temperature causes a phase transition of TiO_2 nanoparticles among rutile (E_{bg} = 3.10 eV), anatase (E_{bg} = 3.36 eV), and brookite (E_{bg} = 3.51 eV).[127] Phromma et al.[115] revealed that increases of calcination temperature results in increases in the particle and crystallite sizes and nanoparticle formation in the crystal state. This group reported that, based on the calcination temperature, one or more phases predominated. There was rutile phase at temperature ≥500 °C, a mixture of three phases (rutile, brookite, and anatase) between 500−600 °C, and rutile phase at 800 °C. Three shapes of TiO_2 in the SEM images, namely, cubic, spherical, and hexagonal, were recognizable. According to the work of Al Farsi et al.,[121] thin films of ZnO photocatalyst doped with Al (AZO) were calcined at different temperatures (350, 450, and 550 °C) and used to evaluate the photocatalytic efficiency toward the degradation of phenol under solar light. The results showed that photodegradation kinetics of AZO (Al: 2.0%) prepared at 550 °C are 3× greater than that of pure ZnO.

Applying certain conditions of synthetic methods render benefits like extended specific surface area, increased adsorption area, improved morphology, crystallinity and porosity, and alterations in particle size and roughness of photocatalysts as the heterogeneous phase.[128,129] An appropriate synthetic method is applied to insist on distinct physicochemical features of the photocatalyst. The increased number of surface hydroxyl groups in the hydrothermal technique and at high calcination temperature, increased surface area in the sol−gel method, and improved crystallinity in the sputtering method and at high calcination temperature meet the need for suitable photocatalytic processes with excellent efficiency.

4.2. Modification of TiO_2 and ZnO Structures. The main aim of the modifying strategy in the synthesis of novel TiO_2- and ZnO-based photocatalysts with doping and grafting is conquering some restrictions of utilizing them in daylight conditions due to their extended band gap and high photon energy demand. These properties reduce the quantum performance of TiO_2 and ZnO because of the low recombination time of photoexcited holes and electrons; therefore, energy waste occurs. Modification processes include adding some compounds in elemental or oxide states on the surface or within the texture of the photocatalyst. Doping, grafting, decorating, and immobilizing external moieties on the surfaces of the hydrothermalized photocatalysts cause changes in the electronic arrangements of the assembled compounds, therefore changing the band gap energy and creating new transfer routes for charge carriers. Some recent attempts of scientific groups to synthesize and evaluate modified ZnO- and TiO_2-based photocatalysts are gathered in Table 2.

4.2.1. Modification without Electrochemical Interactions. One approach to improve photocatalytic activity without electrochemical interactions of photocatalysts is to provide appropriate dispersion in the slurry or suspension through the sonication technique[144] and immobilize photocatalyst nanoparticles on an inert support, such as 3D-printed biocompatible polymer (polylactic acid, PLA)[145] and porous sulfonated polystyrene microspheres,[146] glass,[147] cellulose,[148] poly aniline,[149] and ceramics,[150] to prevent agglomeration, enhance the specific surface area, and increase the opportunity for adsorption of pollutants on the photocatalyst surface, as well as desorption of products from the surface.[151] Immobilization of photocatalysts overcomes two main restrictions of photocatalytic utilization, including agglomeration during and separation after the photoreaction. Aminuddin et al.[152] synthesized TiO_2-modified photocatalysts via a step by step preparation process. Immobilization of TiO_2 was performed by coating a photo-

https://doi.org/10.1021/acsomega.3c08717
ACS Omega 2024, 9, 25457−25492

catalyst layer on the external layer of porous PANI-poly(vinyl alcohol)-glutaraldehyde (PPG), and ferric ions were doped as cross-linking agents within PPG to improve the photocatalytic activity by extending the surface area and electrochemically assisting Fe^{3+}, respectively. Mousa et al.[153] improved the photocatalytic efficiency of TiO_2 doped with ZnO and immobilized it on the cellulose acetate by the electrospinning and immersion method to prepare a CTZO composite. Dispersion of TiO_2 as a core within the cellulose acetate matrix and deposition of ZnO on the surface of the modified cellulose acetate were considered in this study. Two modification approaches, namely, immobilization and doping, improve photocatalytic activity by narrowing the band gap energy from 3.27 and 3.52 eV based on pure ZnO and TiO_2, respectively, to 1.17 eV in composite structures. Lal et al.[154] synthesized TiO_2 doped with Nd by the sol−gel sonication method to evaluate the photodegradation of MB under UV (photocatalytic efficiency of 99.11%) and solar light irradiation (photocatalytic efficiency of 96.42%). The synergic effect of both sol−gel and sonication techniques led to a smaller size and higher surface area, which improved the photocatalytic activity of the product. Ge et al.[155] reported the synthesis of TiO_2 photocatalysts by the solvothermal method (T-S) in oleylamine as a solvent and in the presence of 1,2-ethanedithiol. T-S is active under wide visible light irradiation due to a decrease in band gap energy from 3.21 eV (P25) to 2.16 eV, which was attributed to improvements in the morphology of T-S nanoparticles during solvothermal synthesis. Photodegradation of MB and RhB under visible light irradiation at 425 nm at a 10 mg/L concentration with more than 95% efficiency was a superb achievement. Solvothermal synthesis in the presence of ethylene glycol instead of 1,2-ethanedithiol did not result in better modification than P25. Xu et al.[156] utilized the ultrasonic technique in conjunction with TiO_2's photocatalytic capacity against RhB under visible light irradiation. They justified the role of sonication as an activator for introducing abundant energy via the production and blowing of cavitation bubbles. Every cavitation bubble passes through the pathway of oscillation, growth, gathering, and blowing. This process occurs immediately, and a large amount of heat (1500−5000 K) and pressure (50 MPa) are released, creating a hotspot that degrades any organic pollutants that are sucked into the cavitation spot. In fact, hot and sonic luminescence (SL) generated by blowing cavitation bubbles resulted in two consequences: (1) hydrothermal degradation of organic pollutants by the heat and the generation of hydroxyl radicals and (2) TiO_2 activation by irradiation of sonic luminescence and generation of charge carrier species. Makama et al.[157] reported that the photodegradation process was a surface-mediated reaction that improved the optimum amount of the photocatalyst. Introducing an excess amount of ZnO/SnS_2 nanocomposite had a preventative effect against light permeability and initiation of the photooxidation reaction. One of the physical approaches to enhance the photocatalytic effect against air pollutant photodegradation is the exploitation of photocatalysts as paint ingredients in the coating procedure. Arekhi et al.[158] used dispersed TiO_2 micro- and nanoparticles by adding Na_2SiO_3 into the acrylic latex. TiO_2, with a dual use as a paint and photocatalyst, was evaluated against the degradation of benzene as an air pollutant.

4.2.2. Modification with Electrochemical Interactions. 4.2.2.1. Metal Doping. Modification of photocatalysts with metals, including transition metals,[159,160] rare earth metals,[161,162] noble metals,[163,164] semimetals,[165] and alkaline earth metals,[166,167] improves organic pollutant treatment. Generally, doping of metals is carried out by reducing and precipitating ion metals into the ZnO and/or TiO_2 nanoparticle suspensions in the presence of a reduction agent. The kind and size of the metal ions and the concentration of the metal salt solution determine the photocatalytic composite activity. Kozlova et al.[48] reported the synthesis of Pt/TiO_2 and CuO_x/TiO_2 (x = 0.68) as photocatalysts and evaluated their photodegradation activity under UV irradiation against the degradation of glycerol according to eq 1.

$$C_3H_8O_3 + 3H_2O \rightarrow 7H_2 + 3CO_2 \quad (1)$$

Reduction of H_2PtCl_6 and $Cu(NO_3)_2{\cdot}6H_2O$ aqueous solutions, individually, occurred in the presence of $NaBH_4$ by the impregnation method on the TiO_2 nanoparticles. Pt^{4+} and Cu^{2+} were reduced to Pt metal and Cu^{1+}, which resulted in the stability of Pt/TiO_2 being higher than that of CuO_x/TiO_2. The maximum speed of glycerol photoreforming and H_2 release was about 1.35 and 0.55 $mmol{\cdot}h^{-1}{\cdot}g^{-1}$ for Pt/TiO_2 and CuO_x/TiO_2, respectively. Gao et al.[168] synthesized a core−shell cocatalyst of Ag@Ni by surrounding Ag nanoparticles with Ni metal and then loading the sample on the TiO_2 surface to prepare $Ag@Ni/TiO_2$ as a photocatalyst through a one-step photoinduced deposition method. In fact, in modified photocatalytic processes, Ag in the metallic form was used to assist H_2 release as a collector of photoexcited electrons and electronics extractor, and Ni as low-cost metal and interfacial active center was used to improve Ag activity. Totally, it resulted in 5.4× more generation of H_2 than conventional process with Ag/TiO_2 or TiO_2. Liu et al.[169] synthesized semiconductor oxide nanocomposites (AZ) using $AgNO_3$ and $Zn(NO_3)_2{\cdot}6H_2O$ as starting materials through a two-step polymer-network gel method. ZnO was prepared using L-(+)-tartaric acid, glucose anhydride, acrylamide, and *N*,*N*′-methylene diacrylamide to assist wet sol preparation of Zn salt, dried at 120 °C to form a xerogel, and calcined at 650 °C to form ZA0, which in step two was loaded with Ag (ZA). The final nanocomposite had superb morphology, a good distribution of Ag nanoparticle loading on the ZnO surface, a high ratio of surface area to volume, and abundant vacant sites of oxygen on the surface of ZnO, which totally resulted in significant photoactivity against degradation of MB, MO, and RhB under sunlight irradiation. According to XPS analysis, the level of oxygen vacancy on the surface of ZnO gradually increased with increased Ag loading. Higher Ag loading caused more vacant surface oxygen as a good photocatalytic efficiency factor, but exceeding from the definite amount weakened the photocatalytic activity due to the shielding effect of Ag at higher concentrations on the ZnO surface and prevented light from accessing ZnO as the photocatalyst center. Lopes et al.[170] reported the photodegradation of anthracene by a Ag/TiO_2 photocatalyst clinched on natural fibers like pretreated sisal and coconuts fiber under UV−visible light irradiation. Biodegradation, bioavailability, suitable mechanical persistence, density, and price are some factors that make these fibers good candidates as supports for the Ag/TiO_2 photocatalyst. Pretreating fibers with hot water and CTAB to remove some main residues such as wax, cellulose, and lignin makes them compatible with photocatalysts. The shift of the absorption wavelength from the UV to the visible region arises from loading Ag metals on the TiO_2 bulk and immobilization.

Adeel et al.[171] synthesized a ZnO photocatalyst doped with cobalt (Co) and assessed its efficiency against the degradation of

https://doi.org/10.1021/acsomega.3c08717
ACS Omega 2024, 9, 25457−25492

MO as a dye pollutant under visible irradiation. Loading with some transition metals like Co is an alternative approach to narrow the band gap energy of pure ZnO and trapped photoexcited electrons and slow down the recombination process of ZnO, which promotes photocatalytic efficiency. According to UV−vis DRS analysis, the band gap measurements of Co-ZnO and pure ZnO were approximately 2.16 and 3.37 eV, respectively.

4.2.2.2. Metal Oxide Doping. Nowadays, semiconductors as heterogeneous solid catalysts play important roles in photoelectrochemical reactions due to their wide band gap energies. Metal oxides from groups II−VI are considered as n-type semiconductors, which are active in UV range of light irradiation, and one main reason for their restricted usability as photocatalysts is fast recombination of photoexcited species. Doping with other metal oxides with lower band gaps and or introducing metal oxides as photoexcited trapping agents improves the base semiconductor quantum efficiency.[172−174] A literature survey shows that some transition metals as d-type and p-type doping groups on the TiO_2 and ZnO surface are Cr_2O_3,[175] SnO,[176] MnO_2,[177,178] FeO,[179] CoO,[180] NiO,[181] Cu_2O,[182] and CuO.[183] Baniamerian et al.[184,185] disclosed the application of a Fe_2O_3/TiO_2 photocatalyst synthesized by ultrasonic co-precipitation method and evaluated MB photodegradation under visible light radiation. Owing to its narrow band gap energy (2.2 eV), Fe_2O_3 causes a decrease in the band gap of modified TiO_2 from 3.2 (P25 TiO_2) to 2.9 eV at 430 nm absorption (2.5% Fe_2O_3/TiO_2). Analysis with some scavengers like IPA for $OH^•$ scavenging, TEA for h^+ scavenging, and BQ for $O_2^{•-}$ showed that h^+ was the most reactive oxidant species in algal degradation. Jiang et al.[186] fabricated a p-n type heterojunction Cu_2O/ZnO nanocomposite through a simple hydrothermal process. In its optimal structure, 1.5% wt. Cu-ZnO, this photocatalyst was able to degrade RhB two times more than pure ZnO under UV irradiation. Cu as a p-type element caused efficient retardation of photogenerated charge carrier recombination, and the amount of Cu impurities also determined the photocatalytic performance improvement. Wang et al.[187] synthesized a Z-scheme photocatalyst, namely, a ZnO-CdS composite, by hydrothermal and chemical bath deposition methods for the preparation of ZnO microspheres and the composite, respectively. Evaluation of the composite showed the effect of CdS loaded on the ZnO surface on the extension of light absorption from the UV to visible region and the photoactivity of the composite. Detection and monitoring of hydroxyl radicals by photoluminescence irradiation and XPS in situ monitoring on the ZnO-CdS composite under visible radiance confirmed the direct Z-scheme arrangement of the charge migration route. Shoueir et al.[188] reported the synthesis of $Au@TiO_2$ with uniform nanoparticles by the photodeposition method and then impregnated these nanoparticles into the chitosan fiber to a prepare plasmonic fiber of $Au@TiO_2$ with photoactivity under visible light irradiation. According to XRD analysis, it was obvious that during loading of Au on the TiO_2 some of the Ti^{4+} ions were converted to Ti^{3+} via reduction by Au, so that steadiness and efficiency of the photocatalyst were improved against photodegradation due to the lattice defect. Photodegradation of MB, carbofuran, and metronidazole as organic pollutants and photoreduction of Cr^{6+} to Cr^{3+} as a hazardous material in the presence of citric acid were evaluated. Four factors play important roles in improving the TiO_2 photocatalyst efficiency, mostly relying on the loading with Au: (1) reduction of Ti^{4+} to Ti^{3+}, (2) enhancing charge carrier dissociation, (3) Au mediating electron transfer between TiO_2 and pollutants, and (4) the presence of acid citric as a reduction agent of hazardous Cr^{6+} to safe Cr^{3+}. Siwińska-Stefańska et al.[189] synthesized binary semiconductors of a TiO_2−ZnO system with a variety of molar ratios between TiO_2 and ZnO from 9:1, 7:3, 3:7, and 1:9. The aim was the evaluation of the molar ratios on the photocatalytic activity of binary systems against photodegradation of C.I. Basic Violet 10 dye under UV irradiation. The best response to photodegradation was obtained in the presence of a Ti_9Zn_1 binary photocatalyst.

4.2.2.3. Nonmetal Doping. Nonmetal-doped photocatalysts constitute a main part of the photocatalytic modification approach due to avoiding hazardous metal doping and the lower thermostability of incorporating metals in the photocatalytic structure. Some elements like N,[190] C,[191] S,[192] B, P, I, and F as dopants are used to narrow the band gap energy and extend the recombination time of electrons and holes to improve the photocatalytic efficiency.[193] Nitrogen, due to its similarity with oxygen in terms of ionic radius and 2p energy level, is commonly used as a modifying agent and replaces with oxygen in the photocatalytic lattice.[194−196] On the other hand, doping with carbon materials is an effective approach to change the optical properties of the photocatalysts and improve photocatalytic activity due to the electron transfer potential, light absorption, and physicochemical durability of carbons as dopants.[197] Sulfur, the same as oxygen, is a VIA group element that has comparable physicochemical properties, but the ionic radius and electronegativity values of sulfur are different. When oxygen is replaced with sulfur in the ZnO structure and S-doped ZnO fabrication, the photocatalytic activity improves due to the creation of sulfur defects in the photocatalytic lattice.[192] Microcrystalline cellulose (MCC),[198] poly(vinyl alcohol) (PVA),[199] glucose,[200] Ti_3C_2 MXene,[201] ethanol, ethylene, triethanolamine, ethylene glycol, resorcinol-formaldehyde, acetylacetone, cyclohexanol, oleylamine, and activated carbon are among the employed carbon sources;[202] urea, ammonium acetate,[194] hydrazine,[203] and glycine[204] are used as nitrogen sources; thiourea is used as a sulfur and nitrogen source;[35,205] and boric acid is used as a boron source.[205] Negi et al.[202] synthesized TiO_2 nanoparticles doped with elemental carbon by the sol−gel method. Polydiallyldimethylammonium chloride (PDADMAC) as a cationic polymer and carbon source was doped on the surface of TiO_2. The decrease in the band gap energy of the composite and red shift to 2.37 eV was attributed to the improvement of the visible light response resulting from the creation of new, more stable levels of impurities for passing and trapping photoexcited electrons. Yu et al.[206] synthesized ZnO photocatalysts and used N, C, and S as dopants introduced into the photocatalytic lattice. N and C as p-type elements create vacancies in the ZnO structures, while it is not possible to create more defects in the lattice in S-doped ZnO structures due to the n-type properties of S. Generally doping ZnO with N, C, and S resulted in a red shift toward the visible area. The order of composite photocatalytic efficiency was reported as C > N > S. Mirzaeifard et al.[205] reported the synthesis of a ZnO photocatalyst doped with sulfur to enhance the photocatalytic activity against the degradation of RhB. Improvement of the photocatalytic efficiency was attributed to the red shift of the band gap energy from 3.33 to 3.02 eV and trapping of photoexcited electrons in the S-doped ZnO structure. In order to reinforce the photocatalytic efficiency by decreasing the photodegradation time, Mirzaeifard and co-workers added $(NH_4)_2S_2O_8$ as an electron trapping agent in to the photocatalytic reaction. Wang

https://doi.org/10.1021/acsomega.3c08717
ACS Omega 2024, 9, 25457−25492

et al.[207] described the synthesis of TiO_2 codoped with C/I (C/I-TiO_2) by the solvothermal-calcination method for photodegradation of MO and RhB (separately and mixed) with superb efficiency under visible and sunlight irradiation. This scientific group supposed that utilizing a codoped instead of monodoped photocatalyst had a synergic effect, increasing the photocatalytic activity. Chung et al.[208] stated the synthesis of nitrogen-doped TiO_2 in an amorphous structure with photocatalytic activity under visible light irradiation against the degradation of MB and formaldehyde as organic pollutants. Evaluation of the optical properties of N-doped TiO_2 demonstrated a red shift from the UV region (3.2 eV) to the visible area (2.4 eV) due nitrogen exchanging with oxygen in the TiO_2 lattice. The amorphous structure due to calcination at 130 °C and anatase structure due to calcination at 500 °C had the same band gap energy.

4.2.2.4. Assembly with 2D Compounds. Improving photocatalytic activity through modification with two-dimensional (2D) compounds is another approach to extend photocatalyst usability from the UV to visible region. 2D materials have large specific surface areas, coordinated unsaturated surface elements, and large amounts of active sites that absorb light irradiation. These properties make them appropriate modifying agents of ZnO and TiO_2 semiconductors.[209] g-C_3N_4[210,211] and MXenes[204,212,213] are among the 2D compounds that modify the photocatalytic efficiency of photocatalysts by increasing specific surface area and trapping photoexcited electrons in Z-scheme[210] and S-scheme[211,214] structures. g-C_3N_4 compound is an n-type semiconductor with two-dimensional metal-free structures. Although g-C_3N_4 has narrow band gap energy that is activated in visible light irradiation, its low potential quantum efficiency results in fast recombination of photogenerated species.[215] Paul et al.[216] reported the photodegradation of MB using a g-C_3N_4/ZnO heterojunction composite as a photocatalyst under visible light irradiation. Differential reflectance spectroscopy analysis demonstrated a lower band gap energy in the optimal g-C_3N_4/ZnO composite than pure ZnO and g-C_3N_4, with energies of 2.56, 3.28, and 2.72 eV, respectively. Some restrictions of ZnO and TiO_2 as photocatalysts such as wide band gap energy, low recombination time of photoexcited charge carriers, photocorrosion, and affinity for agglomeration require the integration of other compounds such as graphene, graphene oxide, and reduced graphene oxide. These two-dimensional compounds with layered structures have significant electron portability, thermal conductivity, an extended specific surface area with a thickness of just one atom, high mechanical strength that generally narrows the band gap energy, and long recombination time and improve the photocatalytic efficiency of the composite.[217−221] Tobaldi et al.[222] synthesized graphene−TiO_2 hybrids to remove VOCs and NOx in the air under solar photochemical interaction. This nanocomposite was prepared by a cost-effective sol−gel method. 1 wt % graphene coupled with TiO_2 demonstrated 2× more efficiency than pristine TiO_2. Simplicity and facilitation of electron transfer and lengthening of recombination time are among the main reason for the improved photocatalytic efficiency. Guo et al.[223] synthesized a graphene−TiO_2−Fe_3O_4 nanocomposite. Magnetic Fe_3O_4 was used to improve composite separation due to its magnetic nature, recyclability, and efficiency; however, its magnetic nature made the composite susceptible to agglomeration. Using graphene as a two-dimensional layered compound with high specific surface area, thermal stability, and mechanical strength resulted in the fabrication of a superb photocatalyst with synergic effects of Fe_3O_4 and titanium photocatalysts and better dispersion of titanium and Fe_3O_4 nanoparticles in the composite structure. Tan et al.[224] synthesized ZnO integrated with GO by the hydrothermal method. Graphene oxide, in contrast to graphene, has a hydrophilic surface full of hydroxyl and carbonyl functional groups, which provide enough affinity toward reaction with ZnO. Graphene oxide has overcome some limitations of graphene like low solubility and high aggregation affinity.

4.2.2.5. Codopants. One of the main restrictions during the design engineering of a fabricated photocatalytic composite is adverse secondary effects resulting from introducing new components. Doping with magnetic compounds like Fe_2O_3, metals, and other metal oxides increases the agglomeration affinity of the nanocomposite and oxidation when exposed to the air. These adverse effects result from reinforcement of the surface energy, which decreases the specific surface area and makes the ultimate goal pointless.[197] These modification strategies, under most conditions, have synergic effects toward improving photocatalytic performance. Therefore, additional modification in order to conquer some drawbacks of introducing new dopants demands consideration.

Tang et al.[225] claimed the synthesis of a Bi_2O_3−Ti^{3+}/TiO_2 heterojunction photocatalytic composite. A p-n heterojunction composite and Ti^{3+} self-doped titanium were two main factors that demonstrated synergic effects. The excellent photocatalytic efficiency resulted from coordination bonding between Bi_2O_3 and the Ti^{3+}/TiO_2 substrate. Photodegradation of tetracycline (TC) antibiotics under sunlight irradiation in the citric acid solution as an electron trapping agent exhibited 100% efficiency. Abdelhaleem et al.[226] reported the synthesis of Fe^{III}N-TiO_2 for the photodegradation of diphenamid in the presence of sulfite as a conventional radical agent under a visible LED. The modified photocatalyst had dual uses: (1) diphenamid degradation and (2) Sulfite activation (see eq 2). Some advantages of this process were cost efficiency because of using low-cost sulfite and iron (as wastes of many industries), low misuse of Fe loaded on the titanium as leachate during the process, and visible light accessibility.

$$SO_3^{-2} + M^{n+} \rightarrow M(SO_3)_x^{n-2x} \rightarrow xSO_3^{-\bullet} + M^{(n-1)+} \quad (2)$$

Fe loaded on the N-doped titanium acts as mediator for electron transfer and subsequently lowers the band gap. However, this group stated that the photocatalytic efficiency did not improve after using Fe because of a decrease of the specific surface area. Kong et al.[227] disclosed the photodegradation of bisphenol A (BPA) via a photocatalytic process in the presence of Fe_2O_3/g-C_3N_4@N-TiO_2 under simulated irradiation of sunlight. Doping and loading with C, N, and Fe caused changes in the crystallinity and in turn decreased the band gap energy from 3.3 to 2.15 eV for the anatase phase of TNAs and Fe_2O_3/g-C_3N_4@N-TiO_2, respectively. g-C_3N_4 acted as mediator to transfer excited electrons, optimized photodegradation speed, and immobilized other photocatalytic participants. Titanium nanotubes were used instead of nanoparticles to facilitate precipitation, filtration, and hydro-cyclone separation and recapture. Sharotri et al.[228] described the synthesis of Mn−N codoped TiO_2 (MnNT) utilizing the cavitation-induced method along with ultrasonic irradiation. MnNT-550 demonstrated good photocatalytic efficiency because of the formation of oxygen cavities at a calcination temperature of 550 °C in the presence of Mn^{2+}, which caused

https://doi.org/10.1021/acsomega.3c08717
ACS Omega 2024, 9, 25457−25492

the anatase phase to convert to the rutile phase. Decreasing the band gap energy in MnNT-550 to 2.4 eV resulted in red shift and photodegradation of quialphos and 2-chlorophenol at 660 nm with 87.5% and 91.7% degradation efficiencies, respectively. Ravichandran et al.[229] synthesized a thin film ZnO photocatalyst activated with Ag and g-C_3N_4 as dopant agents and subsequently evaluated its photocatalytic activity against the degradation of MB and MG under visible light irradiation. The following were considered three determining factors on the photodegradation activity: (1) incorporation of Ag as an electron mediator between conduction bands of ZnO, (2) participation of g-C_3N_4 as a delaying agent for electron−hole recombination, and finally (3) enhanced roughness of the ZnO/g-C_3N_4/Ag thin film, which resulted in more pollutant adsorption. Vignesh et al.[230] prepared a new PVP-capped Cd:Ag:ZnO nanocomposite through the microwave-assisted precipitation method. The analyses confirmed that any dopant agents including Cd and Ag act as impurities with proportions of $Zn_{1-x}(Cd_xAg_x)O$:PVP (x = 10%), which improved the photocatalytic efficiency of ZnO by playing the role of charge carrier mediators. Increased specific surface area, increased transfer of charge carriers at interface regions of semiconductors, and increased charge carrier recombination time were the other reasons in favor of the enhancement of the photocatalytic activity.

Modifying TiO_2 and ZnO structures improved their photocatalytic efficiency by combining them with external participants. The creation of a new path to transfer photoexcited electrons and holes is the reason for the enhancement of the photocatalyst performance. Selecting a suitable dopant, which has appropriate agreement with the band gap of the base photocatalyst, decreases the hybrid band gap of the composite and delays recombination due to the trapping of photoexcited species. In the following, mechanistic routes of several pristine and modified TiO_2- and ZnO-based photocatalysts against the photodegradation of water-soluble and air pollutants are provided.

5. MECHANISM OF PHOTOCATALYTIC DEGRADATION OF WATER-SOLUBLE AND AIR POLLUTANTS

Photocatalytic degradation under light irradiation in the UV to visible range of the electromagnetic spectrum generally follows a distinct oxidation−reduction photochemical process on the surface of the photocatalyst.[252] Photocatalysts with semiconductor natures have distinct band gap energies (E_{bg} (eV)) between the occupied VB and vacant CB. For example, titanium as a customary photocatalyst has different band gap energies in the anatase phase and rutile phases equal to 3.2 and 3.0 eV, respectively. Also, the band gap energy of ZnO at the wurtzite phase is 3.2 eV. The exact value of the band gap energy is a function of several preparation method factors, like synthesis methods and their variable factors like temperature, time, solvent, pH, time, and temperature of calcination. Generally, the synthesis method is determined by the accessibility and facility of the precursors and workup, respectively. Defining a distinct mechanistic route is not possible. There is some evidence that points toward a specific reaction route. Adsorption of a pollutant on the surface of the photocatalyst is considered as the initiation of the photodegradation reaction. Electron transfer and photogenerated species complete the oxidation−reduction reaction to destroy organic pollutants in a water or air environment. Some analyses elucidate the dominant mechanistic route, while other routes are also possible. Some theoretical investigations by density functional theory (DFT) calculations and kinetic studies are considered usable alternatives to predict the mechanistic route (see section 5.1), while trapping active species by adding distinct scavengers determines the main route of the photodegradation mechanism (see section 5.6.3).

5.1. Theoretical Study. Theoretical evaluations of the photocatalytic activity of the TiO_2- and ZnO-based photocatalysts by DFT calculations, experimental design programs, and kinetics studies elucidate their potential during the photodegradation process, reduce cost, and save time. Xu et al.[253] studied the photocatalytic activity of six different morphologies of pristine ZnO using DFT calculations to obtain some theoretical results about the effect of the morphology and adsorption−desorption energies of the preradical molecules on the photocatalytic efficiency. The experimental results showed that different morphologies of ZnO only affected the adsorption−desorption energies and determined the superoxide anion radical as the main active species of photodegradation by ZnO ($O_2^{\bullet-}$ > holes > $OH^\bullet$), which was in agreement with DFT calculation outcomes. Xu et al.[254] studied the kinetics of acetaldehyde removal from the air by N-modified titanium in a fluidized bed photoreactor system. The optimum flow rate of pollutant gas, concentration, humidity, irradiation light intensity, O_2 concentration, residence time, catalyst loading, and temperature as main factors affecting the kinetics were calculated. The results showed that low flow rate and decreased gas pollutant concentration are better conditions to photooxidize acetaldehyde from the air.

5.2. Photogenerated Species. Striking photons with energy equivalent to or higher than E_{bg} of the photocatalyst results in the excitation of electrons and transfer from the VB to CB, which subsequently leaves holes behind at the VB. These photoexcited species, denoted as electrons (e^-_{CB}) and holes (h^+_{VB}), play critical roles as initiators of photoredox reactions to degrade organic pollutants (i.e., dyes, phenolic, and any volatile organic compounds) in the air and wastewater media. Exchanging energy between irradiated photons and chemical bonds in order to purify wastewater is an attractive field according to cost-effectiveness, convenient accessibility, and easy employment of photocatalysts.[255,256]

5.3. Photogenerated Species Pathway. Photogenerated e^-_{CB} reach toward the surface of the photocatalyst to reduce adsorbed O_2 and generate an oxygen anion, i.e., a superoxide radical ($O_2^{\bullet-}$), which in turn reduces H_2O to $OH^\bullet$ and $HOO^\bullet$ or is directly consumed for organic pollutant degradation through the surface of the nanocomposite. The photoreduction process on the surface of TiO_2 is presented in eqs 3−5.

$$TiO_2 + h\nu \rightarrow TiO_2[e^-_{CB} + h^+_{VB}] \quad (3)$$

$$e^-_{CB} + O_2 \rightarrow O_2^{\bullet-} \quad (4)$$

$$O_2^{\bullet-} + H_2O \rightarrow HOO^\cdot + OH^- \quad (5)$$

Photogenerated h^+_{VB} oxidizes a hydroxyl anion on the photocatalyst surface to a hydroxyl radical ($OH^\bullet$). Oxidation of H_2O to $OH^\bullet$ and H^+ occurs by the photooxidation activity of h^+_{VB}. Equations 6−8 represent photo-oxidation reactions in the presence of titanium as the photocatalyst.

$$TiO_2 + h\nu \rightarrow TiO_2[e^-_{CB} + h^+_{VB}] \quad (6)$$

$$h^+_{VB} + OH^- \rightarrow OH^\bullet \quad (7)$$

https://doi.org/10.1021/acsomega.3c08717
ACS Omega 2024, 9, 25457−25492

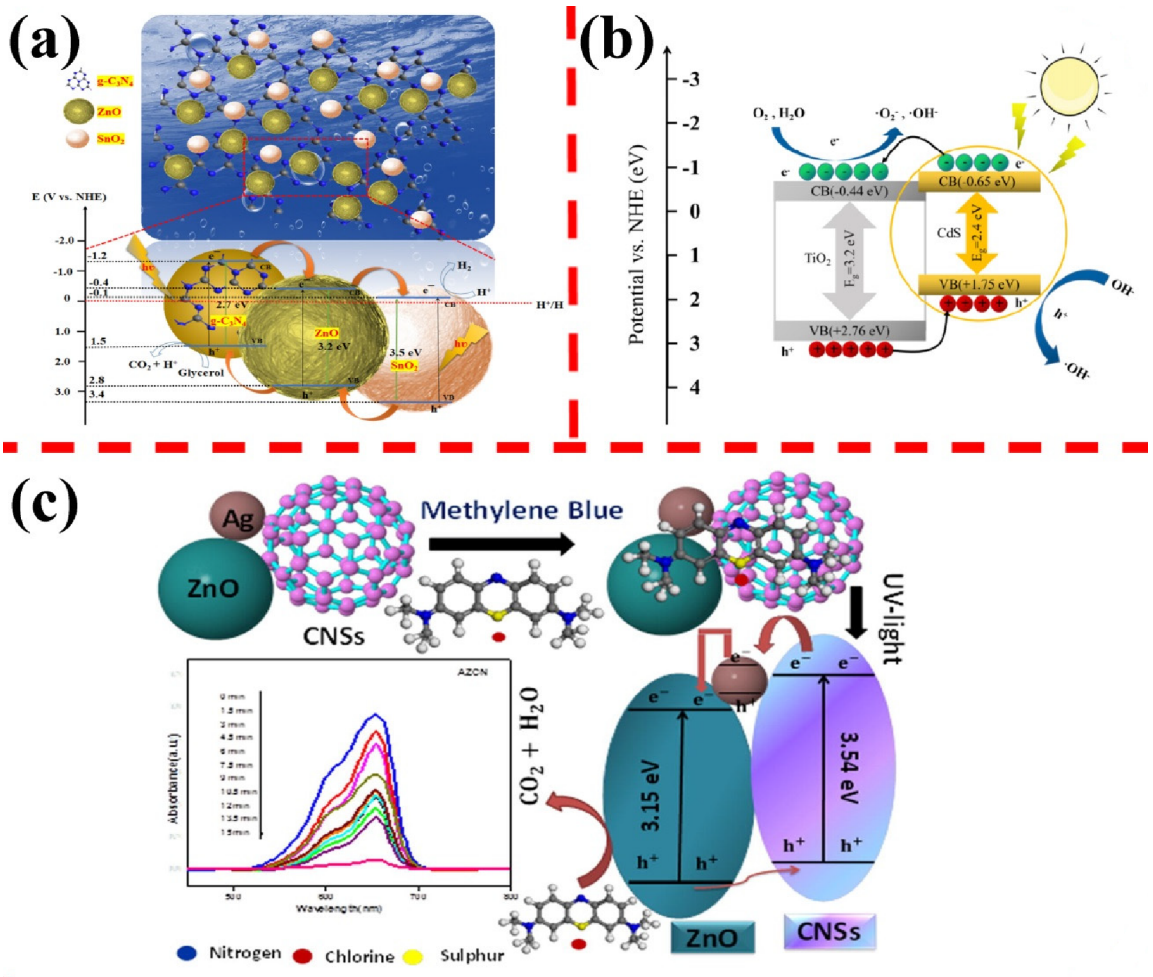

Figure 1. (a) Schematic illustration of the mechanism of the transfer and separation of photogenerated charges. Reprinted in part with permission from ref 260. Copyright 2018 American Chemical Society. (b) Mechanistic route of the transfer and separation of photogenerated charges in the TiO_2−CdS nanocomposite. Reprinted in part with permission from ref 261. Copyright 2021 American Chemical Society. (c) Mechanistic route of the transfer and separation of photogenerated charges in the AZCN nanocomposite. Reprinted in part with permission from ref 263. Copyright 2018 Elsevier.

$$h^+_{VB} + [H_2O \leftrightarrow H^+ + OH^-] \rightarrow H^+ + OH^\bullet \quad (8)$$

At the end step, similar to any radical reactions, as demonstrated in eqs 9 and 10, the radical species react with the adsorbed organic pollutant on the surface of the photocatalyst and degrade it to some nontoxic compounds, resulting in the mineral compounds of CO_2 and H_2O.[257]

$$OH^\bullet + \text{organic pollutants} \rightarrow \text{oxidized products} \quad (9)$$

$$O_2^{\bullet -} + \text{organic products} \rightarrow \text{oxidized productions} \quad (10)$$

5.4. Recombination Pathway of Photogenerated Species. Recombination of h^+_{VB} and e^-_{CB} is one important factor that affects the performance and efficiency of photocatalysts. This happens if photoexcited e^-_{CB} without more reaction with adsorbed O_2 returns to the VB, as demonstrated in eq 11. A higher E_{bg} (eV) of the photocatalyst can generally be equal to increased recombination occurrence followed by heat release.

$$TiO_2[e^-_{CB} + h^+_{VB}] \rightarrow TiO_2 + \text{heat} \quad (11)$$

5.5. The Mechanism of TiO_2 and ZnO Photocatalytic Reactions. The principle of the photocatalytic mechanism of TiO_2 and ZnO in the photodegradation of organic pollutants was evaluated. The mechanistic basis of these two semiconductors as photocatalysts (TiO_2 and ZnO) is that they have wide band gap energies (approximately 3.2 eV), such that photons just in the UV region (≤380 nm) are able to excite and move electrons from the VB and to the CB.[33] Narrowing the band gap energy to shift toward the visible light region (400−700 nm) enhances the photocatalytic efficiency to operate in moderate conditions and leads to benefits from daylight for the photodegradation of organic pollutants.[258] Several modification techniques are used to conquer this limitation in TiO_2 and ZnO photocatalysts, such as doping with metal, nonmetal, and semimetal oxides.[259] There are two ways dopant agents decrease the band gap energy (E_{bg}) and improve the photocatalytic efficiency to degrade organic pollutants. The first is through embedding two band gaps from the dopant and photocatalyst into each other, which act as electron trapping intermediates and increase the recombination time of the charge carrier species (electrons and holes). This approach has been seen with metal, nonmetal, and semimetal oxides. Ali et al.[107] synthesized a ternary composite of ZnO, SnO_2, and TiO_2 denoted as ZST that acted as photocatalyst for degradation of 2,4-dichlorophenol (DCP) and bisphenol A (BPA) under UV light irradiation. Every component in the ternary nanocomposite of SnO_2, ZnO, and TiO_2 has its distinct CB and VB levels, and all the electrons in the VB can be excited by UV light irradiation. According to

https://doi.org/10.1021/acsomega.3c08717
ACS Omega 2024, 9, 25457−25492

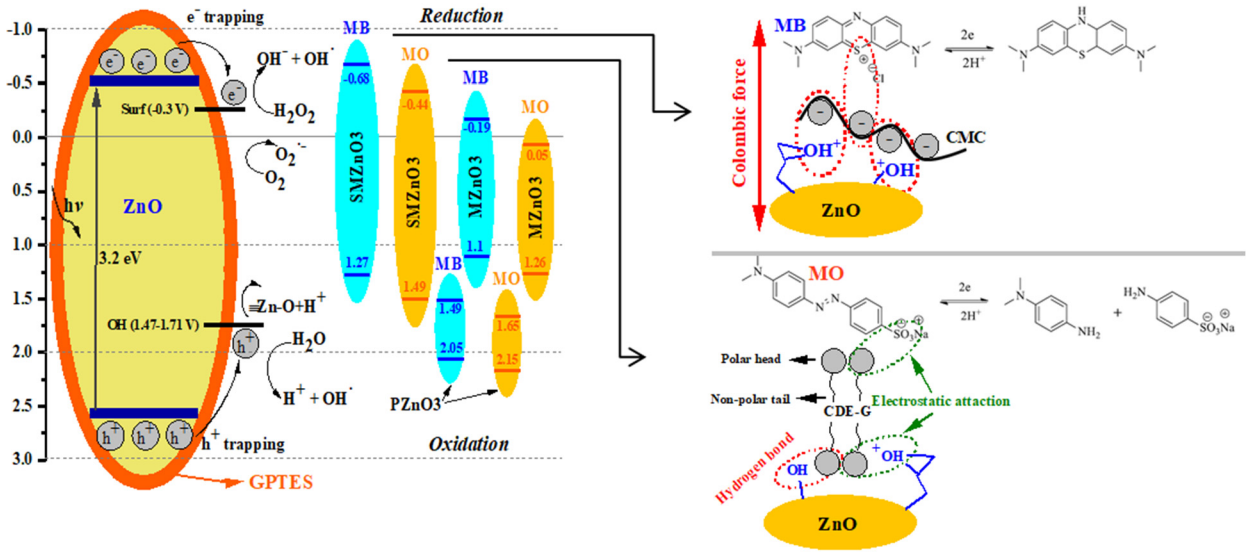

Figure 2. Schematic route of the transfer of charge carriers during photodegradation in the presence of GPTES@ZnO and a surfactant-mediated photocatalytic reaction. Reprinted in part with permission from ref 267. Copyright 2023 Elsevier.

the CBs of SnO_2, ZnO, and TiO_2, photoexcited electrons shift from the CB of ZnO to TiO_2 and then SnO_2, while according to the VBs of SnO_2, ZnO, and TiO_2 the transfer of photogenerated holes occurs from the VB of SnO_2 to TiO_2 and then ZnO. CB and VB levels of TiO_2 are between the CBs and VBs of SnO_2 and ZnO. This system made a staggered type II heterojunction. As demonstrated in Figure 1a, Vattikuti et al.[260] prepared similar three component composites of ZnO/SnO/g-C_3N_4 and evaluated their photocatalytic efficiency against organic contamination removal and H_2 release.

Ye et al.[261] synthesized a binary composite of TiO_2−CdS as a photocatalyst and used it against the photodegradation of penicillin under sunlight irradiation. As demonstrated in Figure 1b, it was concluded that photon irradiation with an energy higher than or equal to the band gap energy (E_{bg}) of CdS (the component with minor E_{bg}) generated photoexcited species, including electrons and holes, according to CB and VB potentials due to differences between the E_{CB} of TiO_2 and the E_{CB} of CdS. The photodegradation enhancement was attributed to the intrinsic heterojunction property of recombination hindrance of the CB from CdS and the VB from titanium.

A mediator transfers photogenerated electrons from the CB to either appropriate compounds on the surface of the photocatalysts like O_2 and H_2O to produce fresh radicals or organic pollutants to degrade them directly. This pathway has been seen with pure metals like Au and Ag loaded on the photocatalyst surface.[262] Singhal et al.[263] synthesized a new ZnO-based photocatalyst with deposited self-assembled Ag, which was loaded on the surface of the carbon nanospheres (CNSs). The new composite denoted as AZCN was utilized to evaluate the photodegradation of MB as an organic pollutant under UV light irradiation. According to Figure 1c, UV light irradiation on the surface of the AZCN nanocomposite caused photoexcited electrons create junctions at the interface of ZnO and CNSs that act as charge transfer bridges between ZnO and CNSs. Participation of CNSs and Ag in the photocatalytic activity of ZnO resulted in a reduction of the overall band gap energy and enhancement of the photodegradation performance.

Ravichandran et al.[229] synthesized thin film of ZnO/g-C_3N_4/Ag. The incorporation of Ag as an electron mediator between conduction bands of ZnO and g-C_3N_4, participation of g-C_3N_4 as an agent delaying electron−hole recombination, and finally increased roughness on the ZnO/g-C_3N_4/Ag thin film, which resulted in more pollutant adsorption, were considered as three determining factors of the photodegradation activity. Optical transmittance spectra of ZnO showed approximately 80% transmittance of irradiated light, while that about the composite was lower than 60%, which is in accordance with increased light absorption by the ZnO/g-C_3N_4/Ag thin film and the improvement of the photodegradation activity. Marschall et al.[264] evaluated the mechanistic route of charge carrier transfer along with temperature increase in TiO_2 (p25), which consisted of both anatase and rutile phases when used as a photocatalyst. Photogenerated electrons generally transfer from the CB of the anatase phase to the CB of the rutile phase, and subsequently holes move from the VB of the rutile phase to the VB of the anatase phase, which in total results in a decrease of the recombination speed and improvement of the photocatalytic efficiency. With an increase in temperature, the recombination of charge carriers in the rutile phase accelerates and causes retardation in the recombination cycle between anatase and rutile phases.[265,266]

Photocatalytic capacity is directly related to the amount of photogenerated electrons that reach to the surface of the catalyst and proceed through the degradation procedure with an oxidative nature due to producing other active species, such as superoxide anion radicals and hydroxyl radicals, or directly degrading organic pollutant adsorbed on the surface of the photocatalyst. Ghamarpoor et al.[267] synthesized a ZnO photocatalyst modified with GPTES as a silane source. The improvement in photocatalytic efficiency was attributed to a decrease in the band gap energy from 3.25 to 3.1 eV due to surface modification by hydrothermal and silanization methods. Utilizing surfactants and preparing a thin film were two other alternatives to obtain more efficiency in MB and MO photodegradation in the wastewater media and benzene in the air. Mechanistic and surfactant-mediated pathways are shown in Figure 2.

Gas emissions into the air from industrial plants are another pollutant source of heavy metals, greenhouse gases, and VOCs.

https://doi.org/10.1021/acsomega.3c08717
ACS Omega 2024, 9, 25457−25492

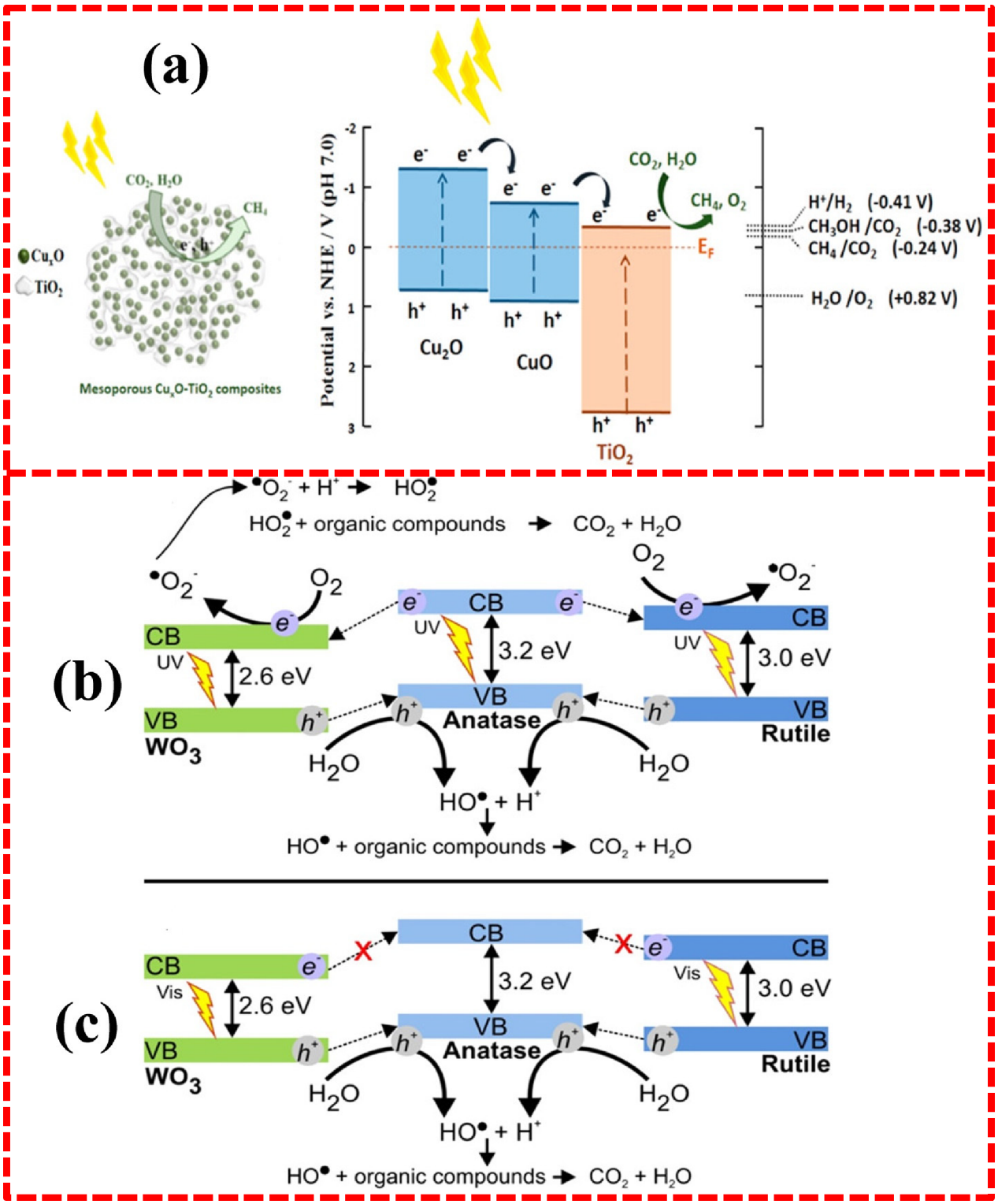

Figure 3. (a) Mechanistic route of CO_2 photoreduction in the presence of the Cu_xO−TiO_2 composite. Reprinted in part with permission from ref 269. Copyright 2016 American Chemical Society. Mechanistic route of photodegradation in the presence of TiO_2 (rutile)/WO_3/TiO_2 (anatase) (b) under UV light irradiation and (c) under visible light irradiation. Reprinted in part with permission from ref 271. Copyright 2021 American Chemical Society.

The removal of this group of contaminants on the surface of photocatalysts in the presence of O_2 and in a humid environment was evaluated in experimental conditions toward the photodegradation of H_2S, NH_3, phenols, and acetaldehyde as types of air pollutants. The mechanistic route of the gas photodecomposition is similar to that under aqueous conditions. H_2O- and O_2-containing air adsorbed on the surface of the photocatalyst is oxidized and reduced, respectively, by holes and electrons as photogenerated species to produce $OH^{\bullet}$ and $O_2^{\bullet-}$ as secondary active species. The surface hydroxyl groups of the nanocomposites, which assembled during hydrothermal treatment, are considered as a hydroxyl radical source; the more,

https://doi.org/10.1021/acsomega.3c08717
ACS Omega 2024, 9, 25457−25492

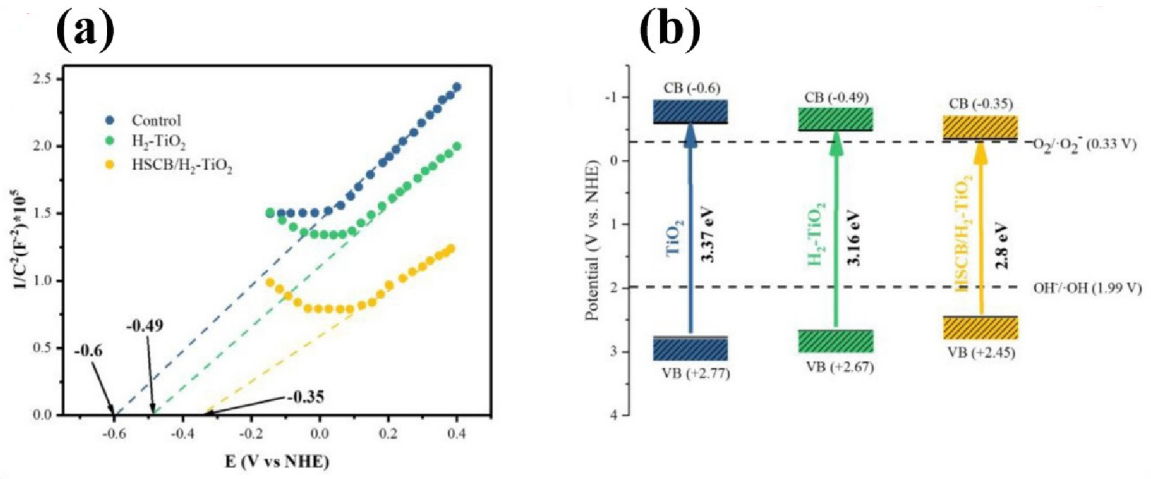

Figure 4. (a) Mott−Schottky plot and (b) mechanistic routes of biochar-H_2/TiO_2. Reprinted in part with permission from ref 276. Copyright 2022 American Chemical Society.

the better in terms of the efficiency of the photocatalytic performance against air pollutant degradation. The main step is the adsorption of gaseous organic pollutants on the surface of the photocatalyst, which along with gas pollutant concentration, flow rate, relative humidity, and temperature define the photocatalytic efficiency. Mohamed et al.[268] reported the removal of toluene as a VOC pollutant of the air using prepared TiO_2/Pt/$Ti_2Fe_2O_7$ nanocomposites. The photocatalytic activity of the photocatalyst results in more than 95% photodegradation of toluene on its surface under solar light irradiation. The participation of $Ti_2Fe_2O_7$ with anatase and rutile phases of TiO_2, as well as the presence of Pt, improves the recombination time of the photo-nanocomposite by trapping photogenerated holes and electrons, respectively. According to the schematic in Figure 3a, Park et al.[269] prepared a heterostructured Cu_xO-TiO_2 composite as a photocatalyst to reduce CO_2 to methane to use as precious fuel. These photoreduction reactions proceed in three levels from a mechanistic point of view. The efficiency of CO_2 removal to methane production was reported as 221.63 $ppm \cdot g^{-1} \cdot h^{-1}$.

Taghizadeh-Lendeh et al.[270] synthesized ZnO/TiO_2 supported by active carbon as a photocatalyst for the degradation of gas refinery effluent (GRE) under sunlight irradiation. Transfer of photoexcited electrons initiates from the CB of ZnO by sunlight irradiation striking the VB, then participation of the CB of TiO_2 cause a delay in recombination time and improves the photocatalytic efficiency of the nanocomposite. Active carbon enhances the surface area of the photocatalyst and hinders agglomeration of the nanoparticles.

Pinedo-Escobar et al.[271] synthesized a photocatalytic active composite with the hybridization of two forms of TiO_2 lattice (rutile and anatase) and WO_3. The photocatalytic efficiency of the prepared composite was evaluated under visible and near-UV irradiation. As demonstrated in Figure 3b and c, movements of photogenerated species start from VB excitation of WO_3 and proceed to generate oxidation reagents for MO photodegradation. Wang et al.[272] reported the removal of NH_3 by a photocatalytic oxidation process in the presence of C-doped titanium grafted with Mo under visible light irradiation due to the creation of a heterojunction with titanium to trap photoactive species. Secondary active species as ROS exhibit oxidation activity through the N_2H_4 mechanism and convert NH_3 to N_2 and H_2O.

5.6. Electrochemical Analysis. Determination of the photocatalytic degradation mechanism has been performed by two groups of experiments, including internal and external analysis. Internal analyses are performed by adding some active species scavengers into the wastewater media to study their affect on the photocatalytic efficiency, while external analyses are several device evaluations that monitor the presence of photogenerated active species in the media, including surface photovoltage (SPV) response, photoluminescence spectroscopy (PL), and electron spin resonance (ESR-DMPO). In the following, several analytical techniques and spectral responses are gathered according to a literature survey and stated to clarify mechanistic routes of charge carrier transfer during photoexcitation processes in semiconductors as photoactive and photocatalytic materials.

5.6.1. Mott−Schottky Plot. Confirmation of heterojunction formation in the composite of the photocatalysts is performed using a Mott−Schottky measurement. According to the Mott−Schottky plot, the flat-band potential (E_{FB}) of any participants and junction type formation between participants are acquired. Extrapolation of the plot with eq 12 determines the conduction type and photoexcited charge carrier density (N_c).[273,274]

$$\frac{1}{C^2} = \pm\frac{2}{\varepsilon\varepsilon_0 A^2 e N_c}\left(V - V_{FB} - \frac{k_B T}{e}\right) \tag{12}$$

Lazau et al.[275] synthesized a heterojunction of TiO_2/$CuMnO_2$ with photocatalytic efficiency, measured its flat-band potential, determined its semiconductor states using a Mott−Schottky plot. According to the slope of the lines, titanium and $CuMnO_2$ are n- and p-type semiconductors, respectively. Additionally, the participants' E_{FB} values confirm the upward and downward shifts of the Fermi levels of $CuMnO_2$ and titanium, respectively, to reach a balanced level. In fact, the Mott−Schottky plot showed the possibility of p-n heterojunction formation. Shi et al.,[276] in a similar work, prepared a photoactive ternary composite of TiO_2 base modified with biochar/H_2. The Mott−Schottky plot and mechanistic route are demonstrated in Figure 4a and b, respectively. Zakir et al.[277] fabricated titanium doped with Ag and Cu to evaluate MB photodegradation under UV irradiation. The Mott−Schottky plot confirmed that the flat-band potential in the composite with

https://doi.org/10.1021/acsomega.3c08717
ACS Omega 2024, 9, 25457−25492

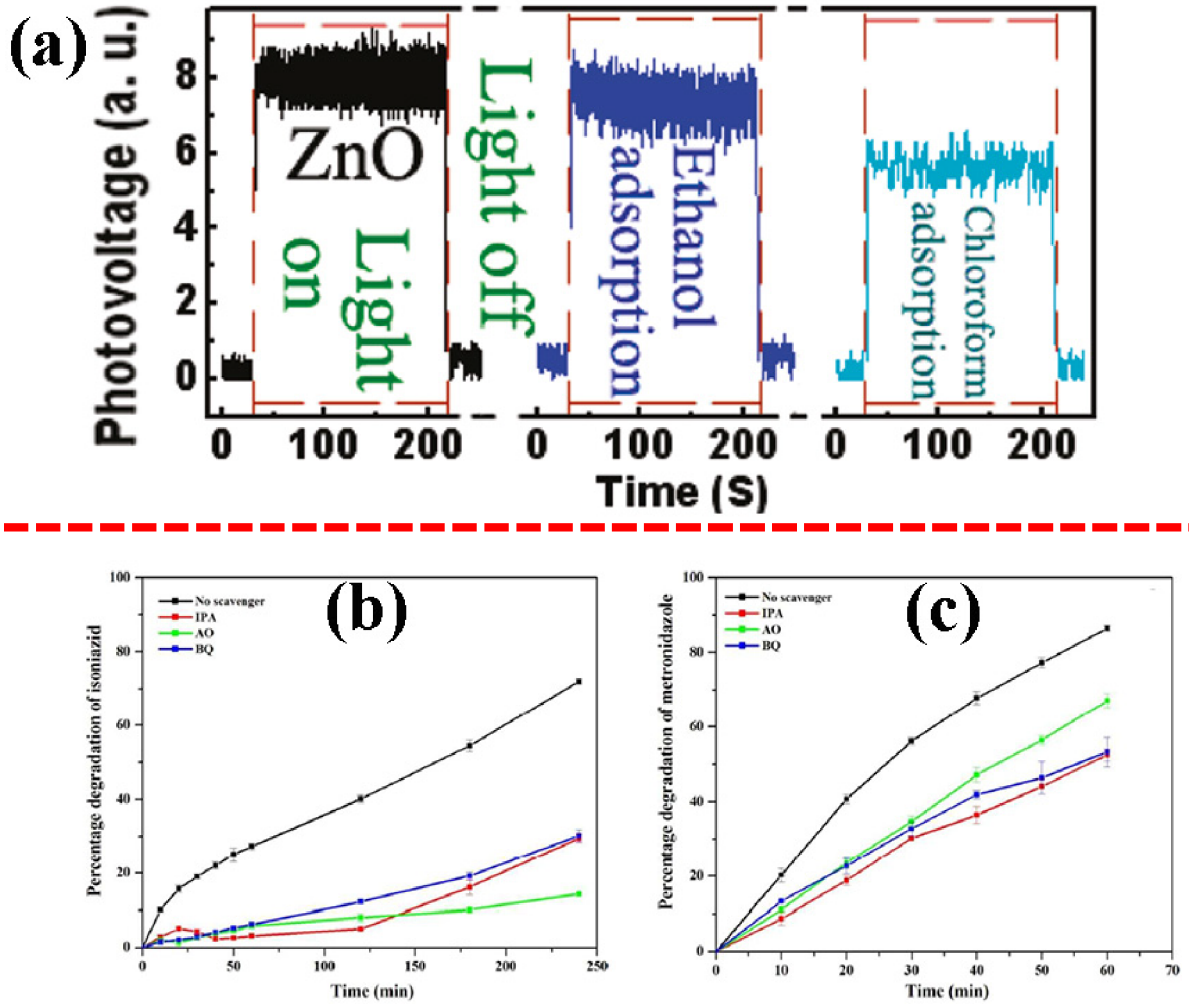

Figure 5. (a) Surface photovoltage (SPV) measurements as a work function response of porous ZnO. Reprinted in part with permission from ref 280. Copyright 2010 American Chemical Society. The photodegradation curves of adding AO, iso-PrOH, and BQ (b) against metroimidazole and (c) against isoniazid. Reprinted in part with permission from ref 293. Copyright 2015 American Chemical Society.

Table 3. Some General Scavengers as Charge Carriers and Reactive Oxygen Species (ROS) Trapping Agents

				photodegradation in the presence of		
no.	active species	scavengers	photocatalyst	photocatalyst	scavenger	ref
1	hydroxyl radical	isopropanol	magnetic mesoporous TiO_2	97.52%	93.72%	283
		t-butyl alcohol	ZnO-doped CuO@Alg bionanocomposite	98.12%	54.16%	284
		EDTA-2Na	B-doped TiO_2	98.8%	60.87%	285
2	electron	$AgNO_3$	ZnO nanowires	83.0%	78.0%	286
3	superoxide anion radical	*para*-benzoquinone (BQ)	Fe_3O_4@SiO_2@g-C_3N_4/TiO_2 nanocomposite	91.0%	~10%	287
		N_2	alkali-treated TiO_2	99.0%	45.0%	288
4	hole	KI	commercial ZnO	99.0% (pH = 3.0)	~75% (pH = 3.0)	289
		triethanolamine (TEOA)	titanium-based MOF	93.5%	48.0%	290
		ammonium oxalate (AO)	CuO supported on ZnO photocatalyst	99.0%	~35.0%	291
		EDTA	TiO_2	97.52%	63.11%	282
		oxalic acid			46.7%	
		benzyl alcohol	ZnO	91.4%	42.6%	292

Ag or Cu dopants shifts negatively, and all participants of the composite are p-type.

5.6.2. Surface Photovoltage (SPV) Measurements. Surface photovoltage (SPV) measurements through the Kelvin probe technique are used to evaluate surface and bulk characterization of semiconductors and find a correlation between photocatalytic activity and SPV response. The SPV response changes with the photocatalytic capacity against the photodegradation of organic pollutants. Modifying photocatalysts and improving their capacity cause stronger SPV responses. Any new response band in the SPV diagram is equal to the surface state population transition created by new dopants on the surface of the photocatalyst.[278] Urs and Kamble[279] evaluated three variables of SPV measurements including temperature, oxygen amounts,

https://doi.org/10.1021/acsomega.3c08717
ACS Omega 2024, 9, 25457−25492

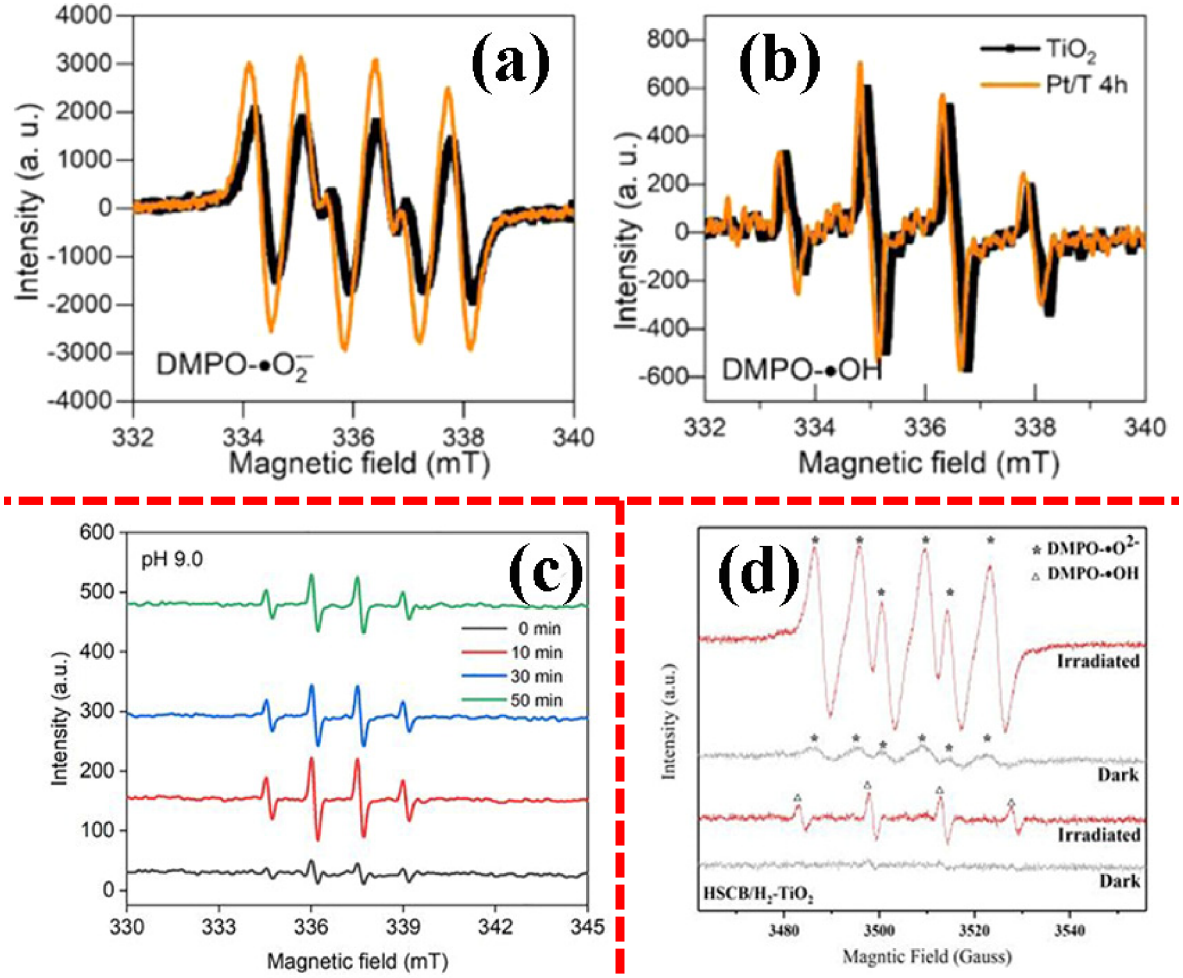

Figure 6. ESR spectra of (a) hydroxide and (b) superoxide radicals trapped under simulated solar irradiation. Reprinted in part with permission from ref 294. Copyright 2021 American Chemical Society. (c) ESR spectral monitoring of DMPO−OH• radicals with time dependence. Reprinted in part with permission from ref 295. Copyright 2020 American Chemical Society. (d) ESR spectrum of biochar/H_2−TiO_2 by spin trapping with DMPO in different light conditions. Reprinted in part with permission from ref 276. Copyright 2022 American Chemical Society.

and a photon energy of a UV laser to report the accumulation density of charge carriers on the surface of the photocatalyst. The SPV response is considered a time analysis of work function measurements of photocatalysts under light irradiation and photoexcitation. SPV curves of porous ZnO as the work function response over time (sec) are plotted in Figure 5a. Li et al.[280] confirmed that intense SPV signals are due to the preparation of ZnO in high temperature and its porous structure.

5.6.3. Confirmation of the Fate of Photogenerated Species by Scavengers. Another way to determine the mechanistic route of photocatalytic degradation of organic pollutants is to introduce some distinct scavengers as active species quenchers into the media. Changes in photodegradation speed in the presence of photocatalysts after the addition of intended scavengers correlate with the effectiveness of supplementary photogenerated active species (whether directly or indirectly).[281] Some scavengers, which are frequently used in active species detection during photocatalytic reactions, are gathered in Table 3. Scavengers are classified as oxidizable or reducible compounds that are used to determine photocatalytic oxidation (PCO) or reduction (PCR) nature in the degradation reactions. In order to improve a photoreduction reaction, adding hole scavengers is appropriate approach due to their smooth oxidation capacity to remove holes from the recombination cycle and improve electron numbers.[282]

Kiwaan et al.[70] employed pure titanium nanoparticles to separately photodegrade RhB and Acid Red57 dyes in water solutions. Photoelectrochemical investigations of photocatalytic routes were performed in the presence of some radical scavengers and terephthalic acid as probe molecules while monitoring the photodegradation speed. They reported that OH• was the determining radical during photodegradation under UV irradiation according to a photoluminescence experiment (PL spectroscopy) at 425 nm. Makama et al.[157] synthesized a ZnO/SnS_2 nanocomposite to degrade ciprofloxacin (CIP) under visible irradiation. The determining agent in the photodegradation pathway was evaluated by adding some scavengers into the wastewater media. The effects of adding DMSO as an electron scavenger, $KBrO_3$ as an O_2 scavenger, BQ as an $O_2^{\bullet-}$ scavenger, KI as and OH• and hole scavenger, and isopropanol as an OH• scavenger were analyzed. The necessity of dissolved O_2 in the photodegradation of CIP was confirmed by purging and comparing argon and air in the wastewater. Jo et al.[293] measured the efficiency of photogenerated species of Z-scheme $CaIn_2S_4/TiO_2$ as a photocatalyst under light excitation by monitoring the competition of different scavengers. The results of Figure 5b and c confirmed that OH• and $O_2^{\bullet-}$ as main

https://doi.org/10.1021/acsomega.3c08717
ACS Omega 2024, 9, 25457−25492

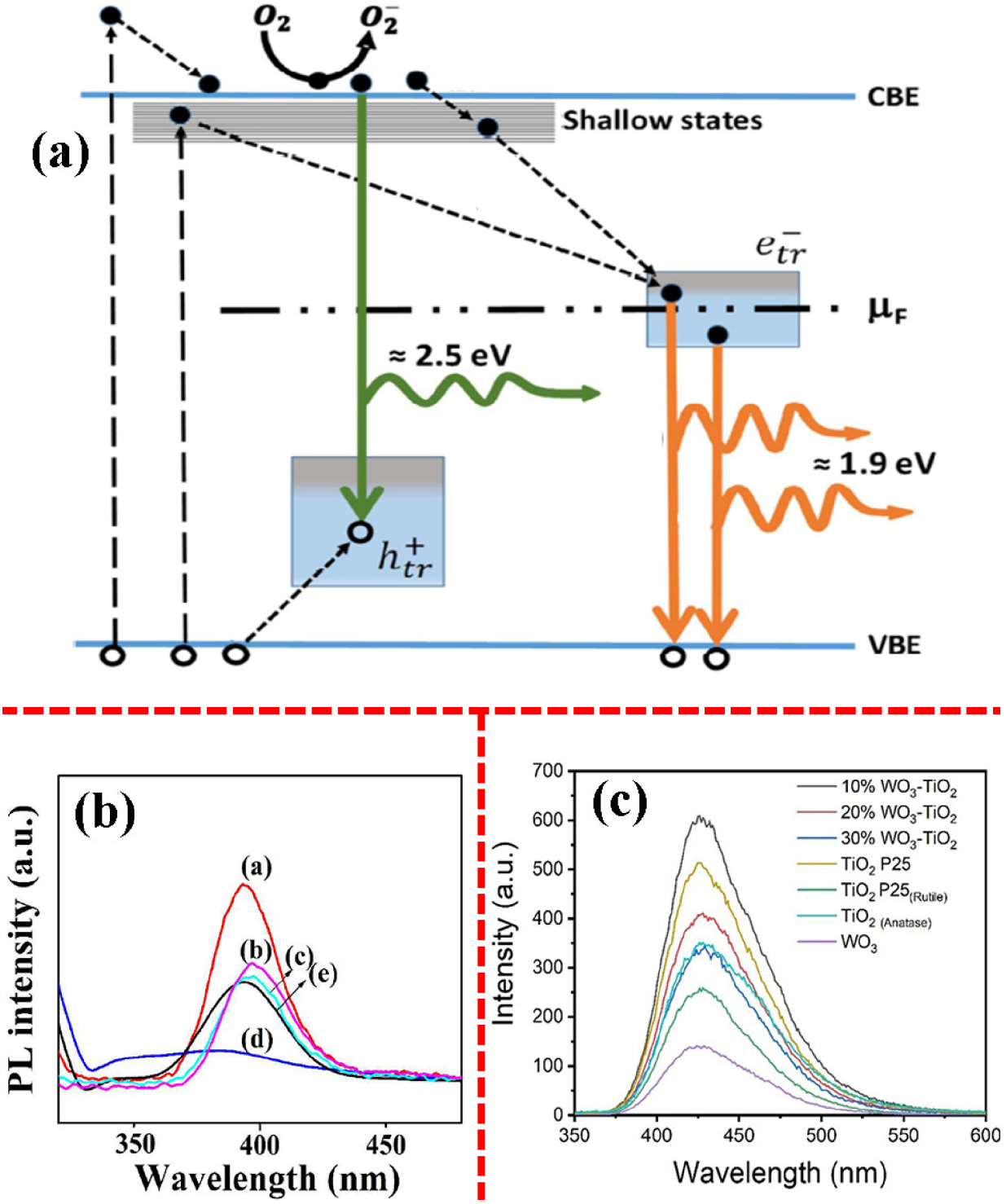

Figure 7. (a) PL mechanism in the anatase structure of TiO_2. Reprinted in part with permission from ref 296. Copyright 2017 American Chemical Society. (b) Recorded fluorescence emission PL spectra of pure (a) ZnO nanocrystals and (b) 1:3, (c) 2:1, and (d) 3:1 molar ratios of glycine to ZnO nanocrystals. Reprinted in part with permission from ref 298. Copyright 2015 American Chemical Society. (c) Intensity of the fluorescence emission in the presence of TiO_2/WO_3. Reprinted in part with permission from ref 271. Copyright 2021 American Chemical Society.

active species proceed directly to the oxidative degradation of metronidazole and isoniazid, respectively, due to their greater effect on decreasing the photocatalytic activity.

5.6.4. ESR Analysis—Spin Trap with DMPO. ESR analysis—spin trap with DMPO (5,5-dimethyl-1-pyrroline *N*-oxide) was carried out to confirm the role of active species in the photocatalytic degradation of organic pollutants under light radiation. As demonstrated in Figure 6, there are two distinct peaks related to the $O_2^{\bullet-}$ (see Figure 6a) and $OH^{\bullet}$ (see Figure 6b)[294] as radical species trapped with DMPO in the ESR spectrum, which are invisible in the absence of light irradiation. The intensity of the recorded signals is in direct proportion with passing time for $O_2^{\bullet-}$ or $OH^{\bullet}$ (see Figure 6c).[295]

https://doi.org/10.1021/acsomega.3c08717
ACS Omega 2024, 9, 25457−25492

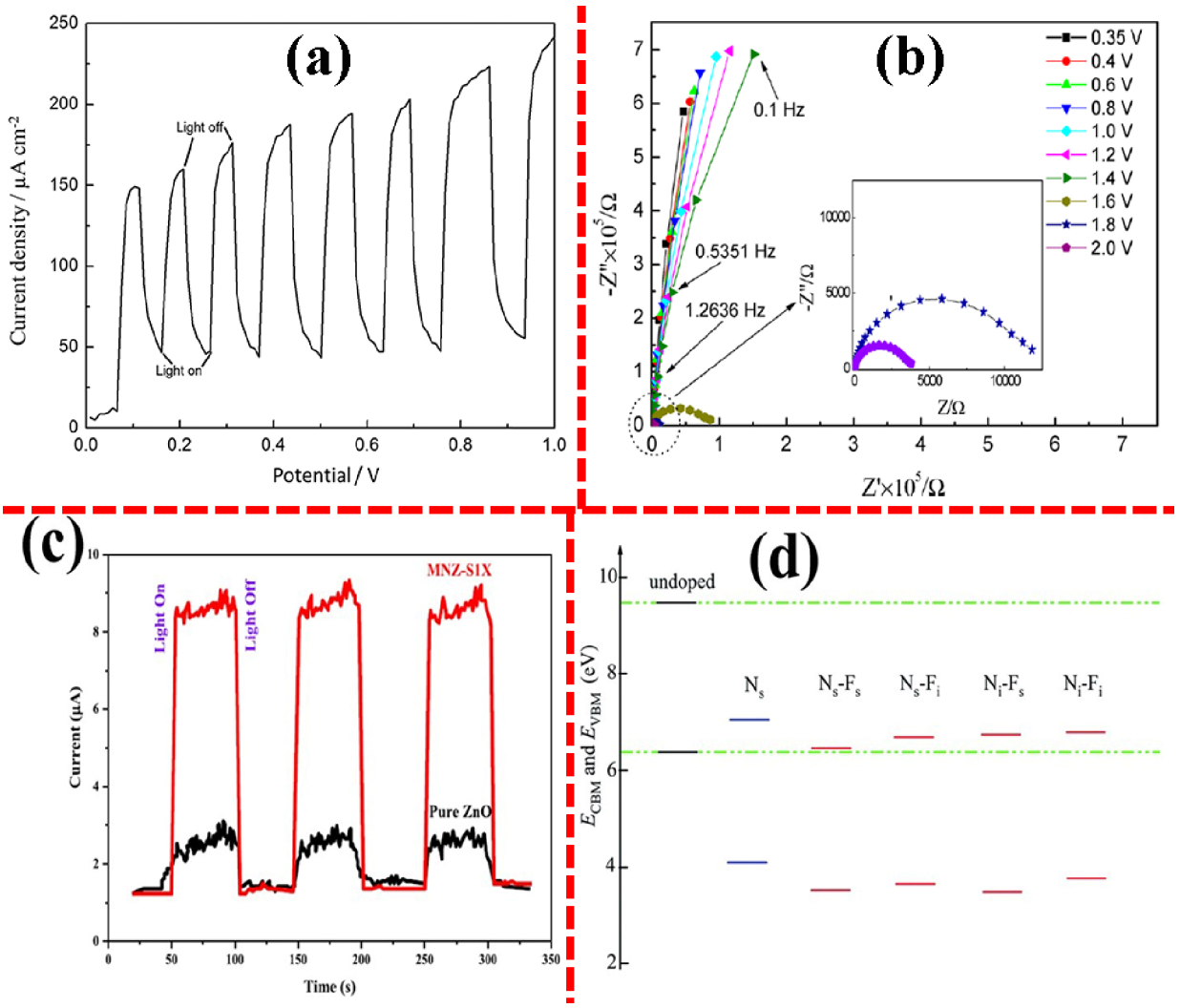

Figure 8. (a) Plot of the EIS response of $Sn_{0.39}Ti_{0.61}O_2$. Reprinted in part with permission from ref 303. Copyright 2020 American Chemical Society. (b) Impedance plot for TiO_2 in the rutile state. Reprinted in part with permission from ref 304. Copyright 2014 American Chemical Society. (c) EIS plot of pure ZnO and silane-modified ZnO. Reprinted in part with permission from ref 305. Copyright 2023 Elsevier. (d) Comparison of E_{CBM} and E_{VBM} of electronic states of N- and F-doped titanium. Reprinted in part with permission from ref 306. Copyright 2017 Royal Society of Chemistry.

Shi et al.[276] prepared a biochar/H_2−TiO_2 composite to evaluate the photoremoval of enrofloxacin under solar radiation. Results of ESR-DMPO spectroscopy are indicated in Figure 6d. As seen in the spectrum, there are no significant signals in the dark condition in the presence of the biochar/H_2−TiO_2 nanocomposite. Some trival signals were attributed to the superoxide anion radicals created during the preparation step and under ambient light irradiation. Distinct and sharp signals can be seen in the presence of the biochar/H_2−TiO_2 nanocomposite under light irradiation, which ascertained the formation of $O_2^{\bullet-}$ in the presence of light.

5.6.5. Photoluminescence (PL) Spectroscopy. Due to the impermanent nature of photogenerated hydroxyl radicals, PL spectroscopy is an indirect method to detect $OH^{\bullet}$ generated during a photoexcitation reaction by introducing a probe molecule like terephthalic acid or cumarin as a scavenger of OH. PL spectroscopy is recommended because of measurable photoluminescence signal emission from the products, e.g., TAOH and 7-OHC at 338 and 315 nm, respectively. A summary of the PL mechanism in the anatase structure of TiO_2 is presented in Figure 7a.[296]

In situ photoluminescence spectroscopy (PL) is a suitable analysis to study the effects of any dopant on the photoexcited recombination speed of photocatalysts. Higher intensity of the PL signal plotted on the spectrum indicates faster photogenerated carrier recombination, which is associated with the decrease in photocatalytic activity and amounts of active sites on the surface of the photocatalyst. Wafi et al.[297] fabricated TiO_2/RGO nanocomposites and evaluated their photocatalytic efficiency against the photodegradation of MB and *p*-aminophenol dyes. Study of the photocatalytic capacity was done by PL spectroscopy to compare pure titanium with the nanocomposite. Fluorescence emission confirmed the photocatalytic improvement of the TiO_2/RGO nanocomposite due to graphene participation in titanium structure and appropriate prevention from recombination. The fluorescence emission intensity increased with time, which resulted from a decrease in the photogenerated population in the solution. Zhang et al.[298] reported the PL analysis of carbon dot-modified ZnO. As demonstrated in Figure 7b, different molar ratios of glycine to ZnO nanocrystals ((a) 1:3, (b) 2:1, and (d) 3:1) and pure ZnO nanocrystals were studied. In the Figure 7c, the resulting fluorescence spectra of some nanocomposites of TiO_2/WO_3 in

https://doi.org/10.1021/acsomega.3c08717
ACS Omega 2024, 9, 25457−25492

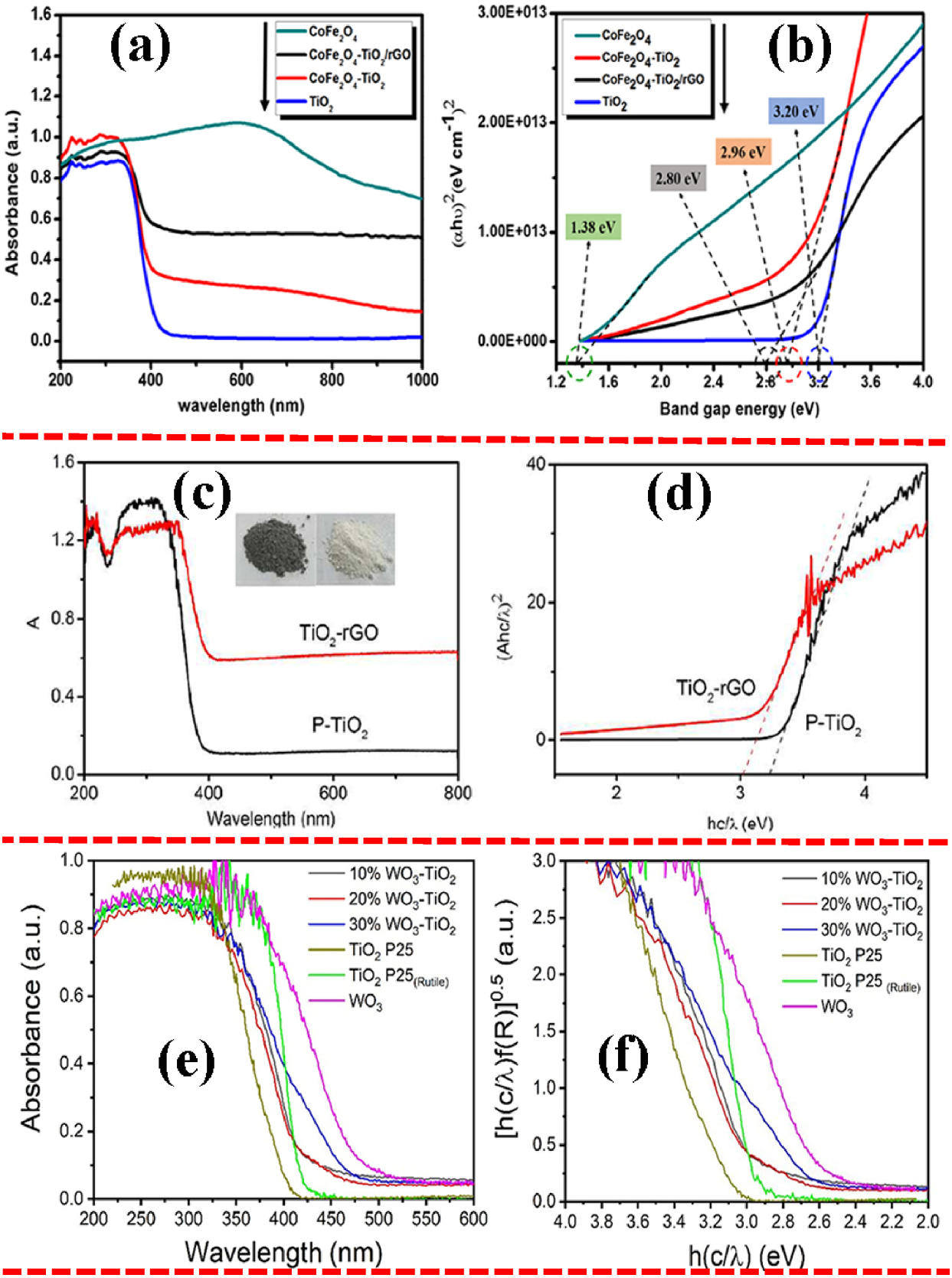

Figure 9. (a) UV−vis absorption spectra and (b) Tauc plot of $CoFeO_4$−TiO_2/rGO. Reprinted in part with permission from ref 309. Copyright 2019 American Chemical Society. (c) UV−vis absorption spectra and (d) Tauc plot of TiO_2/rGO. Reprinted in part with permission from ref 310. Copyright 2017 American Chemical Society. (e) Absorption spectra and (f) KM plot of pristine TiO_2(rutile)/WO_3/TiO_2 (anatase). Reprinted in part with permission from ref 271. Copyright 2021 American Chemical Society.

https://doi.org/10.1021/acsomega.3c08717
ACS Omega 2024, 9, 25457−25492

the presence of 2-hydroxy-terphthalic acid under a 315 nm excitation wave are shown, as reported by Pinedo-Escobar et al.[271] As can be seen, the TiO_2 loaded with 10% WO_3 responded better to the excitation light; therefore, increased production of hydroxyl radicals and holes is expected.

5.6.6. Electrochemical Impedance Spectroscopy (EIS). According to the charge transfer process, electrochemical impedance spectroscopy (EIS) was performed to measure charge carrier recombination time and photoexcited electron lifetime in photocatalysts, fuel cells, and Li-based batteries. The EIS response of photocatalysts determines their efficiency against the photodegradation of pollutants. EIS diagrams show the photocurrent density over time throughout several cycles of photon irradiation. Based on the work of Li et al.,[299] a good photocatalyst shows good photostability and intense pulses of photocurrent during cycles. The Nyquist plots are in line with the EIS response diagram due to assessing resistance against the interfacial photoexcited charge transfer. The curvature of any plot confirms its resistance against the movement of charge carriers. Less curvature means better efficiency of the photocatalysts.[300−302] As demonstrated in Figure 8a, Sohail et al.[303] reported EIS analysis of TiO_2 doped with Sn as a $Sn_{0.39}Ti_{0.61}O_2$·TiO_2 nanocomposite. According to Figure 8b, Ge et al.[304] reported an impedance plot of TiO_2 in the rutile state. The results of the $NaSO_4$ solution (0.1 M) at several anodizing potentials show some semicircles due to the space charge layer on the semiconductors. Eftekharipour et al.[305] synthesized silane-modified nano-ZnO heterojunction photocatalysts (NZ-HT) by the hydrothermal method and investigated their efficiency against the photodegradation of benzene. As can be seen in Figure 8c, the EIS plot (time response curve) of the fabricated photocatalysts confirmed that nano-ZnO modified with BTPA (as silane source) showed more flexibility than pure ZnO and less resistance against charge transient and optical flow. The photoelectrochemical improvement was due to the strong interaction between the chemical bond of BTPA and nano-ZnO, which facilitated electron transfer.

5.6.7. Band Gap Energy (E_{bg}) Calculation. Tauc's relation (eq 13) is used to calculate band gap energy of photoactive compounds at a distinct photon striking energy.

$$(\alpha h\upsilon) = A(h\upsilon - E_{bg})^n \tag{13}$$

Here, α, $h\upsilon$, and E_{bg} correspond to absorbance, the energy of incidental light (eV), and the band gap energy (eV), respectively, along with a representative of a relevant characteristic parameter and n equal to 1/2. In the following, wavelength (λ, nm) is converted to corresponding band gap energy (eV) by using eq 14.

$$E_{bg}(\text{eV}) = 1240/\lambda(\text{nm}) \tag{14}$$

According to the Tauc plot, the band gap energy of the compounds participating in the nanocomposite structures is calculated by extrapolating the linear part of the $(\alpha h\upsilon)_2$ vs $h\upsilon$ plot.

Kaur et al.[307] measured band gap energies of pristine titanium and some structures modified with PANI (TP2, TP4, TP6, and TP8) by plotting absorbance versus wavelength (λ, nm). The range of absorption peaks was set at 314−325 nm, which was a function of wt % PANI. E_{bg} (eV) was calculated according to the Tauc equation.

Schünemann et al.[308] reported the result of the Tauc plot. The band gap energy of bare TiO_2 decreased from 3.0 to 2.3 eV after preparing $CsPbBr_3/TiO_2$. In fact, sensitizing titanium with a halide perovskite ($CsPbBr_3$) caused a red shift from the UV region (413 nm) to the visible area (530 nm). Hafeez et al.[309] plotted DRS and Tauc results of a ternary composite of $CoFeO_4$−TiO_2/rGO, as demonstrated in Figure 9a and b.

Singhal et al.[263] synthesized a new ZnO-based photocatalyst with deposited self-assembled Ag, which was loaded on the surface of the carbon nanospheres (CNSs). Reduction of the band gap energy with modification techniques is consistent with the improvement of photocatalytic activity. The photodegradation efficiency of MB in the presence of CNSs, ZNO/CNSs, and AZCN with band gap energies of 3.54 3.15, and 3.04 eV, respectively, obtained 65.0% (60 min), 85.6% (25 min), and 95.0% (15 min), respectively, under UV light irradiation (315 nm). Zhang et al.[310] prepared a composite of TiO_2/rGO, and the results of DRS and Tauc plot are represented in Figure 9c and d, respectively. The Tauc plot confirms narrowing band gap of the TiO_2/rGO nanocomposite against pure TiO_2.

Another way to calculate E_{bg} is plotting the Kubelka−Munk (KM) function of any participating components in the photocatalytic structures. Diffuse reflectance spectroscopy (DRS) is used to estimate the optical band gap energy. The intercept of the DRS plot $(F(R)h\upsilon)^{1/2}$ vs $h\upsilon$ determines the band gap energy of participating compounds in photocatalytic structures.[311,312]

Mohamed et al.[313] studied photocatalytic effects of titanium quantum dots (TDs) by the sol−gel method in some polar solvents, which resulted in excellent specific surface area. Investigation and calculation of band gap energies were done by UV−vis DRS spectroscopy and the KM function, respectively. According to the mentioned plots, the enhancement in band gap energy was attributed to the smaller quantum size of TDs in comparison with TiO_2 (P25). TD1 had smaller particle size than TD2, therefore having more specific area and in turn having more efficiency in the photodegradation of the textile dye. Pinedo-Escobar et al.[271] reported the synthesis of new composites of TiO_2 in rutile and anatase forms with WO_3 and evaluated their photocatalytic activity against MO photodegradation. Absorption spectra and KM plots of these nanocomposites are illustrated in Figure 9e and f, respectively.

Priya et al.[314] synthesized a visible-active photocatalyst denoted as $BiFeWO_6$/ZnO for the decomposition of RhB. The Kubelka−Munk (KM) function was plotted to obtain the band gap energy of any participating components in the photocatalytic study. It should be noted that although $BiFeWO_6$ has a narrow band gap energy, its charge carrier recombination is too fast to use individually as a photocatalyst.

5.6.8. E_{CBM} and E_{VBM}. The other electronic properties of photocatalysts are band edge energies (E_{CBM} and E_{VBM}), which are affected by the orbital coordination of modifying agents. In bare TiO_2 and ZnO, the 2p orbital of O and 3d orbitals of Ti or Zn determine electronic properties, while doped agents cause the rearrangement and tuning of novel electronic states. Zhao et al.[306] studied N- and F-doped titanium as modified photocatalysts and evaluated their E_{CBM} and E_{VBM} theoretically to determine the redox potential of the photocatalytic system. According to Figure 8d, doping with N and F made the photoelectronic system of titanium more stable (more than 2.33 eV) and shifted it to the red region; therefore, titanium functionality was enhanced in terms of absorption of an extended light irradiation region.

https://doi.org/10.1021/acsomega.3c08717
ACS Omega 2024, 9, 25457−25492

6. CONCLUSION AND FUTURE PROSPECTS

A literature survey was performed to investigate the removal of organic pollutants in the air and wastewater via a photocatalytic process utilizing TiO_2- and ZnO-based photocatalysts. Some main advantages of photocatalytic reactions are the consumption of illimitable energy sources, conversion of organic pollutants to nontoxic compounds, and removal of trace amounts of organic pollutants. Three steps toward perform launching a photocatalytic reaction were studied, including synthesis, modification, and mechanistic routes. According to the heterogeneous nature of photocatalytic compounds, several synthetic methods were exemplified for the preparation of solid forms of photocatalysts with distinct properties like crystallinity, pore size, and specific surface area. Modification of TiO_2- and ZnO-based photocatalysts was done to shift high photoexcitation energy toward the red area of the electromagnetic region. Doping with metal or nonmetals as well as other semiconductors is among the modification strategies. What was the most important area in the photocatalytic field was identifying mechanistic routes of charge carrier transfer between the VB and CB in order to reach the surface of the photocatalysts and degrade adsorbed organic pollutants via the absorption of light irradiation. Detection of photoexcited species and other ROSs with some scavengers are useful techniques to determine photocatalytic efficiency against an organic pollutant photodegradation process. On the basis of the cost-effectiveness and easy accessibility of TiO_2- and ZnO-based photocatalysts, it would be precious to extend their scope of use from laboratory scale to the industrial area for removing organic pollutants from liquid, solid, and gas effluents. Novel treatment and structural sophistication of TiO_2 and/or ZnO composites improve their photocatalytic activity. Distribution on films, modification with other impurities, and fixation with an inert framework are some approaches to enhance their physical and chemical limitations toward photodegradation of air and water-soluble pollutants. It seems that theoretical calculations and kinetic studies of designed structures would be helpful before experimental steps. Trying new applications toward more extensive use, particularly in building materials and paints, causes effective photodegradation of air pollutants. As future aspects, designing new hybrids of TiO_2 and ZnO with conductive 2D materials, distributing photocatalysts on a resin film, and combining them with building paints would be an applicable approach against selective photoremoval of air or water-soluble pollutants.

AUTHOR INFORMATION

Corresponding Author

Reza Ghamarpoor − *Department of Petroleum Engineering, Faculty of Engineering, University of Garmsar, Garmsar 3588115589, Iran; Constructional Polymers and Composites Research Lab, School of Chemical, Petroleum and Gas Engineering, Iran University of Science and Technology (IUST), Tehran 1311416846, Iran;* orcid.org/0009-0006-6582-351X; Phone: ++98-912-972-4374; Email: reza_ghamarpoor@alumni.iust.ac.ir

Authors

Akram Fallah − *Department of Chemical Technologies, Iranian Research Organization for Science and Technology (IROST), Tehran 3313193685, Iran*

Masoud Jamshidi − *Constructional Polymers and Composites Research Lab, School of Chemical, Petroleum and Gas Engineering, Iran University of Science and Technology (IUST), Tehran 1311416846, Iran;* orcid.org/0000-0002-3512-6370

Complete contact information is available at: https://pubs.acs.org/10.1021/acsomega.3c08717

Notes

The authors declare no competing financial interest.

ACKNOWLEDGMENTS

The corresponding author of this work appreciates all of the team members.

REFERENCES

(1) Bhattu, M.; Singh, J. Recent advances in nanomaterials based sustainable approaches for mitigation of emerging organic pollutants. *Chemosphere* **2023**, *321*, No. 138072.

(2) Ghamarpoor, R.; Jamshidi, M. Silanizing nano SiO2 and its application in recycled nitrile rubber to prepare super oil resistant/superhydrophobic/superoleophilic oil/water separator. *Journal of Environmental Chemical Engineering* **2022**, *10* (3), No. 107971.

(3) Ma, J.; Wang, Y.; Zhang, Z.; Wang, X.; Hou, X.; Hu, Q. Conventional and toxic pollutants removal of toxic herbal wastewater by using moving bed biofilm reactor, coagulation, and adsorption. *Journal of Environmental Chemical Engineering* **2024**, *12*, No. 112705.

(4) Devendrapandi, G.; Balu, R.; Ayyappan, K.; Ayyamperumal, R.; Alhammadi, S.; Lavanya, M.; Senthilkumar, R.; Karthika, P. Unearthing Earth's secrets: Exploring the environmental legacy of contaminants in soil, water, and sediments. *Environmental Research* **2024**, *249*, No. 118246.

(5) Ma, D.; Wang, D.; Wang, X.; Wang, Q.; Hu, Y. Efficient treatment of old landfill leachate by peroxodisulfate assisted electro-oxidation and electro-coagulation combined system. *Chemosphere* **2024**, *346*, No. 140675.

(6) Booton, A.; Mayer, B. K.; Zitomer, D. H. Chemical oxidation as an alternative for municipal wastewater secondary treatment: a review. *Rev. Environ. Sci. Biotechnol.* **2024**, *23*, 43−65.

(7) Shi, W.; Ren, H.; Huang, X.; Li, M.; Tang, Y.; Guo, F. Low cost red mud modified graphitic carbon nitride for the removal of organic pollutants in wastewater by the synergistic effect of adsorption and photocatalysis. *Sep. Purif. Technol.* **2020**, *237*, No. 116477.

(8) Opoku, F.; Kiarii, E. M.; Govender, P. P.; Mamo, M. A. Metal oxide polymer nanocomposites in water treatments. In *Descriptive inorganic chemistry researches of metal compounds*; Akitsu, T., Ed.; IntechOpen: London, UK, 2017; pp 173−199.

(9) Son, B. T.; Long, N. V.; Hang, N. T. N. Fly ash-, foundry sand-, clay-, and pumice-based metal oxide nanocomposites as green photocatalysts. *RSC Adv.* **2021**, *11* (49), 30805−30826.

(10) Jabbar, Z. H.; Graimed, B. H.; Ammar, S. H.; Sabit, D. A.; Najim, A. A.; Radeef, A. Y.; Taher, A. G. The latest progress in the design and application of semiconductor photocatalysis systems for degradation of environmental pollutants in wastewater: Mechanism insight and theoretical calculations. *Materials Science in Semiconductor Processing* **2024**, *173*, No. 108153.

(11) Louis, J.; Padmanabhan, N. T.; Jayaraj, M. K.; John, H. Exploring enhanced interfacial charge separation in ZnO/reduced graphene oxide hybrids on alkaline photoelectrochemical water splitting and photocatalytic pollutant degradation. *Mater. Res. Bull.* **2024**, *169*, No. 112542.

(12) Omar, S.; Omar, M.; Attia, N. F.; El-Subruiti, G. M.; Eltaweil, A. Rational engineering and fabrication of efficient nanophotocatalysts based on ZnO-SrO-CdS for pharmaceutical pollutants based wastewater degradation. *Surfaces and Interfaces* **2024**, *45*, No. 103817.

(13) Montalvo, D.; Corro, G.; Bañuelos, F.; Olivares-Xometl, O.; Arellanes, P.; Pal, U. Selective alcohols production through CO2 photoreduction using Co3O4/TiO2 photocatalyst exploiting synergetic interactions between Ti3+, Co2+ and Co3+. *Applied Catalysis B: Environmental* **2023**, *330*, No. 122652.

(14) Rad, A. S.; Afshar, A.; Azadeh, M. Antireflection and photocatalytic single layer and double layer ZnO and ZnO−TiO2 thin films. *Opt. Mater.* **2023**, *136*, No. 113501.
(15) Esquivel-Castro, T.; Robledo-Trujillo, G.; Oliva, J.; Rosu, H.; Rodríguez-González, V. A functional SiO2-TiO2 mesoporous assembly designed for the controlled release of carvacrol. *Applied Surface Science Advances* **2023**, *13*, No. 100378.
(16) Yao, Y.; Wang, Z.; Han, Y.; Xie, L.; Zhao, X.; Shahrokhian, S.; Barsan, N.; Zhu, Z. Conductometric Cr2O3/TiO2/Ti3C2Tx gas sensor for detecting triethylamine at room temperature. *Sens. Actuators, B* **2023**, *381*, No. 133412.
(17) Amu-Darko, J. N. O.; Hussain, S.; Zhang, X.; Alothman, A. A.; Ouladsmane, M.; Nazir, M. T.; Qiao, G.; Liu, G. Metal-organic frameworks-derived In2O3/ZnO porous hollow nanocages for highly sensitive H2S gas sensor. *Chemosphere* **2023**, *314*, No. 137670.
(18) El Gohary, H. G.; Alhagri, I. A.; Qahtan, T. F.; Al-Hakimi, A. N.; Saeed, A.; Abolaban, F.; Alshammari, E. M.; Asnag, G. Reinforcement of structural, thermal and electrical properties and antibacterial activity of PVA/SA blend filled with hybrid nanoparticles (Ag and TiO2 NPs): Nanodielectric for energy storage and food packaging industries. *Ceram. Int.* **2023**, *49* (12), 20174−20184.
(19) Yıldırım, H. Excitons in nonpolar ZnO/BeZnO quantum wells: Their binding energy and its dependence on the dimensions of the structures. *Physica B: Condensed Matter* **2022**, *639*, No. 413974.
(20) Karthikeyan, C.; Arunachalam, P.; Ramachandran, K.; Al-Mayouf, A. M.; Karuppuchamy, S. Recent advances in semiconductor metal oxides with enhanced methods for solar photocatalytic applications. *J. Alloys Compd.* **2020**, *828*, No. 154281.
(21) Chen, X.; Wu, Z.; Liu, D.; Gao, Z. Preparation of ZnO photocatalyst for the efficient and rapid photocatalytic degradation of azo dyes. *Nanoscale Res. Lett.* **2017**, *12*, 143.
(22) Saldaña-Ramírez, A.; Cruz, M. A.; Juárez-Ramírez, I.; Torres-Martínez, L. M. Influence of the power density and working pressure in the magnetron co-sputtering deposition of ZnO−SnO2 thin films and their effect in photocatalytic hydrogen production. *Opt. Mater.* **2020**, *110*, No. 110501.
(23) Ghamarpoor, R.; Fallah, A.; Jamshidi, M. Investigating the use of titanium dioxide (TiO2) nanoparticles on the amount of protection against UV irradiation. *Sci. Rep.* **2023**, *13*, 9793.
(24) Ghamarpoor, R.; Fallah, A.; Jamshidi, M.; Salehfekr, S. Using waste silver metal in synthesis of Z-scheme Ag@ WO3-CeO2 heterojunction to increase photodegradation and electrochemical performances. *Journal of Industrial and Engineering Chemistry* **2023**, *128*, 459−471.
(25) Moradi, N.; Jamshidi, M.; Ghamarpoor, R.; Moghbeli, M. R. Surface functionalization/silane modification of CeO2 nanoparticles and their influences on photocatalytic activity of acrylic films for methylene blue removal. *Prog. Org. Coat.* **2023**, *183*, No. 107787.
(26) Chen, S.; Zhao, W.; Liu, W.; Zhang, S. Preparation, characterization and activity evaluation of p−n junction photocatalyst p-ZnO/n-TiO2. *Appl. Surf. Sci.* **2008**, *255* (5), 2478−2484.
(27) Han, J.; Liu, Y.; Singhal, N.; Wang, L.; Gao, W. Comparative photocatalytic degradation of estrone in water by ZnO and TiO2 under artificial UVA and solar irradiation. *Chemical Engineering Journal* **2012**, *213*, 150−162.
(28) Wang, L.; Liu, S.; Wang, Z.; Zhou, Y.; Qin, Y.; Wang, Z. L. Piezotronic effect enhanced photocatalysis in strained anisotropic ZnO/TiO2 nanoplatelets via thermal stress. *ACS Nano* **2016**, *10* (2), 2636−2643.
(29) Pérez-González, M.; Tomás, S.; Morales-Luna, M.; Arvizu, M.; Tellez-Cruz, M. Optical, structural, and morphological properties of photocatalytic TiO2−ZnO thin films synthesized by the sol−gel process. *Thin Solid Films* **2015**, *594*, 304−309.
(30) Ghamarpoor, R.; Fallah, A.; Eghbali, T. Design of Bifunctional Sandwich-like Co@ Si/Ox-MXene Nanocomposite to Increase the Supercapacitor Properties and Removal of Pollutants from Wastewater. *J. Alloys Compd.* **2024**, *983*, No. 173920.
(31) Kumar, S. G.; Rao, K. K. Comparison of modification strategies towards enhanced charge carrier separation and photocatalytic degradation activity of metal oxide semiconductors (TiO2, WO3 and ZnO). *Appl. Surf. Sci.* **2017**, *391*, 124−148.
(32) Patil, S. B.; Basavarajappa, P. S.; Ganganagappa, N.; Jyothi, M.; Raghu, A.; Reddy, K. R. Recent advances in non-metals-doped TiO2 nanostructured photocatalysts for visible-light driven hydrogen production, CO2 reduction and air purification. *Int. J. Hydrogen Energy* **2019**, *44* (26), 13022−13039.
(33) Rehman, S.; Ullah, R.; Butt, A.; Gohar, N. Strategies of making TiO2 and ZnO visible light active. *Journal of hazardous materials* **2009**, *170* (2−3), 560−569.
(34) Singhal, N.; Kumar, U. Noble metal modified TiO2: selective photoreduction of CO2 to hydrocarbons. *Molecular Catalysis* **2017**, *439*, 91−99.
(35) Farhadian, N.; Akbarzadeh, R.; Pirsaheb, M.; Jen, T.-C.; Fakhri, Y.; Asadi, A. Chitosan modified N, S-doped TiO2 and N, S-doped ZnO for visible light photocatalytic degradation of tetracycline. *Int. J. Biol. Macromol.* **2019**, *132*, 360−373.
(36) Ding, Z.; Sun, M.; Liu, W.; Meng, X.; Zheng, Y.; Sun, W.; Zhou, Q. In-situ growth of N−TiO2 on delaminated N−Ti3C2 with highly strengthened photocatalytic activity. *Int. J. Hydrogen Energy* **2022**, *47* (49), 21204−21219.
(37) Inturi, S. N. R.; Boningari, T.; Suidan, M.; Smirniotis, P. G. Visible-light-induced photodegradation of gas phase acetonitrile using aerosol-made transition metal (V, Cr, Fe, Co, Mn, Mo, Ni, Cu, Y, Ce, and Zr) doped TiO2. *Applied Catalysis B: Environmental* **2014**, *144*, 333−342.
(38) Sukhadeve, G.; Bandewar, H.; Janbandhu, S.; Jayaramaiah, J.; Gedam, R. Photocatalytic hydrogen production, dye degradation, and antimicrobial activity by Ag-Fe co-doped TiO2 nanoparticles. *J. Mol. Liq.* **2023**, *369*, No. 120948.
(39) Kim, S.-S.; Yum, J.-H.; Sung, Y.-E. Flexible dye-sensitized solar cells using ZnO coated TiO2 nanoparticles. *J. Photochem. Photobiol., A* **2005**, *171* (3), 269−273.
(40) Xiao, L.; Youji, L.; Feitai, C.; Peng, X.; Ming, L. Facile synthesis of mesoporous titanium dioxide doped by Ag-coated graphene with enhanced visible-light photocatalytic performance for methylene blue degradation. *Rsc Advances* **2017**, *7* (41), 25314−25324.
(41) Wang, Q.; Zhao, Y.; Zhang, Z.; Liao, S.; Deng, Y.; Wang, X.; Ye, Q.; Wang, K. Hydrothermal preparation of Sn3O4/TiO2 nanotube arrays as effective photocatalysts for boosting photocatalytic dye degradation and hydrogen production. *Ceram. Int.* **2023**, *49* (4), 5977−5985.
(42) Kovács, Z.; Molnár, C.; Gyulavári, T.; Magyari, K.; Tóth, Z.-R.; Baia, L.; Pap, Z.; Hernádi, K. Solvothermal synthesis of ZnO spheres: Tuning the structure and morphology from nano-to micro-meter range and its impact on their photocatalytic activity. *Catal. Today* **2022**, *397*, 16−27.
(43) Ahmad, S.; Aadil, M.; Ejaz, S. R.; Akhtar, M. U.; Noor, H.; Haider, S.; Alsafari, I. A.; Yasmin, G. Sol-gel synthesis of nanostructured ZnO/SrZnO2 with boosted antibacterial and photocatalytic activity. *Ceram. Int.* **2022**, *48* (2), 2394−2405.
(44) Shawky, A.; Alshaikh, H. Cobalt ferrite-modified sol-gel synthesized ZnO nanoplatelets for fast and bearable visible light remediation of ciprofloxacin in water. *Environmental Research* **2022**, *205*, No. 112462.
(45) Saeed, M.; Khan, I.; Adeel, M.; Akram, N.; Muneer, M. Synthesis of a CoO−ZnO photocatalyst for enhanced visible-light assisted photodegradation of methylene blue. *New J. Chem.* **2022**, *46* (5), 2224−2231.
(46) Li, J.; Chu, B.; Xie, Z.; Deng, Y.; Zhou, Y.; Dong, L.; Li, B.; Chen, Z. Mechanism and DFT study of degradation of organic pollutants on rare earth ions doped TiO2 photocatalysts prepared by sol-hydrothermal synthesis. *Catal. Lett.* **2022**, *152* (2), 489−502.
(47) Hu, W.; Zhou, W.; Zhang, K.; Zhang, X.; Wang, L.; Jiang, B.; Tian, G.; Zhao, D.; Fu, H. Facile strategy for controllable synthesis of stable mesoporous black TiO 2 hollow spheres with efficient solar-driven photocatalytic hydrogen evolution. *Journal of Materials Chemistry A* **2016**, *4* (19), 7495−7502.

https://doi.org/10.1021/acsomega.3c08717
ACS Omega 2024, 9, 25457−25492

(48) Kozlova, E. A.; Kurenkova, A. Y.; Gerasimov, E. Y.; Gromov, N. V.; Medvedeva, T. B.; Saraev, A. A.; Kaichev, V. V. Comparative study of photoreforming of glycerol on Pt/TiO2 and CuOx/TiO2 photocatalysts under UV light. *Mater. Lett.* **2021**, *283*, No. 128901.
(49) Maheswari, P.; Sugapriya, S.; Krishnaveni, N.; Senthil, T. Investigation of Pure and CuO-and ZnO-Loaded TiO2 Nanocomposites Prepared by Modified Hydrothermal Cum Green Synthesis (Hybanthus enneaspermus Extract) Method for Photocatalytic and Antioxidant Applications. *Braz. J. Phys.* **2022**, *52* (4), 142.
(50) Dong, D.; Wang, K.; Yi, M.; Liang, Y.; Muhammad, Y.; Wei, E.; Wei, Y.; Fujita, T. Preparation of TiO2 photocatalyst microspheres by geopolymer technology for the degradation of tetracycline. *Journal of Cleaner Production* **2022**, *339*, No. 130734.
(51) Xiao, X.; Tu, S.; Lu, M.; Zhong, H.; Zheng, C.; Zuo, X.; Nan, J. Discussion on the reaction mechanism of the photocatalytic degradation of organic contaminants from a viewpoint of semiconductor photo-induced electrocatalysis. *Applied Catalysis B: Environmental* **2016**, *198*, 124−132.
(52) Qiang, C.; Li, N.; Zuo, S.; Guo, Z.; Zhan, W.; Li, Z.; Ma, J. Microwave-assisted synthesis of RuTe2/black TiO2 photocatalyst for enhanced diclofenac degradation: Performance, mechanistic investigation and intermediates analysis. *Sep. Purif. Technol.* **2022**, *283*, No. 120214.
(53) Popay, J.; Roberts, H.; Sowden, A.; Petticrew, M.; Arai, L.; Rodgers, M.; Britten, N.; Roen, K.; Duffy, S. *Guidance on the conduct of narrative synthesis in systematic reviews: A product from the ESRC methods programme*; Lancaster University: Lancaster, UK, 2006.
(54) Tranfield, D.; Denyer, D.; Smart, P. Towards a methodology for developing evidence-informed management knowledge by means of systematic review. *British journal of management* **2003**, *14* (3), 207−222.
(55) Centobelli, P.; Cerchione, R.; Esposito, E. Environmental sustainability in the service industry of transportation and logistics service providers: Systematic literature review and research directions. *Transportation Research Part D: Transport and Environment* **2017**, *53*, 454−470.
(56) Cambra-López, M.; Aarnink, A. J.; Zhao, Y.; Calvet, S.; Torres, A. G. Airborne particulate matter from livestock production systems: A review of an air pollution problem. *Environmental pollution* **2010**, *158* (1), 1−17.
(57) Urashima, K.; Chang, J.-S. Removal of volatile organic compounds from air streams and industrial flue gases by non-thermal plasma technology. *IEEE Trans. Dielect. Electr. Insul.* **2000**, *7* (5), 602−614.
(58) Li, F.; Liu, G.; Liu, F.; Wu, J.; Yang, S. Synergetic effect of CQD and oxygen vacancy to TiO2 photocatalyst for boosting visible photocatalytic NO removal. *Journal of Hazardous Materials* **2023**, *452*, No. 131237.
(59) Mohamed, Y. M.; Attia, Y. A. Nano Pt/TiO2 photocatalyst for ultrafast production of sulfamic acid derivatives using 4-nitroacetanilides as nitrogen precursor in continuous flow reactors. *Environmental Science and Pollution Research* **2023**, *30* (17), 51344−51355.
(60) Bashal, A. H.; Alkanad, K.; Al-Ghorbani, M.; Aoun, S. B.; Bajiri, M. A. Synergistic effect of cocatalyst and S-scheme heterojunction over 2D/2D g-C3N4/MoS2 heterostructure coupled Cu nanoparticles for selective photocatalytic CO2 reduction to CO under visible light irradiation. *J. Environ. Chem. Eng.* **2023**, *11* (2), No. 109545.
(61) Lee, J.; Jang, J.; Kim, J.; Lim, S.-H. A recyclable indoor air filter system based on a photocatalytic metal−organic framework for the removal of harmful volatile organic compounds. *Chemical Engineering Journal* **2022**, *430*, No. 132891.
(62) Boviatsis, M.; Alexopoulos, A.; Vlachos, G. Evaluation of the response to emerging environmental threats, focusing on carbon dioxide (CO2), volatile organic compounds (VOCs), and scrubber wash water (SOx). *Euro-Mediterranean Journal for Environmental Integration* **2022**, *7* (3), 391−398.
(63) Islam, A.; Teo, S. H.; Ng, C. H.; Taufiq-Yap, Y. H.; Choong, S. Y. T.; Awual, M. R. Progress in recent sustainable materials for greenhouse gas (NOx and SOx) emission mitigation. *Prog. Mater. Sci.* **2023**, *132*, No. 101033.
(64) Zhang, X.; Gao, B.; Creamer, A. E.; Cao, C.; Li, Y. Adsorption of VOCs onto engineered carbon materials: A review. *Journal of hazardous materials* **2017**, *338*, 102−123.
(65) Lewis, A. C.; Hopkins, J. R.; Carslaw, D. C.; Hamilton, J. F.; Nelson, B. S.; Stewart, G.; Dernie, J.; Passant, N.; Murrells, T. An increasing role for solvent emissions and implications for future measurements of volatile organic compounds. *Philosophical Transactions of the Royal Society A* **2020**, *378* (2183), No. 20190328.
(66) Sharma, R.; Agrawal, P. R.; Chankit; Chanchal; Ittishree; Kashyap, V.; Sharma, A. K.; Alagesan, V. Industrial Waste-Derived Materials for Adsorption of Heavy Metals from Polluted Water. *Remediation of Heavy Metals: Sustainable Technologies and Recent Advances* **2024**, 169−197.
(67) Talukdar, A.; Kundu, P.; Bhattacharya, S.; Dutta, N. Microplastic contamination in wastewater: Sources, distribution, detection and remediation through physical and chemical-biological methods. *Science of The Total Environment* **2024**, *916*, No. 170254.
(68) Ghamarpoor, R.; Jamshidi, M. Preparation of Superhydrophobic/Superoleophilic nitrile rubber (NBR) nanocomposites contained silanized nano silica for efficient oil/water separation. *Sep. Purif. Technol.* **2022**, *291*, No. 120854.
(69) Ghamarpoor, R.; Jamshidi, M. Synergistic effect of microwave assisted devulcanization of waste NBR rubber and using superhydrophobic/superoleophilic silica nanoparticles on oil-water separation. *Alexandria Engineering Journal* **2023**, *69*, 67−84.
(70) Kiwaan, H.; Atwee, T.; Azab, E.; El-Bindary, A. Photocatalytic degradation of organic dyes in the presence of nanostructured titanium dioxide. *J. Mol. Struct.* **2020**, *1200*, No. 127115.
(71) Mao, Y.; Li, Y.; Zou, Y.; Shen, X.; Zhu, L.; Liao, G. Solvothermal synthesis and photocatalytic properties of ZnO micro/nanostructures. *Ceram. Int.* **2019**, *45* (2), 1724−1729.
(72) Dave, S. R.; Patel, T. L.; Tipre, D. R. Bacterial degradation of azo dye containing wastes. *Microbial degradation of synthetic dyes in wastewaters* **2015**, 57−83.
(73) Katheresan, V.; Kansedo, J.; Lau, S. Y. Efficiency of various recent wastewater dye removal methods: A review. *Journal of environmental chemical engineering* **2018**, *6* (4), 4676−4697.
(74) Solayman, H.M.; Hossen, M. A.; Abd Aziz, A.; Yahya, N. Y.; Leong, K. H.; Sim, L. C.; Monir, M. U.; Zoh, K.-D. Performance evaluation of dye wastewater treatment technologies: A review. *J. Environ. Chem. Eng.* **2023**, *11*, No. 109610.
(75) Ahmaruzzaman, M. Adsorption of phenolic compounds on low-cost adsorbents: a review. *Advances in colloid and interface science* **2008**, *143* (1−2), 48−67.
(76) Zhong, W.; Wang, D.; Xu, X. Phenol removal efficiencies of sewage treatment processes and ecological risks associated with phenols in effluents. *Journal of Hazardous Materials* **2012**, *217*, 286−292.
(77) Zhang, Y.; Zhang, L.; Huang, Z.; Li, Y.; Li, J.; Wu, N.; He, J.; Zhang, Z.; Liu, Y.; Niu, Z. Pollution of polycyclic aromatic hydrocarbons (PAHs) in drinking water of China: Composition, distribution and influencing factors. *Ecotoxicology and Environmental Safety* **2019**, *177*, 108−116.
(78) Behera, B. K.; Das, A.; Sarkar, D. J.; Weerathunge, P.; Parida, P. K.; Das, B. K.; Thavamani, P.; Ramanathan, R.; Bansal, V. Polycyclic Aromatic Hydrocarbons (PAHs) in inland aquatic ecosystems: Perils and remedies through biosensors and bioremediation. *Environmental pollution* **2018**, *241*, 212−233.
(79) Suman, S.; Sinha, A.; Tarafdar, A. Polycyclic aromatic hydrocarbons (PAHs) concentration levels, pattern, source identification and soil toxicity assessment in urban traffic soil of Dhanbad, India. *Sci. Total Environ.* **2016**, *545*, 353−360.
(80) Ghamarpoor, R.; Ebrahimabadi, A. Optimum design of water-based drilling fluid in shale formations in Khangiran oilfields. *Progress in Industrial Ecology, an International Journal* **2019**, *13* (1), 42−62.
(81) Shahsavari, E.; Schwarz, A.; Aburto-Medina, A.; Ball, A. S. Biological degradation of polycyclic aromatic compounds (PAHs) in soil: a current perspective. *Current Pollution Reports* **2019**, *5*, 84−92.

https://doi.org/10.1021/acsomega.3c08717
ACS Omega 2024, 9, 25457−25492

(82) Agrawal, N.; Verma, P.; Shahi, S. K. Degradation of polycyclic aromatic hydrocarbons (phenanthrene and pyrene) by the ligninolytic fungi Ganoderma lucidum isolated from the hardwood stump. *Bioresour. Bioprocess.* **2018**, *5*, 11.
(83) Gupta, S.; Graham, D. W.; Sreekrishnan, T.; Ahammad, S. Z. Heavy metal and antibiotic resistance in four Indian and UK rivers with different levels and types of water pollution. *Science of The Total Environment* **2023**, *857*, No. 159059.
(84) Nguyen, M.-K.; Lin, C.; Nguyen, H.-L.; Hung, N. T. Q.; La, D. D.; Nguyen, X. H.; Chang, S. W.; Chung, W. J.; Nguyen, D. D. Occurrence, fate, and potential risk of pharmaceutical pollutants in agriculture: Challenges and environmentally friendly solutions. *Science of The Total Environment* **2023**, *899*, No. 165323.
(85) Gupta, T.; Samriti; Cho, J.; Prakash, J. Hydrothermal synthesis of TiO2 nanorods: formation chemistry, growth mechanism, and tailoring of surface properties for photocatalytic activities. *Mater. Today Chem.* **2021**, *20*, No. 100428.
(86) Ho, W.; Yu, J. C.; Lee, S. Low-temperature hydrothermal synthesis of S-doped TiO2 with visible light photocatalytic activity. *J. Solid State Chem.* **2006**, *179* (4), 1171−1176.
(87) Siwińska-Stefańska, K.; Kubiak, A.; Piasecki, A.; Dobrowolska, A.; Czaczyk, K.; Motylenko, M.; Rafaja, D.; Ehrlich, H.; Jesionowski, T. Hydrothermal synthesis of multifunctional TiO2-ZnO oxide systems with desired antibacterial and photocatalytic properties. *Appl. Surf. Sci.* **2019**, *463*, 791−801.
(88) Saleh, S. M. ZnO nanospheres based simple hydrothermal route for photocatalytic degradation of azo dye. *Spectrochimica Acta Part A: Molecular and Biomolecular Spectroscopy* **2019**, *211*, 141−147.
(89) Danks, A. E.; Hall, S. R.; Schnepp, Z. The evolution of 'sol−gel'chemistry as a technique for materials synthesis. *Materials Horizons* **2016**, *3* (2), 91−112.
(90) Phin, H.-Y.; Ong, Y.-T.; Sin, J.-C. Effect of carbon nanotubes loading on the photocatalytic activity of zinc oxide/carbon nanotubes photocatalyst synthesized via a modified sol-gel method. *Journal of Environmental Chemical Engineering* **2020**, *8* (3), No. 103222.
(91) Palanisamy, B.; Babu, C.; Sundaravel, B.; Anandan, S.; Murugesan, V. Sol−gel synthesis of mesoporous mixed Fe2O3/TiO2 photocatalyst: application for degradation of 4-chlorophenol. *Journal of hazardous materials* **2013**, *252*, 233−242.
(92) Fan, Z.; Meng, F.; Zhang, M.; Wu, Z.; Sun, Z.; Li, A. Solvothermal synthesis of hierarchical TiO2 nanostructures with tunable morphology and enhanced photocatalytic activity. *Appl. Surf. Sci.* **2016**, *360*, 298−305.
(93) Kusiak-Nejman, E.; Wojnarowicz, J.; Morawski, A.; Narkiewicz, U.; Sobczak, K.; Gierlotka, S.; Lojkowski, W. Size-dependent effects of ZnO nanoparticles on the photocatalytic degradation of phenol in a water solution. *Appl. Surf. Sci.* **2021**, *541*, No. 148416.
(94) Huang, D.-G.; Liao, S.-J.; Liu, J.-M.; Dang, Z.; Petrik, L. Preparation of visible-light responsive N−F-codoped TiO2 photocatalyst by a sol−gel-solvothermal method. *J. Photochem. Photobiol., A* **2006**, *184* (3), 282−288.
(95) Ramakrishnan, V. M.; Natarajan, M.; Santhanam, A.; Asokan, V.; Velauthapillai, D. Size controlled synthesis of TiO2 nanoparticles by modified solvothermal method towards effective photo catalytic and photovoltaic applications. *Mater. Res. Bull.* **2018**, *97*, 351−360.
(96) Zulfiqar, M.; Sufian, S.; Mansor, N.; Rabat, N. E. Synthesis and characterization of TiO2-based nanostructures via fluorine-free solvothermal method for enhancing visible light photocatalytic activity: Experimental and theoretical approach. *J. Photochem. Photobiol., A* **2021**, *404*, No. 112834.
(97) Wu, L.; Wang, X.; Wang, W.; Li, J.; Li, X. Fabrication of amorphous TiO2 shell layer on Ag2CO3 surface with enhanced photocatalytic activity and photostability. *J. Alloys Compd.* **2019**, *806*, 603−610.
(98) Henni, A.; Harfouche, N.; Karar, A.; Zerrouki, D.; Perrin, F.; Rosei, F. Synthesis of graphene−ZnO nanocomposites by a one-step electrochemical deposition for efficient photocatalytic degradation of organic pollutant. *Solid State Sci.* **2019**, *98*, No. 106039.
(99) Çırak, B. B.; Caglar, B.; Kılınç, T.; Karadeniz, S. M.; Erdoğan, Y.; Kılıç, S.; Kahveci, E.; Ekinci, A. E.; Çırak, Ç. Synthesis and characterization of ZnO nanorice decorated TiO2 nanotubes for enhanced photocatalytic activity. *Mater. Res. Bull.* **2019**, *109*, 160−167.
(100) Lang, J.; Takahashi, K.; Kubo, M.; Shimada, M. Preparation of TiO2-CNT-Ag ternary composite film with enhanced photocatalytic activity via plasma-enhanced chemical vapor deposition. *Catalysts* **2022**, *12* (5), 508.
(101) Wong, Y.; Li, Y.; Lin, Z.; Kafizas, A. Studying the effects of processing parameters in the aerosol-assisted chemical vapour deposition of TiO2 coatings on glass for applications in photocatalytic NOx remediation. *Applied Catalysis A: General* **2022**, *648*, No. 118924.
(102) Taylor, M.; Pullar, R. C.; Parkin, I. P.; Piccirillo, C. Nanostructured titanium dioxide coatings prepared by aerosol assisted chemical vapour deposition (AACVD). *J. Photochem. Photobiol., A* **2020**, *400*, No. 112727.
(103) Yang, W.-D.; Li, Y.-R.; Lee, Y.-C. Synthesis of r-GO/TiO2 composites via the UV-assisted photocatalytic reduction of graphene oxide. *Appl. Surf. Sci.* **2016**, *380*, 249−256.
(104) Andronic, L.; Enesca, A. Black TiO2 synthesis by chemical reduction methods for photocatalysis applications. *Frontiers in Chemistry* **2020**, *8*, No. 565489.
(105) Malik, A. R.; Sharif, S.; Shaheen, F.; Khalid, M.; Iqbal, Y.; Faisal, A.; Aziz, M. H.; Atif, M.; Ahmad, S.; Fakhar-e-Alam, M.; et al. Green synthesis of RGO-ZnO mediated Ocimum basilicum leaves extract nanocomposite for antioxidant, antibacterial, antidiabetic and photocatalytic activity. *J. Saudi Chem. Soc.* **2022**, *26* (2), No. 101438.
(106) Revathi, J.; Abel, M. J.; Archana, V.; Sumithra, T.; Thiruneelakandan, R.; Joseph Prince, J. Synthesis and characterization of CoFe2O4 and Ni-doped CoFe2O4 nanoparticles by chemical Co-precipitation technique for photo-degradation of organic dyestuffs under direct sunlight. *Physica B: Condensed Matter* **2020**, *587*, No. 412136.
(107) Ali, W.; Ullah, H.; Zada, A.; Muhammad, W.; Ali, S.; Shaheen, S.; Alamgir, M. K.; Ansar, M. Z.; Khan, Z. U.; Bilal, H.; et al. Synthesis of TiO2 modified self-assembled honeycomb ZnO/SnO2 nanocomposites for exceptional photocatalytic degradation of 2, 4-dichlorophenol and bisphenol A. *Sci. Total Environ.* **2020**, *746*, No. 141291.
(108) Lassoued, M. S.; Lassoued, A.; Ammar, S.; Gadri, A.; Salah, A. B.; García-Granda, S. Synthesis and characterization of Co-doped nano-TiO 2 through co-precipitation method for photocatalytic activity. *Journal of Materials Science: Materials in Electronics* **2018**, *29*, 8914−8922.
(109) Mahendran, V.; Gogate, P. R. Degradation of Acid Scarlet 3R dye using oxidation strategies involving photocatalysis based on Fe doped TiO2 photocatalyst, ultrasound and hydrogen peroxide. *Sep. Purif. Technol.* **2021**, *274*, No. 119011.
(110) Bazazi, S.; Arsalani, N.; Khataee, A.; Tabrizi, A. G. Comparison of ball milling-hydrothermal and hydrothermal methods for synthesis of ZnO nanostructures and evaluation of their photocatalytic performance. *Journal of industrial and engineering chemistry* **2018**, *62*, 265−272.
(111) Wu, D.; Li, C.; Zhang, D.; Wang, L.; Zhang, X.; Shi, Z.; Lin, Q. Enhanced photocatalytic activity of Gd3+ doped TiO2 and Gd2O3 modified TiO2 prepared via ball milling method. *Journal of Rare Earths* **2019**, *37* (8), 845−852.
(112) Yu, F.; Tian, F.; Zou, H.; Ye, Z.; Peng, C.; Huang, J.; Zheng, Y.; Zhang, Y.; Yang, Y.; Wei, X.; et al. ZnO/biochar nanocomposites via solvent free ball milling for enhanced adsorption and photocatalytic degradation of methylene blue. *J. Hazard. Mater.* **2021**, *415*, No. 125511.
(113) Ye, M.; Pan, J.; Guo, Z.; Liu, X.; Chen, Y. Effect of ball milling process on the photocatalytic performance of CdS/TiO2 composite. *Nanotechnol. Rev.* **2020**, *9* (1), 558−567.
(114) Shafei, A.; Salarpour, M.; Sheibani, S. Effect of intermediate ball milling on the synthesis of Cu-doped TiO 2 nano-photocatalyst by sol−gel method. *J. Sol-Gel Sci. Technol.* **2019**, *92*, 173−185.
(115) Phromma, S.; Wutikhun, T.; Kasamechonchung, P.; Eksangsri, T.; Sapcharoenkun, C. Effect of calcination temperature on photo-

https://doi.org/10.1021/acsomega.3c08717
ACS Omega 2024, 9, 25457−25492

catalytic activity of synthesized TiO2 nanoparticles via wet ball milling sol-gel method. *Applied Sciences* **2020**, *10* (3), 993.
(116) Bouarioua, A.; Zerdaoui, M. Photocatalytic activities of TiO2 layers immobilized on glass substrates by dip-coating technique toward the decolorization of methyl orange as a model organic pollutant. *Journal of Environmental Chemical Engineering* **2017**, *5* (2), 1565−1574.
(117) Away, R. D. Y.; Takai-Yamashita, C.; Ban, T.; Ohya, Y. Photocatalytic properties of TiO2-SiO2 sandwich multilayer films prepared by sol-gel dip-coating. *Thin Solid Films* **2021**, *720*, No. 138522.
(118) Parul; Kaur, K.; Badru, R.; Singh, P. P.; Kaushal, S. Photodegradation of organic pollutants using heterojunctions: A review. *J. Environ. Chem. Eng.* **2020**, *8* (2), No. 103666.
(119) Thongsuriwong, K.; Amornpitoksuk, P.; Suwanboon, S. Structure, morphology, photocatalytic and antibacterial activities of ZnO thin films prepared by sol−gel dip-coating method. *Advanced Powder Technology* **2013**, *24* (1), 275−280.
(120) Tekin, D.; Kiziltas, H.; Ungan, H. Kinetic evaluation of ZnO/TiO2 thin film photocatalyst in photocatalytic degradation of Orange G. *J. Mol. Liq.* **2020**, *306*, No. 112905.
(121) Al Farsi, B.; Souier, T.; Al Marzouqi, F.; Al Maashani, M.; Bououdina, M.; Widatallah, H.; Al Abri, M. Structural and optical properties of visible active photocatalytic Al doped ZnO nanostructured thin films prepared by dip coating. *Opt. Mater.* **2021**, *113*, No. 110868.
(122) Navío, J. A.; Colon, G.; Trillas, M. a.; Peral, J.; Domenech, X.; Testa, J. J.; Padron, J.; Rodríguez, D.; Litter, M. I. Heterogeneous photocatalytic reactions of nitrite oxidation and Cr (VI) reduction on iron-doped titania prepared by the wet impregnation method. *Applied Catalysis B: Environmental* **1998**, *16* (2), 187−196.
(123) Mishra, S.; Chakinala, N.; Chakinala, A. G.; Surolia, P. K. Photocatalytic degradation of methylene blue using monometallic and bimetallic Bi-Fe doped TiO2. *Catal. Commun.* **2022**, *171*, No. 106518.
(124) Kumaresan, N.; Ramamurthi, K. Synthesis of ZnO/rGO nanocomposites by wet impregnation method for photocatalytic performance against RhB dye and 4-chlorophenol under UV light irradiation. *Journal of Materials Science: Materials in Electronics* **2020**, *31*, 3361−3374.
(125) Bernareggi, M.; Chiarello, G. L.; West, G.; Ratova, M.; Ferretti, A. M.; Kelly, P.; Selli, E. Cu and Pt clusters deposition on TiO2 powders by DC magnetron sputtering for photocatalytic hydrogen production. *Catalysis today* **2019**, *326*, 15−21.
(126) Mekasuwandumrong, O.; Jantarasorn, N.; Panpranot, J.; Ratova, M.; Kelly, P.; Praserthdam, P. Synthesis of Cu/TiO2 catalysts by reactive magnetron sputtering deposition and its application for photocatalytic reduction of CO2 and H2O to CH4. *Ceram. Int.* **2019**, *45* (17), 22961−22971.
(127) Tao, T.; Bae, I.-T.; Woodruff, K. B.; Sauer, K.; Cho, J. Hydrothermally-grown nanostructured anatase TiO2 coatings tailored for photocatalytic and antibacterial properties. *Ceram. Int.* **2019**, *45* (17), 23216−23224.
(128) Wei, K.; Faraj, Y.; Yao, G.; Xie, R.; Lai, B. Strategies for improving perovskite photocatalysts reactivity for organic pollutants degradation: A review on recent progress. *Chemical Engineering Journal* **2021**, *414*, No. 128783.
(129) Petronella, F.; Truppi, A.; Ingrosso, C.; Placido, T.; Striccoli, M.; Curri, M.; Agostiano, A.; Comparelli, R. Nanocomposite materials for photocatalytic degradation of pollutants. *Catal. Today* **2017**, *281*, 85−100.
(130) Yaqoob, A. A.; Mohd Noor, N. H. b.; Serrà, A.; Mohamad Ibrahim, M. N. Advances and challenges in developing efficient graphene oxide-based ZnO photocatalysts for dye photo-oxidation. *Nanomaterials* **2020**, *10* (5), 932.
(131) Kumar, R.; Ansari, M. O.; Taleb, M. A.; Oves, M.; Barakat, M. A.; Alghamdi, M. A.; Al Makishah, N. H. Integrated Adsorption-Photocatalytic Decontamination of Oxytetracycline from Wastewater Using S-Doped TiO2/WS2/Calcium Alginate Beads. *Catalysts* **2022**, *12* (12), 1676.
(132) Ortiz, G. M. H.; Parra, R.; Fuchs, V.; Fanovich, M. A. TiO 2-HA composites obtained by combination of sol−gel synthesis and a supercritical CO2 drying process. *J. Sol-Gel Sci. Technol.* **2022**, *101*, 205−214.
(133) Shankar, S.; Rhim, J.-W. Effect of types of zinc oxide nanoparticles on structural, mechanical and antibacterial properties of poly (lactide)/poly (butylene adipate-co-terephthalate) composite films. *Food Packaging and Shelf Life* **2019**, *21*, No. 100327.
(134) Li, L.; Wang, L.; Hu, T.; Zhang, W.; Zhang, X.; Chen, X. Preparation of highly photocatalytic active CdS/TiO2 nanocomposites by combining chemical bath deposition and microwave-assisted hydrothermal synthesis. *J. Solid State Chem.* **2014**, *218*, 81−89.
(135) Ferreira-Neto, E. P.; Ullah, S.; Simões, M. B.; Perissinotto, A. P.; de Vicente, F. S.; Noeske, P.-L. M.; Ribeiro, S. J.; Rodrigues-Filho, U. P. Solvent-controlled deposition of titania on silica spheres for the preparation of SiO2@ TiO2 core@ shell nanoparticles with enhanced photocatalytic activity. *Colloids Surf., A* **2019**, *570*, 293−305.
(136) Zhang, Q.; Li, C. TiO2 coated ZnO nanorods by mist chemical vapor deposition for application as photoanodes for dye-sensitized solar cells. *Nanomaterials* **2019**, *9* (9), 1339.
(137) Javed, M.; Qamar, M. A.; Shahid, S.; Alsaab, H. O.; Asif, S. Highly efficient visible light active Cu−ZnO/SgC 3 N 4 nanocomposites for efficient photocatalytic degradation of organic pollutants. *RSC Adv.* **2021**, *11* (59), 37254−37267.
(138) Abomuti, M. A.; Danish, E. Y.; Firoz, A.; Hasan, N.; Malik, M. A. Green synthesis of zinc oxide nanoparticles using salvia officinalis leaf extract and their photocatalytic and antifungal activities. *Biology* **2021**, *10* (11), 1075.
(139) Wirunchit, S.; Gansa, P.; Koetniyom, W. Synthesis of ZnO nanoparticles by Ball-milling process for biological applications. *Materials Today: Proceedings* **2021**, *47*, 3554−3559.
(140) Rinaudo, M. G.; Beltrán, A. M.; Fernández, M. A.; Cadús, L. E.; Morales, M. R. Tailoring materials by high-energy ball milling: TiO2 mixtures for catalyst support application. *Materials Today Chemistry* **2020**, *17*, No. 100340.
(141) Benaboud, A.; Zaabat, M.; Aida, M.; Boudine, B.; Benzitouni, S.; Saidani, T. Fe2O4/ZnO-nanowires synthesis by dip-coating for Orange II-dye photodegradation. *Optik* **2017**, *144*, 397−405.
(142) Hu, J.; Zhong, Z.; Zhang, F.; Xing, W.; Low, Z.-X.; Fan, Y. Coating of ZnO nanoparticles onto the inner pore channel surface of SiC foam to fabricate a novel antibacterial air filter material. *Ceram. Int.* **2015**, *41* (5), 7080−7090.
(143) Cao, Y.-Q.; Zi, T.-Q.; Zhao, X.-R.; Liu, C.; Ren, Q.; Fang, J.-B.; Li, W.-M.; Li, A.-D. Enhanced visible light photocatalytic activity of Fe2O3 modified TiO2 prepared by atomic layer deposition. *Sci. Rep.* **2020**, *10*, No. 13437.
(144) Turcu, E.; Coromelci, C. G.; Harabagiu, V.; Ignat, M. Enhancing the photocatalytic activity of TiO2 for the degradation of congo red dye by adjusting the ultrasonication regime applied in its synthesis procedure. *Catalysts* **2023**, *13* (2), 345.
(145) Kennedy, A. J.; McQueen, A. D.; Ballentine, M. L.; May, L. R.; Fernando, B. M.; Das, A.; Klaus, K. L.; Williams, C. B.; Bortner, M. J. Degradation of microcystin algal toxin by 3D printable polymer immobilized photocatalytic TiO2. *Chemical Engineering Journal* **2023**, *455*, No. 140866.
(146) Zakia, M.; Yoo, S. I. Enhanced Photocatalytic Activity of TiO2 Nanoparticles Immobilized on Porous-Sulfonated Polystyrene Microspheres through Multiple Scattering Process. *Macromol. Res.* **2022**, *30* (9), 677−683.
(147) Vaiano, V.; Iervolino, G. Facile method to immobilize ZnO particles on glass spheres for the photocatalytic treatment of tannery wastewater. *J. Colloid Interface Sci.* **2018**, *518*, 192−199.
(148) Habibi, S.; Jamshidi, M. Synthesis of TiO2 nanoparticles coated on cellulose nanofibers with different morphologies: Effect of the template and sol-gel parameters. *Materials Science in Semiconductor Processing* **2020**, *109*, No. 104927.
(149) Monfared, A. H.; Jamshidi, M. Synthesis of polyaniline/titanium dioxide nanocomposite (PAni/TiO2) and its application as

https://doi.org/10.1021/acsomega.3c08717
ACS Omega 2024, 9, 25457−25492

photocatalyst in acrylic pseudo paint for benzene removal under UV/VIS lights. *Prog. Org. Coat.* **2019**, *136*, No. 105257.
(150) Gyulavári, T.; Márta, V.; Kovács, Z.; Magyari, K.; Kása, Z.; Veréb, G.; Pap, Z.; Hernadi, K. Immobilization of highly active titanium dioxide and zinc oxide hollow spheres on ceramic paper and their applicability for photocatalytic water treatment. *J. Photochem. Photobiol., A* **2022**, *427*, No. 113791.
(151) Hou, L.; Wang, L.; Royer, S.; Zhang, H. Ultrasound-assisted heterogeneous Fenton-like degradation of tetracycline over a magnetite catalyst. *Journal of hazardous materials* **2016**, *302*, 458−467.
(152) Aminuddin, N.; Nawi, M.; Bahrudin, N. Enhancing the optical properties of immobilized TiO2/polyaniline bilayer photocatalyst for methyl orange decolorization. *React. Funct. Polym.* **2022**, *174*, No. 105248.
(153) Mousa, H. M.; Alenezi, J. F.; Mohamed, I. M.; Yasin, A. S.; Hashem, A.-F. M.; Abdal-Hay, A. Synthesis of TiO2@ ZnO heterojunction for dye photodegradation and wastewater treatment. *J. Alloys Compd.* **2021**, *886*, No. 161169.
(154) Lal, M.; Sharma, P.; Ram, C. Synthesis and photocatalytic potential of Nd-doped TiO2 under UV and solar light irradiation using a sol-gel ultrasonication method. *Results in Materials* **2022**, *15*, No. 100308.
(155) Ge, Y.; Luo, H.; Huang, J.; Zhang, Z. Visible-light-active TiO2 photocatalyst for efficient photodegradation of organic dyes. *Opt. Mater.* **2021**, *115*, No. 111058.
(156) Xu, D.; Ma, H. Degradation of rhodamine B in water by ultrasound-assisted TiO2 photocatalysis. *Journal of Cleaner Production* **2021**, *313*, No. 127758.
(157) Makama, A.; Salmiaton, A.; Choong, T.; Hamid, M.; Abdullah, N.; Saion, E. Influence of parameters and radical scavengers on the visible-light-induced degradation of ciprofloxacin in ZnO/SnS2 nanocomposite suspension: Identification of transformation products. *Chemosphere* **2020**, *253*, No. 126689.
(158) Arekhi, M.; Jamshidi, M. Influences of inorganic binder on photocatalytic oxidation (PCO) and degradation of nano/micro TiO2 containing acrylic composites. *Prog. Org. Coat.* **2018**, *115*, 1−8.
(159) Wang, J.; Wang, Z.; Zhao, D.; Liang, Y.; Wang, H.; Wang, N.; Jiang, W.; Liu, S.; Liu, C.; Ding, W.; et al. Preparation, structural and photocatalytic activity of Sn/Fe co-doped TiO2 nanoparticles by sol-gel method. *Ceram. Int.* **2022**, *48* (6), 8297−8305.
(160) Sukhadeve, G.; Janbandhu, S.; Kumar, R.; Lataye, D.; Ramteke, D.; Gedam, R. Visible light assisted photocatalytic degradation of Indigo Carmine dye and NO2 removal by Fe doped TiO2 nanoparticles. *Ceram. Int.* **2022**, *48* (19), 29121−29135.
(161) Lee, H.; Park, J.; Lam, S. S.; Park, Y.-K.; Kim, S.-C.; Jung, S.-C. Diclofenac degradation properties of a La-doped visible light-responsive TiO2 photocatalyst. *Sustainable Chemistry and Pharmacy* **2022**, *25*, No. 100564.
(162) Viet, N. M.; Huong, N. T. M.; Hoai, P. T. T. Enhanced photocatalytic decomposition of phenol in wastewater by using La−TiO2 nanocomposite. *Chemosphere* **2023**, *313*, No. 137605.
(163) Bazyar, Z.; Tavakoliana, M.; Hosseini-Sarvari, M. Au−Pd@ ZnO alloy nanoparticles: a promising heterogeneous photocatalyst toward decarboxylative trifluoromethylation under visible-light irradiation. *New J. Chem.* **2022**, *46* (31), 14903−14909.
(164) Arumugam, M.; Koutavarapu, R.; Seralathan, K.-K.; Praserthdam, S.; Praserthdam, P. Noble metals (Pd, Ag, Pt, and Au) doped bismuth oxybromide photocatalysts for improved visible light-driven catalytic activity for the degradation of phenol. *Chemosphere* **2023**, *324*, No. 138368.
(165) Ataabadi, M. R.; Jamshidi, M. Improved photocatalytic degradation of methylene blue under visible light using acrylic nanocomposite contained silane grafted nano TiO2. *J. Photochem. Photobiol., A* **2023**, *443*, No. 114832.
(166) Asadi, A.; Daglioglu, N.; Hasani, T.; Farhadian, N. Construction of Mg-doped ZnO/g-C3N4@ ZIF-8 multi-component catalyst with superior catalytic performance for the degradation of illicit drug under visible light. *Colloids Surf., A* **2022**, *650*, No. 129536.
(167) Tanji, K.; El Mrabet, I.; Fahoul, Y.; Soussi, A.; Belghiti, M.; Jellal, I.; Naciri, Y.; El Gaidoumi, A.; Kherbeche, A. Experimental and theoretical investigation of enhancing the photocatalytic activity of Mg doped ZnO for nitrophenol degradation. *Reaction Kinetics, Mechanisms and Catalysis* **2023**, *136* (2), 1125−1142.
(168) Gao, D.; Liu, W.; Xu, Y.; Wang, P.; Fan, J.; Yu, H. Core-shell Ag@ Ni cocatalyst on the TiO2 photocatalyst: one-step photoinduced deposition and its improved H2-evolution activity. *Applied Catalysis B: Environmental* **2020**, *260*, No. 118190.
(169) Liu, Y.; Zhang, Q.; Xu, M.; Yuan, H.; Chen, Y.; Zhang, J.; Luo, K.; Zhang, J.; You, B. Novel and efficient synthesis of Ag-ZnO nanoparticles for the sunlight-induced photocatalytic degradation. *Appl. Surf. Sci.* **2019**, *476*, 632−640.
(170) Lopes, F. C. S.M.R.; da Rocha, M. d. G. C.; Bargiela, P.; Sousa Ferreira, H.; Pires, C. A. d. M. Ag/TiO2 photocatalyst immobilized onto modified natural fibers for photodegradation of anthracene. *Chem. Eng. Sci.* **2020**, *227*, No. 115939.
(171) Adeel, M.; Saeed, M.; Khan, I.; Muneer, M.; Akram, N. Synthesis and characterization of Co−ZnO and evaluation of its photocatalytic activity for photodegradation of methyl orange. *ACS omega* **2021**, *6* (2), 1426−1435.
(172) Hassan, S. M.; Ahmed, A. I.; Mannaa, M. A. Preparation and characterization of SnO2 doped TiO2 nanoparticles: Effect of phase changes on the photocatalytic and catalytic activity. *Journal of Science: Advanced Materials and Devices* **2019**, *4* (3), 400−412.
(173) Ramírez, A. E.; Montero-Muñoz, M.; López, L. L.; Ramos-Ibarra, J. E.; Coaquira, J. A.; Heinrichs, B.; Páez, C. A. Significantly enhancement of sunlight photocatalytic performance of ZnO by doping with transition metal oxides. *Sci. Rep.* **2021**, *11*, 2804.
(174) Singh, A. R.; Dhumal, P. S.; Bhakare, M. A.; Lokhande, K. D.; Bondarde, M. P.; Some, S. In-situ synthesis of metal oxide and polymer decorated activated carbon-based photocatalyst for organic pollutants degradation. *Sep. Purif. Technol.* **2022**, *286*, No. 120380.
(175) Mohamed, R. M.; Ismail, A. A.; Alhaddad, M. A novel design of porous Cr2O3@ ZnO nanocomposites as highly efficient photocatalyst toward degradation of antibiotics: a case study of ciprofloxacin. *Sep. Purif. Technol.* **2021**, *266*, No. 118588.
(176) Chen, C.; Mei, W.; Wang, C.; Yang, Z.; Chen, X. a.; Chen, X.; Liu, T. Synthesis of a flower-like SnO/ZnO nanostructure with high catalytic activity and stability under natural sunlight. *J. Alloys Compd.* **2020**, *826*, No. 154122.
(177) Lam, S.-M.; Lim, C.-L.; Sin, J.-C.; Zeng, H.; Lin, H.; Li, H. Facile synthesis of MnO2/ZnO coated on cotton fabric for boosted antimicrobial, self-cleaning and photocatalytic activities under sunlight. *Mater. Lett.* **2021**, *305*, No. 130818.
(178) Xie, C.; Xu, L.; Xia, Y.; Gang, R.; Ye, Q.; Koppala, S. Evaluation of visible photocatalytic performance of microwave hydrothermal synthesis of MnO2/TiO2 core-shell structures and gaseous mercury removal. *Microporous Mesoporous Mater.* **2022**, *334*, No. 111788.
(179) Shoneye, A.; Jiao, H.; Tang, J. Bimetallic FeO x−MO x Loaded TiO2 (M= Cu, Co) Nanocomposite Photocatalysts for Complete Mineralization of Herbicides. *J. Phys. Chem. C* **2023**, *127*, 1388.
(180) Rini, N. P.; Istiqomah, N. I.; Sunarta; Suharyadi, E. Enhancing photodegradation of methylene blue and reusability using CoO/ZnO composite nanoparticles. *Case Studies Chem. Environ. Eng.* **2023**, *7*, No. 100301.
(181) Yu, G.; Hu, J.; Xiao, W.; Zhu, Y.; Dai, Y. Fabrication of black NiO/Sr2FeTaO6 heterojunctions with rapid interface charge transfer for efficient photocatalytic hydrogen evolution. *Frontiers in Chemistry* **2023**, *10*, No. 1118540.
(182) Wu, X.; Zhang, J.; Wang, H.; Huo, Y.; Xie, Z. Construction of 2D/0D Graphene Oxide/Copper (I) Oxide-Incorporated Titanium Dioxide Mixed-Dimensional Membranes with Ultrafast Water Transport and Enhanced Antifouling Properties. *ACS Appl. Mater. Interfaces* **2023**, *15*, 31561.
(183) Nekooie, R.; Shamspur, T.; Mostafavi, A. Novel CuO/TiO2/PANI nanocomposite: Preparation and photocatalytic investigation for chlorpyrifos degradation in water under visible light irradiation. *J. Photochem. Photobiol., A* **2021**, *407*, No. 113038.

https://doi.org/10.1021/acsomega.3c08717
ACS Omega 2024, 9, 25457−25492

(184) Baniamerian, H.; Safavi, M.; Alvarado-Morales, M.; Tsapekos, P.; Angelidaki, I.; Shokrollahzadeh, S. Photocatalytic inactivation of Vibrio fischeri using Fe2O3-TiO2-based nanoparticles. *Environmental research* **2018**, *166*, 497−506.
(185) Baniamerian, H.; Tsapekos, P.; Alvarado-Morales, M.; Shokrollahzadeh, S.; Safavi, M.; Angelidaki, I. Anti-algal activity of Fe2O3−TiO2 photocatalyst on Chlorella vulgaris species under visible light irradiation. *Chemosphere* **2020**, *242*, No. 125119.
(186) Jiang, J.; Mu, Z.; Xing, H.; Wu, Q.; Yue, X.; Lin, Y. Insights into the synergetic effect for enhanced UV/visible-light activated photodegradation activity via Cu-ZnO photocatalyst. *Appl. Surf. Sci.* **2019**, *478*, 1037−1045.
(187) Wang, S.; Zhu, B.; Liu, M.; Zhang, L.; Yu, J.; Zhou, M. Direct Z-scheme ZnO/CdS hierarchical photocatalyst for enhanced photocatalytic H2-production activity. *Applied Catalysis B: Environmental* **2019**, *243*, 19−26.
(188) Shoueir, K.; Kandil, S.; El-hosainy, H.; El-Kemary, M. Tailoring the surface reactivity of plasmonic Au@ TiO2 photocatalyst bio-based chitosan fiber towards cleaner of harmful water pollutants under visible-light irradiation. *Journal of Cleaner Production* **2019**, *230*, 383−393.
(189) Siwińska-Stefańska, K.; Kubiak, A.; Piasecki, A.; Goscianska, J.; Nowaczyk, G.; Jurga, S.; Jesionowski, T. TiO2-ZnO binary oxide systems: Comprehensive characterization and tests of photocatalytic activity. *Materials* **2018**, *11* (5), 841.
(190) Zhou, L.; Cai, M.; Zhang, X.; Cui, N.; Chen, G.; Zou, G.-y. In-situ nitrogen-doped black TiO2 with enhanced visible-light-driven photocatalytic inactivation of Microcystis aeruginosa cells: Synthesization, performance and mechanism. *Applied Catalysis B: Environmental* **2020**, *272*, No. 119019.
(191) Wang, Y.; Liu, X.; Guo, L.; Shang, L.; Ge, S.; Song, G.; Naik, N.; Shao, Q.; Lin, J.; Guo, Z. Metal organic framework-derived C-doped ZnO/TiO2 nanocomposite catalysts for enhanced photodegradation of Rhodamine B. *J. Colloid Interface Sci.* **2021**, *599*, 566−576.
(192) Gupta, B.; Gupta, A. K.; Ghosal, P. S.; Tiwary, C. S. Photo-induced degradation of bio-toxic Ciprofloxacin using the porous 3D hybrid architecture of an atomically thin sulfur-doped g-C3N4/ZnO nanosheet. *Environmental research* **2020**, *183*, No. 109154.
(193) Zhu, G.; Yang, X.; Liu, Y.; Zeng, Y.; Wang, T.; Yu, H. One-pot synthesis of C-modified and N-doped TiO2 for enhanced visible-light photocatalytic activity. *J. Alloys Compd.* **2022**, *902*, No. 163677.
(194) Mandor, H.; Amin, N. K.; Abdelwahab, O.; El-Ashtoukhy, E.-S. Z. Preparation and characterization of N-doped ZnO and N-doped TiO2 beads for photocatalytic degradation of phenol and ammonia. *Environmental Science and Pollution Research* **2022**, *29* (37), 56845−56862.
(195) Ghanbarnezhad, M.; Parvareh, A.; Moraveji, M. K.; Jorfi, S. La, S, N tri-doped TiO2/nickel foam as efficient photoelectrode for degradation of BTX solution under visible light irradiation. *J. Photochem. Photobiol., A* **2022**, *431*, No. 114044.
(196) Navarra, W.; Sacco, O.; Daniel, C.; Venditto, V.; Vaiano, V.; Vignati, D. A. L.; Bojic, C.; Libralato, G.; Lofrano, G.; Carotenuto, M. Photocatalytic degradation of atrazine by an N-doped TiO2/polymer composite: catalytic efficiency and toxicity evaluation. *Journal of Environmental Chemical Engineering* **2022**, *10* (4), No. 108167.
(197) Chen, J.; Liu, L.; Zheng, L.; Liu, M.; Gao, Y.; Zhao, K. Structural and optical properties of Fe@ C doped TiO2 thin films prepared by sol−gel method. *Inorg. Chem. Commun.* **2023**, *153*, No. 110776.
(198) Habibi, S.; Jamshidi, M. Sol−gel synthesis of carbon-doped TiO2 nanoparticles based on microcrystalline cellulose for efficient photocatalytic degradation of methylene blue under visible light. *Environ. Technol.* **2020**, *41* (24), 3233−3247.
(199) Kwak, C. H.; Im, U.-S.; Seo, S. W.; Kim, M. I.; Huh, Y. S.; Im, J. S. Effects of carbon doping on TiO2 for enhanced visible light-driven NO sensing performance. *Mater. Lett.* **2021**, *288*, No. 129313.
(200) Lin, X.; Rong, F.; Ji, X.; Fu, D. Carbon-doped mesoporous TiO2 film and its photocatalytic activity. *Microporous Mesoporous Mater.* **2011**, *142* (1), 276−281.
(201) Lv, X.; Deng, Z.; Wang, M.; Deng, J. Ti3C2MXene derived carbon-doped TiO2 multilayers anchored with Fe2O3 nanoparticles as anode for enhanced lithium-ion storage. *J. Alloys Compd.* **2022**, *918*, No. 165697.
(202) Negi, C.; Kandwal, P.; Rawat, J.; Sharma, M.; Sharma, H.; Dalapati, G.; Dwivedi, C. Carbon-doped titanium dioxide nanoparticles for visible light driven photocatalytic activity. *Appl. Surf. Sci.* **2021**, *554*, No. 149553.
(203) Khalid, N.; Ishtiaq, H.; Ali, F.; Tahir, M.; Naeem, S.; Ul-Hamid, A.; Ikram, M.; Iqbal, T.; Kamal, M. R.; Alrobei, H.; et al. Synergistic effects of Bi and N doped on ZnO nanorods for efficient photocatalysis. *Mater. Chem. Phys.* **2022**, *289*, No. 126423.
(204) Jiang, D.; Wei, M.; Du, X.; Qin, M.; Shan, X.; Chen, Z. One-pot synthesis of ZnO quantum dots/N-doped Ti3C2MXene: Tunable nitrogen-doping properties and efficient electrochemiluminescence sensing. *Chemical Engineering Journal* **2022**, *430*, No. 132771.
(205) Mirzaeifard, Z.; Shariatinia, Z.; Jourshabani, M.; Rezaei Darvishi, S. M. ZnO photocatalyst revisited: effective photocatalytic degradation of emerging contaminants using S-doped ZnO nanoparticles under visible light radiation. *Ind. Eng. Chem. Res.* **2020**, *59* (36), 15894−15911.
(206) Yu, W.; Zhang, J.; Peng, T. New insight into the enhanced photocatalytic activity of N-, C-and S-doped ZnO photocatalysts. *Applied Catalysis B: Environmental* **2016**, *181*, 220−227.
(207) Wang, J.-C.; Lou, H.-H.; Xu, Z.-H.; Cui, C.-X.; Li, Z.-J.; Jiang, K.; Zhang, Y.-P.; Qu, L.-B.; Shi, W. Natural sunlight driven highly efficient photocatalysis for simultaneous degradation of rhodamine B and methyl orange using I/C codoped TiO2 photocatalyst. *Journal of hazardous materials* **2018**, *360*, 356−363.
(208) Chung, K.-H.; Kim, B.-J.; Park, Y.-K.; Kim, S.-C.; Jung, S.-C. Photocatalytic properties of amorphous n-doped TiO2 photocatalyst under visible light irradiation. *Catalysts* **2021**, *11* (8), 1010.
(209) Hu, R.; Liao, G.; Huang, Z.; Qiao, H.; Liu, H.; Shu, Y.; Wang, B.; Qi, X. Recent advances of monoelemental 2D materials for photocatalytic applications. *Journal of Hazardous Materials* **2021**, *405*, No. 124179.
(210) Jung, H.; Pham, T.-T.; Shin, E. W. Effect of g-C3N4 precursors on the morphological structures of g-C3N4/ZnO composite photocatalysts. *J. Alloys Compd.* **2019**, *788*, 1084−1092.
(211) Lee, J.-T.; Lee, S.-W.; Wey, M.-Y. S-scheme g-C3N4/ZnO heterojunction photocatalyst with enhanced photodegradation of azo dye. *Journal of the Taiwan Institute of Chemical Engineers* **2022**, *134*, No. 104357.
(212) Chen, K.; Yan, K.; Xie, Q.; Zhu, H.; Li, X.; Dong, Z.; Yuan, G.; Zhang, J.; Cong, Y. MXene-derived C-doped TiO2/Ti3C2 heterojunction as a high-performance visible-light photocatalyst. *Res. Chem. Intermed.* **2022**, *48* (11), 4443−4458.
(213) Biswal, L.; Mohanty, R.; Nayak, S.; Parida, K. Review on MXene/TiO2 nanohybrids for photocatalytic hydrogen production and pollutant degradations. *Journal of Environmental Chemical Engineering* **2022**, *10*, No. 107211.
(214) Yang, W.; Ma, G.; Fu, Y.; Peng, K.; Yang, H.; Zhan, X.; Yang, W.; Wang, L.; Hou, H. Rationally designed Ti3C2MXene@ TiO2/CuInS2 Schottky/S-scheme integrated heterojunction for enhanced photocatalytic hydrogen evolution. *Chemical Engineering Journal* **2022**, *429*, No. 132381.
(215) Yu, X.; Xie, J.; Liu, Q.; Dong, H.; Li, Y. The origin of enhanced photocatalytic activity in g-C3N4/TiO2 heterostructure revealed by DFT calculations. *J. Colloid Interface Sci.* **2021**, *593*, 133−141.
(216) Paul, D. R.; Gautam, S.; Panchal, P.; Nehra, S. P.; Choudhary, P.; Sharma, A. ZnO-modified g-C3N4: a potential photocatalyst for environmental application. *ACS omega* **2020**, *5* (8), 3828−3838.
(217) Sodeinde, K.; Olusanya, S.; Lawal, O.; Sriariyanun, M.; Adediran, A. Enhanced adsorptional-photocatalytic degradation of chloramphenicol by reduced graphene oxide-zinc oxide nanocomposite. *Sci. Rep.* **2022**, *12*, No. 17054.
(218) Shaheen, S.; Iqbal, A.; Ikram, M.; Imran, M.; Naz, S.; Ul-Hamid, A.; Shahzadi, A.; Nabgan, W.; Haider, J.; Haider, A. Graphene oxide-ZnO nanorods for efficient dye degradation, antibacterial and in-silico analysis. *Appl. Nanosci.* **2022**, *12*, 165−177.

https://doi.org/10.1021/acsomega.3c08717
ACS Omega 2024, 9, 25457−25492

(219) Luo, L.; Meng, D.; He, L.; Wang, X.; Xia, L.; Pan, X.; Jiang, F.; Wang, H.; Dai, J. Photocatalytic activation of peroxydisulfate by a new porous g-C3N4/reduced graphene oxide/TiO2 nanobelts composite for efficient degradation of 17α-ethinylestradiol. *Chemical Engineering Journal* **2022**, *446*, No. 137325.
(220) Tai, X. H.; Lai, C. W.; Yang, T. C. K.; Johan, M. R.; Lee, K. M.; Chen, C.-Y.; Juan, J. C. Highly effective removal of volatile organic pollutants with pn heterojunction photoreduced graphene oxide-TiO2 photocatalyst. *Journal of Environmental Chemical Engineering* **2022**, *10* (2), No. 107304.
(221) Tan, L. L.; Chai, S. P.; Mohamed, A. R. Synthesis and applications of graphene-based TiO2 photocatalysts. *ChemSusChem* **2012**, *5* (10), 1868−1882.
(222) Tobaldi, D.; Dvoranová, D.; Lajaunie, L.; Rozman, N.; Figueiredo, B.; Seabra, M.; Škapin, A. S.; Calvino, J.; Brezová, V.; Labrincha, J. Graphene-TiO2 hybrids for photocatalytic aided removal of VOCs and nitrogen oxides from outdoor environment. *Chemical Engineering Journal* **2021**, *405*, No. 126651.
(223) Guo, H.; Wang, Y.; Yao, X.; Zhang, Y.; Li, Z.; Pan, S.; Han, J.; Xu, L.; Qiao, W.; Li, J.; et al. A comprehensive insight into plasma-catalytic removal of antibiotic oxytetracycline based on graphene-TiO2-Fe3O4 nanocomposites. *Chem. Eng. J.* **2021**, *425*, No. 130614.
(224) Tan, S. Y.; Chong, W. C.; Sethupathi, S.; Pang, Y. L.; Sim, L. C.; Mahmoudi, E. Optimisation of Aqueous Phase Low Density Polyethylene Degradation by Graphene Oxide-Zinc Oxide Photocatalysts. *Chem. Eng. Res. Des.* **2023**, *190*, 550.
(225) Tang, T.; Yin, Z.; Chen, J.; Zhang, S.; Sheng, W.; Wei, W.; Xiao, Y.; Shi, Q.; Cao, S. Novel pn heterojunction Bi2O3/Ti3+-TiO2 photocatalyst enables the complete removal of tetracyclines under visible light. *Chemical Engineering Journal* **2021**, *417*, No. 128058.
(226) Abdelhaleem, A.; Chu, W.; Liang, X. Diphenamid degradation via sulfite activation under visible LED using Fe (III) impregnated N-doped TiO2 photocatalyst. *Applied Catalysis B: Environmental* **2019**, *244*, 823−835.
(227) Kong, X.; Li, J.; Yang, C.; Tang, Q.; Wang, D. Fabrication of Fe2O3/g-C3N4@ N-TiO2 photocatalyst nanotube arrays that promote bisphenol A photodegradation under simulated sunlight irradiation. *Sep. Purif. Technol.* **2020**, *248*, No. 116924.
(228) Sharotri, N.; Sharma, D.; Sud, D. Experimental and theoretical investigations of Mn-N-co-doped TiO2 photocatalyst for visible light induced degradation of organic pollutants. *Journal of Materials Research and Technology* **2019**, *8* (5), 3995−4009.
(229) Ravichandran, K.; Sindhuja, E. Fabrication of cost effective g-C3N4+ Ag activated ZnO photocatalyst in thin film form for enhanced visible light responsive dye degradation. *Mater. Chem. Phys.* **2019**, *221*, 203−215.
(230) Vignesh, S.; Suganthi, S.; Sundar, J. K.; Raj, V.; Devi, P. R. I. Highly efficient visible light photocatalytic and antibacterial performance of PVP capped Cd: Ag: ZnO photocatalyst nanocomposites. *Appl. Surf. Sci.* **2019**, *479*, 914−929.
(231) Liao, G.; Yao, W. Upcycling of waste concrete powder into a functionalized host for nano-TiO2 photocatalyst: Binding mechanism and enhanced photocatalytic efficiency. *Journal of Cleaner Production* **2022**, *366*, No. 132918.
(232) Manojkumar, P.; Premchand, C.; Lokeshkumar, E.; Subrahmanyam, C.; Viswanathan, A.; Krishna, L. R.; Rameshbabu, N. Development of immobilised sunlight active W-Mo/Mo-V/VW co-doped TiO2 photocatalyst by plasma electrolytic oxidation. *J. Alloys Compd.* **2022**, *919*, No. 165781.
(233) Kader, S.; Al-Mamun, M. R.; Suhan, M. B. K.; Shuchi, S. B.; Islam, M. S. Enhanced photodegradation of methyl orange dye under UV irradiation using MoO3 and Ag doped TiO2 photocatalysts. *Environmental Technology & Innovation* **2022**, *27*, No. 102476.
(234) Yang, J.; Shi, C.; Dong, Y.; Su, H.; Sun, H.; Guo, Y.; Yin, S. Efficient hydrogen generation of vector Z-scheme CaTiO3/Cu/TiO2 photocatalyst assisted by cocatalyst Cu nanoparticles. *J. Colloid Interface Sci.* **2022**, *605*, 373−384.
(235) Tang, Q.; Xiong, P.; Wang, H.; Wu, Z. Boosted CO2 photoreduction performance on Ru-Ti3CN MXene-TiO2 photocatalyst synthesized by non-HF Lewis acidic etching method. *J. Colloid Interface Sci.* **2022**, *619*, 179−187.
(236) Zhang, X.; Wang, Y.; Chang, K.; Yang, S.; Liu, H.; Chen, Q.; Xie, Z.; Kuang, Q. Constructing hollow porous Pd/H-TiO2 photocatalyst for highly selective photocatalytic oxidation of methane to methanol with O2. *Applied Catalysis B: Environmental* **2023**, *320*, No. 121961.
(237) Tao, X.; Zhu, L.; Wang, X.; Chen, X.; Liu, X. Preparation of Zr/Y co-doped TiO2 photocatalyst and degradation performance of hydroquinone. *Environmental Science and Pollution Research* **2022**, *29* (27), 40854−40864.
(238) Xia, Z.; Xing, S.; Wang, H.; Zhao, D.; Wu, S.; Jiang, W.; Wang, N.; Liu, S.; Liu, C.; Ding, W.; et al. Weak-visible-light-driven Fe doped TiO2 photocatalyst prepared by coprecipitation method and degradation of methyl orange. *Opt. Mater.* **2022**, *129*, No. 112522.
(239) Tashkandi, N. Y.; Albukhari, S. M.; Ismail, A. A. Visible-light driven of heterostructured LaFeO3/TiO2 photocatalysts for degradation of antibiotics: Ciprofloxacin as case study. *J. Photochem. Photobiol., A* **2022**, *432*, No. 114078.
(240) Sebuso, D. P.; Kuvarega, A. T.; Lefatshe, K.; King'ondu, C. K.; Numan, N.; Maaza, M.; Muiva, C. M. Green synthesis of multilayer Graphene/ZnO nanocomposite for photocatalytic applications. *J. Alloys Compd.* **2022**, *900*, No. 163526.
(241) Yadav, R.; Chundawat, T. S.; Surolia, P. K.; Vaya, D. Photocatalytic degradation of textile dyes using β-CD-CuO/ZnO nanocomposite. *J. Phys. Chem. Solids* **2022**, *165*, No. 110691.
(242) Karthik, K.; Raghu, A.; Reddy, K. R.; Ravishankar, R.; Sangeeta, M.; Shetti, N. P.; Reddy, C. V. Green synthesis of Cu-doped ZnO nanoparticles and its application for the photocatalytic degradation of hazardous organic pollutants. *Chemosphere* **2022**, *287*, No. 132081.
(243) Nguyen, L. T.; Vo, D.-V. N.; Nguyen, L. T.; Duong, A. T.; Nguyen, H. Q.; Chu, N. M.; Nguyen, D. T. C.; Van Tran, T. Synthesis, characterization, and application of ZnFe2O4@ ZnO nanoparticles for photocatalytic degradation of Rhodamine B under visible-light illumination. *Environ. Technol. Innov.* **2022**, *25*, No. 102130.
(244) Choudhary, S.; Hasina, D.; Saini, M.; Ranjan, M.; Mohapatra, S. Facile synthesis, morphological, structural, photocatalytic and optical properties of ZnFe2O4-ZnO hybrid nanostructures. *J. Alloys Compd.* **2022**, *895*, No. 162723.
(245) Hunge, Y. M.; Yadav, A.; Kang, S.-W.; Lim, S. J.; Kim, H. Visible light activated MoS2/ZnO composites for photocatalytic degradation of ciprofloxacin antibiotic and hydrogen production. *J. Photochem. Photobiol., A* **2023**, *434*, No. 114250.
(246) Santos Anholeti, M.; Rocha Honorio de Oliveira, A.; Castro da Cruz, J.; Andrade Luciano, V.; Aparecida Nascimento, M.; Alves Puiatti, G.; de Carvalho Teixeira, A. P.; Pereira Lopes, R. Zn/ZnO heterostructures photocatalyst obtained by sustainable processes from alkaline batteries waste: Synthesis, characterization and application. *Mater. Chem. Phys.* **2022**, *284*, No. 126058.
(247) Sabouri, Z.; Sabouri, S.; Moghaddas, S. S. T. H.; Mostafapour, A.; Gheibihayat, S. M.; Darroudi, M. Plant-based synthesis of Ag-doped ZnO/MgO nanocomposites using Caccinia macranthera extract and evaluation of their photocatalytic activity, cytotoxicity, and potential application as a novel sensor for detection of Pb2+ ions. *Biomass Convers. Biorefin.* **2024**, *14*, 8293−8305.
(248) Chinnathambi, A. Synthesis and characterization of spinel FeV2O4 coupled ZnO nanoplates for boosted white light photocatalysis and antibacterial applications. *J. Alloys Compd.* **2022**, *890*, No. 161742.
(249) Alharbi, F.; Manzoor, S.; Munawar, T.; Nisa, M. U.; Abid, A. G.; Iqbal, F.; Aman, S.; Ehsan, M. F.; Najam-Ul-Haq, M.; Ashiq, M. N. Sunlight activated S-scheme ZnO-CoTe binary photocatalyst for effective degradation of dye pollutants from wastewater. *Surfaces and Interfaces* **2022**, *31*, No. 101991.
(250) AlAbdulaal, T.; AlShadidi, M.; Hussien, M. S.; Ganesh, V.; Bouzidi, A.; Algarni, H.; Zahran, H.; Abdel-wahab, M. S.; Yahia, I.; Elfiky, D.; et al. One-pot synthesis of multifunctionalized Nd2O3 dispersed ZnO nanocomposites for enhancing electrical, optical, and photocatalytic applications. *J. Mater. Res. Technol.* **2022**, *19*, 967−988.

https://doi.org/10.1021/acsomega.3c08717
ACS Omega 2024, 9, 25457−25492

(251) Arun, V.; Manikandan, V.; AlSalhi, M. S.; Devanesan, S.; Priyadharsan, A.; KA, R. K.; Maadeswaran, P. An efficient optical properties of Sn doped ZnO/CdS based solar light driven nanocomposites for enhanced photocatalytic degradation applications. *Chemosphere* **2022**, *300*, No. 134460.
(252) Ibhadon, A. O.; Fitzpatrick, P. Heterogeneous photocatalysis: recent advances and applications. *Catalysts* **2013**, *3* (1), 189−218.
(253) Xu, H.-Y.; Zhang, S.-Q.; Wang, Y.-F.; Xu, Y.; Dong, L.-M.; Komarneni, S. New insights into the photocatalytic mechanism of pristine ZnO nanocrystals: From experiments to DFT calculations. *Appl. Surf. Sci.* **2023**, *614*, No. 156225.
(254) Xu, P.; Ding, C.; Li, Z.; Yu, R.; Cui, H.; Gao, S. Photocatalytic degradation of air pollutant by modified nano titanium oxide (TiO2) in a fluidized bed photoreactor: Optimizing and kinetic modeling. *Chemosphere* **2023**, *319*, No. 137995.
(255) Heidari, Z.; Alizadeh, R.; Ebadi, A.; Oturan, N.; Oturan, M. A. Efficient photocatalytic degradation of furosemide by a novel sonoprecipited ZnO over ion exchanged clinoptilolite nanorods. *Sep. Purif. Technol.* **2020**, *242*, No. 116800.
(256) Mohadesi, M.; Sanavi Fard, M.; Shokri, A. The application of modified nano-TiO2 photocatalyst for wastewater treatment: A review. *International Journal of Environmental Analytical Chemistry* **2022**, 1−22.
(257) Baradaran, M.; Ghodsi, F.; Bittencourt, C.; Llobet, E. The role of Al concentration on improving the photocatalytic performance of nanostructured ZnO/ZnO: Al/ZnO multilayer thin films. *J. Alloys Compd.* **2019**, *788*, 289−301.
(258) Sanakousar, F.; Vidyasagar, C.; Jiménez-Pérez, V.; Prakash, K. Recent progress on visible-light-driven metal and non-metal doped ZnO nanostructures for photocatalytic degradation of organic pollutants. *Materials Science in Semiconductor Processing* **2022**, *140*, No. 106390.
(259) Tang, B.; Chen, H.; Peng, H.; Wang, Z.; Huang, W. Graphene modified TiO2 composite photocatalysts: Mechanism, progress and perspective. *Nanomaterials* **2018**, *8* (2), 105.
(260) Vattikuti, S. P.; Reddy, P. A. K.; Shim, J.; Byon, C. Visible-light-driven photocatalytic activity of SnO2−ZnO quantum dots anchored on g-C3N4 nanosheets for photocatalytic pollutant degradation and H2 production. *ACS omega* **2018**, *3* (7), 7587−7602.
(261) Wang, S.; Liu, D.; Yu, J.; Zhang, X.; Zhao, P.; Ren, Z.; Sun, Y.; Li, M.; Han, S. Photocatalytic penicillin degradation performance and the mechanism of the fragmented TiO2 modified by CdS quantum dots. *ACS omega* **2021**, *6* (28), 18178−18189.
(262) Khaki, M. R. D.; Shafeeyan, M. S.; Raman, A. A. A.; Daud, W. M. A. W. Application of doped photocatalysts for organic pollutant degradation-A review. *Journal of environmental management* **2017**, *198*, 78−94.
(263) Singhal, S.; Dixit, S.; Shukla, A. Self-assembly of the Ag deposited ZnO/carbon nanospheres: a resourceful photocatalyst for efficient photocatalytic degradation of methylene blue dye in water. *Advanced Powder Technology* **2018**, *29* (12), 3483−3492.
(264) Marschall, R. Semiconductor composites: strategies for enhancing charge carrier separation to improve photocatalytic activity. *Adv. Funct. Mater.* **2014**, *24* (17), 2421−2440.
(265) Zong, H.; Zhao, T.; Zhou, G.; Qian, R.; Feng, T.; Pan, J. H. Revisiting structural and photocatalytic properties of g-C3N4/TiO2: is surface modification of TiO2 by calcination with urea an effective route to "solar" photocatalyst? *Catal. Today* **2019**, *335*, 252−261.
(266) Devi, L. G.; Kavitha, R. A review on non metal ion doped titania for the photocatalytic degradation of organic pollutants under UV/solar light: Role of photogenerated charge carrier dynamics in enhancing the activity. *Applied Catalysis B: Environmental* **2013**, *140*, 559−587.
(267) Ghamarpoor, R.; Jamshidi, M.; Fallah, A.; Eftekharipour, F. Preparation of dual-use GPTES@ ZnO photocatalyst from waste warm filter cake and evaluation of its synergic photocatalytic degradation for air-water purification. *Journal of environmental management* **2023**, *342*, No. 118352.
(268) Mohamed, E. F.; Ali, H. New Pt/TiO2/Ti2Fe2O7 nanocomposite using sugarcane bagasse agro-waste for photodegradation of toluene gas pollutant under sunlight. *Materials Science and Engineering: B* **2023**, *295*, No. 116583.
(269) Park, S.-M.; Razzaq, A.; Park, Y. H.; Sorcar, S.; Park, Y.; Grimes, C. A.; In, S.-I. Hybrid Cu x O−TiO2 Heterostructured Composites for Photocatalytic CO2 Reduction into Methane Using Solar Irradiation: Sunlight into Fuel. *ACS omega* **2016**, *1* (5), 868−875.
(270) Taghizadeh-Lendeh, P.; Sarrafi, A. H. M.; Alihosseini, A.; Bahri-Laleh, N. Synthesis and characterisation ZnO/TiO2 incorporated activated carbon as photocatalyst for gas refinery effluent treatment. *Polyhedron* **2024**, *247*, No. 116715.
(271) Pinedo-Escobar, J. A.; Fan, J.; Moctezuma, E.; Gomez-Solís, C.; Carrillo Martinez, C. J.; Gracia-Espino, E. Nanoparticulate double-heterojunction photocatalysts comprising TiO2 (Anatase)/WO3/TiO2 (Rutile) with enhanced photocatalytic activity toward the degradation of methyl orange under near-ultraviolet and visible light. *ACS omega* **2021**, *6* (18), 11840−11848.
(272) Wang, Y.; Huang, L.; Zhang, T. C.; Wang, Y.; Yuan, S. Visible-Light-Induced photocatalytic oxidation of gaseous ammonia on Mo, c-codoped TiO2: Synthesis, performance and mechanism. *Chemical Engineering Journal* **2024**, *482*, No. 148811.
(273) Huang, C.; Li, J. A synergistic effect between ZnO/CdS S-scheme heterojunction and GO cocatalyst for boosting photocatalytic performance. *Opt. Mater.* **2023**, *139*, No. 113726.
(274) Preethi, S.; Vivek, S.; Priya, R.; Balakumar, S.; Suresh Babu, K. Enhanced Photocatalytic Performance of CuFeO2-ZnO Heterostructures for Methylene Blue Degradation under Sunlight. *J. Mater. Sci.: Mater. Electron.* **2021**, *32*, 22256−22269.
(275) Lazau, C.; Poienar, M.; Orha, C.; Ursu, D.; Nicolaescu, M.; Vajda, M.; Bandas, C. Development of a new "np" heterojunction based on TiO2 and CuMnO2 synergy materials. *Mater. Chem. Phys.* **2021**, *272*, No. 124999.
(276) Shi, J.; Huang, W.; Zhu, H.; Xiong, J.; Bei, H.; Wang, S. Facile fabrication of durable biochar/H2-TiO2 for highly efficient solar-driven degradation of enrofloxacin: properties, degradation pathways, and mechanism. *ACS omega* **2022**, *7* (14), 12158−12170.
(277) Zakir, O.; Ait Karra, A.; Idouhli, R.; Elyaagoubi, M.; Khadiri, M.; Dikici, B.; Aityoub, A.; Abouelfida, A.; Outzourhit, A. Fabrication and characterization of Ag-and Cu-doped TiO2 nanotubes (NTs) by in situ anodization method as an efficient photocatalyst. *J. Solid State Electrochem.* **2022**, *26* (10), 2247−2260.
(278) Xie, T.-f.; Wang, D.-j.; Zhu, L.-j.; Li, T.-j.; Xu, Y.-j. Application of surface photovoltage technique in photocatalysis studies on modified TiO2 photo-catalysts for photo-reduction of CO2. *Materials chemistry and physics* **2001**, *70* (1), 103−106.
(279) Urs, K. M.; Kamble, V. Surface photovoltage response of zinc oxide microrods on prismatic planes: effect of UV, temperature and oxygen ambience. *Journal of Materials Science: Materials in Electronics* **2021**, *32*, 6414−6424.
(280) Li, M.; Meng, G.; Huang, Q.; Yin, Z.; Wu, M.; Zhang, Z.; Kong, M. Prototype of a porous ZnO SPV-based sensor for PCB detection at room temperature under visible light illumination. *Langmuir* **2010**, *26* (16), 13703−13706.
(281) Chen, L.; Zhao, C.; Dionysiou, D. D.; O'Shea, K. E. TiO2 photocatalytic degradation and detoxification of cylindrospermopsin. *J. Photochem. Photobiol., A* **2015**, *307*, 115−122.
(282) Shah, B. R.; Patel, U. D. Mechanistic aspects of photocatalytic degradation of Lindane by TiO2 in the presence of Oxalic acid and EDTA as hole-scavengers. *Journal of Environmental Chemical Engineering* **2021**, *9* (4), No. 105458.
(283) Erdem, B.; Sevinç, S.; Erdem, S.; Öksüzoğlu, R. M. Comparative influence of adsorption assisted magnetic mesoporous TiO2 photocatalyst for the removal of methylene blue and rhodamine B. *Reaction Kinetics, Mechanisms and Catalysis* **2023**, *136* (2), 1049−1065.
(284) Hasan, I.; Shekhar, C.; Bin Sharfan, I. I.; Khan, R. A.; Alsalme, A. Ecofriendly green synthesis of the ZnO-doped CuO@ Alg bionanocomposite for efficient oxidative degradation of p-nitrophenol. *Acs Omega* **2020**, *5* (49), 32011−32022.
(285) Xiao, C.; Chen, X.; Tao, X.; Liu, X.; Wang, X.; Zhu, L. In situ generation of hydroxyl radicals by B-doped TiO2 for efficient

https://doi.org/10.1021/acsomega.3c08717
ACS Omega 2024, 9, 25457−25492

photocatalytic degradation of acetaminophen in wastewater. *Environmental Science and Pollution Research* **2023**, *30* (16), 46997−47011.
(286) Kiwaan, H. A.; Atwee, T. M.; Azab, E. A.; El-Bindary, A. A. Efficient photocatalytic degradation of Acid Red 57 using synthesized ZnO nanowires. *Journal of the Chinese Chemical Society* **2019**, *66* (1), 89−98.
(287) Narzary, S.; Alamelu, K.; Raja, V.; Ali, B. J. Visible light active, magnetically retrievable Fe3O4@ SiO2@ g-C3N4/TiO2 nanocomposite as efficient photocatalyst for removal of dye pollutants. *J. Environ. Chem. Eng.* **2020**, *8* (5), No. 104373.
(288) Li, D.; Song, H.; Meng, X.; Shen, T.; Sun, J.; Han, W.; Wang, X. Effects of particle size on the structure and photocatalytic performance by alkali-treated TiO2. *Nanomaterials* **2020**, *10* (3), 546.
(289) Ranjbari, A.; Kim, J.; Kim, J. H.; Yu, J.; Demeestere, K.; Heynderickx, P. M. Enhancement of commercial ZnO adsorption and photocatalytic degradation capacity of methylene blue by oxygen vacancy modification: Kinetic study. *Catal. Today* **2023**, *413*, No. 113976.
(290) Peng, W.; Lin, Y.; Wan, Z.; Ji, H.; Ma, W.; Zhao, J. An unusual dependency on the hole-scavengers in photocatalytic reductions mediated by a titanium-based metal-organic framework. *Catal. Today* **2020**, *340*, 86−91.
(291) Acedo-Mendoza, A.; Infantes-Molina, A.; Vargas-Hernández, D.; Chávez-Sánchez, C.; Rodríguez-Castellón, E.; Tánori-Córdova, J. Photodegradation of methylene blue and methyl orange with CuO supported on ZnO photocatalysts: The effect of copper loading and reaction temperature. *Materials science in semiconductor processing* **2020**, *119*, No. 105257.
(292) Weerathunga, H.; Tang, C.; Brock, A. J.; Sarina, S.; Wang, T.; Liu, Q.; Zhu, H.-Y.; Du, A.; Waclawik, E. R. Nanostructure shape-effects in ZnO heterogeneous photocatalysis. *J. Colloid Interface Sci.* **2022**, *606*, 588−599.
(293) Jo, W.-K.; Sivakumar Natarajan, T. Facile synthesis of novel redox-mediator-free direct Z-scheme CaIn2S4 marigold-flower-like/TiO2 photocatalysts with superior photocatalytic efficiency. *ACS Appl. Mater. Interfaces* **2015**, *7* (31), 17138−17154.
(294) Mahmood, A.; Wang, X.; Xie, X.; Sun, J. Atomically dispersed Pt on TiO2 nanosheets for catalytic gaseous acetaldehyde abatement. *ACS Applied Nano Materials* **2021**, *4* (4), 3799−3810.
(295) Wang, L.; Fu, Y.; Li, Q.; Wang, Z. EPR evidence for mechanistic diversity of Cu (II)/peroxygen oxidation systems by tracing the origin of DMPO spin adducts. *Environ. Sci. Technol.* **2022**, *56* (12), 8796−8806.
(296) Pallotti, D. K.; Passoni, L.; Maddalena, P.; Di Fonzo, F.; Lettieri, S. Photoluminescence mechanisms in anatase and rutile TiO2. *J. Phys. Chem. C* **2017**, *121* (16), 9011−9021.
(297) Wafi, M. A. E.; Ahmed, M.; Abdel-Samad, H. S.; Medien, H. Exceptional removal of methylene blue and p-aminophenol dye over novel TiO2/RGO nanocomposites by tandem adsorption-photocatalytic processes. *Materials Science for Energy Technologies* **2022**, *5*, 217−231.
(298) Zhang, X.-Y.; Liu, J.-K.; Wang, J.-D.; Yang, X.-H. Mass production, enhanced visible light photocatalytic efficiency, and application of modified ZnO nanocrystals by carbon dots. *Ind. Eng. Chem. Res.* **2015**, *54* (6), 1766−1772.
(299) Li, J.; Liu, B.; Han, X.; Liu, B.; Jiang, J.; Liu, S.; Zhang, J.; Shi, H. Direct Z-scheme TiO2-x/AgI heterojunctions for highly efficient photocatalytic degradation of organic contaminants and inactivation of pathogens. *Sep. Purif. Technol.* **2021**, *261*, No. 118306.
(300) Braiek, Z.; Naceur, J. B.; Jrad, F.; Assaker, I. B.; Chtourou, R. Novel synthesis of graphene oxide/In2S3/TiO2 NRs heterojunction photoanode for enhanced photoelectrochemical (PEC) performance. *Int. J. Hydrogen Energy* **2022**, *47* (6), 3655−3666.
(301) Khedri, N.; Sani, M. J.; Mahjoub, A. R.; Khavar, A. H. C. Effect of synergy between reduced graphene oxide and a Dysprosium complex on sensitization of TiO2 nanoparticles for photocatalytic degradation of atrazine under visible light. *Opt. Mater.* **2023**, *135*, No. 113271.
(302) Parsaei-Khomami, A.; Mousavi, M.; Habibi, M. M.; Shirzad, K.; Ghasemi, J. B.; Wang, L.; Yu, J.; Yu, H.; Li, X. Highly efficient visible light photoelectrochemical degradation of ciprofloxacin and azo dyes by novel TiO2/AgBiS2 photoelectrocatalyst. *Solid State Sci.* **2022**, *134*, No. 107044.
(303) Sohail, M.; Baig, N.; Sher, M.; Jamil, R.; Altaf, M.; Akhtar, S.; Sharif, M. A novel tin-doped titanium oxide nanocomposite for efficient photo-anodic water splitting. *ACS omega* **2020**, *5* (12), 6405−6413.
(304) Ge, H.; Tian, H.; Zhou, Y.; Wu, S.; Liu, D.; Fu, X.; Song, X.-M.; Shi, X.; Wang, X.; Li, N. Influence of surface states on the evaluation of the flat band potential of TiO2. *ACS Appl. Mater. Interfaces* **2014**, *6* (4), 2401−2406.
(305) Eftekharipour, F.; Jamshidi, M.; Ghamarpoor, R. Fabricating core-shell of silane modified nano ZnO; Effects on photocatalytic degradation of benzene in air using acrylic nanocomposite. *Alexandria Engineering Journal* **2023**, *70*, 273−288.
(306) Zhao, Y.; Wang, W.; Li, C.; He, L. Electronic and photocatalytic properties of N/F co-doped anatase TiO 2. *RSC Adv.* **2017**, *7* (87), 55282−55287.
(307) Kaur, H.; Kumar, S.; Kaushal, S.; Badru, R.; Singh, P. P.; Pugazhendhi, A. Highly customized porous TiO2-PANI nanoparticles with excellent photocatalytic efficiency for dye degradation. *Environmental Research* **2023**, *225*, No. 114960.
(308) Schünemann, S.; van Gastel, M.; Tüysüz, H. A CsPbBr3/TiO2 composite for visible-light-driven photocatalytic benzyl alcohol oxidation. *ChemSusChem* **2018**, *11* (13), 2057−2061.
(309) Hafeez, H. Y.; Lakhera, S. K.; Narayanan, N.; Harish, S.; Hayakawa, Y.; Lee, B.-K.; Neppolian, B. Environmentally sustainable synthesis of a CoFe2O4−TiO2/rGO ternary photocatalyst: a highly efficient and stable photocatalyst for high production of hydrogen (solar fuel). *ACS omega* **2019**, *4* (1), 880−891.
(310) Zhang, S.; Xu, J.; Hu, J.; Cui, C.; Liu, H. Interfacial growth of TiO2-rGO composite by pickering emulsion for photocatalytic degradation. *Langmuir* **2017**, *33* (20), 5015−5024.
(311) Gnanasekaran, L.; Pachaiappan, R.; Kumar, P. S.; Hoang, T. K.; Rajendran, S.; Durgalakshmi, D.; Soto-Moscoso, M.; Cornejo-Ponce, L.; Gracia, F. Visible light driven exotic p (CuO)-n (TiO2) heterojunction for the photodegradation of 4-chlorophenol and antibacterial activity. *Environ. Pollut.* **2021**, *287*, No. 117304.
(312) Landi, S., Jr Comment on "Photocatalytic degradation of RhB from an aqueous solution using Ag3PO4/N-TiO2 heterostructure" and "Evaluation of the effect of dose change of Fe3O4 nanoparticles on electrochemical biosensor compatibility using hydrogels as an experimental living organism model. *J. Mol. Liq.* **2021**, *338*, No. 116635.
(313) Mohamed, W. A.; Abd El-Gawad, H. H.; Handal, H. T.; Galal, H. R.; Mousa, H. A.; ElSayed, B. A.; Labib, A. A.; Abdel-Mottaleb, M. Study of phytotoxicity, remarkable photocatalytic activity, recycling process and energy consumption cost of TiO2 quantum dots photocatalyst for photodegradation of Coomassie brilliant blue R dye. *Opt. Mater.* **2023**, *137*, No. 113607.
(314) Priya, A.; Arumugam, M.; Arunachalam, P.; Al-Mayouf, A. M.; Madhavan, J.; Theerthagiri, J.; Choi, M. Y. Fabrication of visible-light active BiFeWO6/ZnO nanocomposites with enhanced photocatalytic activity. *Colloids Surf. A* **2020**, *586*, No. 124294.

https://doi.org/10.1021/acsomega.3c08717
ACS Omega 2024, 9, 25457−25492